nature portfolio

Peer Review File

# Elucidating and Decoupling Diverse Fatigue Mechanisms Toward Static Self-Recovery in ZrO2-Based Antiferroelectrics

Corresponding Author: Dr Haoji Qian

**This file contains all editorial decision letters in order by version, followed by all author rebuttals in order by version.**

Version 0:

Decision Letter:

** Please ensure you delete the link to your author home page in this e-mail if you wish to forward it to your coauthors **

Dear Dr Qian,

Thank you for submitting your manuscript, "Elucidating and Decoupling Diverse Fatigue Mechanisms Toward Static Self-Recovery in ZrO2-Based Antiferroelectrics", to Communications Materials. It has now been seen by 3 referees, whose comments are appended below. You will see that while they find your work of potential interest, they have raised substantial concerns that must be addressed. In light of these comments, we cannot accept the manuscript for publication, but are interested in considering a revised version that addresses these serious concerns.

We hope you will find the referees' comments useful as you decide how to proceed. Additional clarification is especially needed regarding the modeling and interpretation of the experimental results, particularly in explaining the fatigue mechanism and the applicability of the proposed static self-recovery method. We also expect all other referee comments to be appropriately addressed, including their requests for further information and discussion.

Should further experimental data or analysis allow you to address these criticisms, we would be happy to look at a substantially revised manuscript. However, please bear in mind that we will be reluctant to approach the referees again in the absence of major revisions. If the revision process takes significantly longer than three months, we will be happy to reconsider your paper at a later date, as long as nothing similar has been accepted for publication at Communications Materials or published elsewhere in the meantime.

We are committed to providing a fair and constructive peer-review process. Please don't hesitate to contact us if you wish to discuss the revision in more detail.

When submitting your revised manuscript, please include the following:

-A response letter with a point-by-point reply to each of the referee comments and a description of changes made. Please include the complete referee report in the response letter. Please note that the response letter must be separate to the cover letter to the editors.

-A marked-up version of the manuscript with all changes to the text in a different colored font. Please do not include tracked changes or comments. Please select the file type ‘Revised Manuscript - Marked Up’ when uploading the manuscript file to our online system.

-A clean version of the manuscript. Please select the file type ‘Article File’.

-An updated <a href="https://www.nature.com/documents/nr-editorial-policy-checklist.zip">Editorial Policy</a> checklist, uploaded as a ‘Related Manuscript File’ type. This checklist is to ensure your paper complies with all relevant editorial policies. If needed, please revise your manuscript in response to these points. Please note that this form is a dynamic ‘smart pdf’ and must therefore be downloaded and completed in Adobe Reader. Clicking this link will download a zip file containing the pdf.

Please use the following link to submit your revised manuscript files:

Link Redacted

** This url links to your confidential home page and associated information about manuscripts you may have submitted or be reviewing for us. If you wish to forward this email to co-authors, please delete the link to your homepage first **

Please do not hesitate to contact me if you have any questions or would like to discuss the required revisions further. Thank you for the opportunity to review your work.

Best regards,

Andreja Bencan Golob, PhD
Editorial Board Member
Communications Materials
orcid.org/0000-0002-2116-3779

Reviewers' comments:

Reviewer #1 (Remarks to the Author):

In this manuscript, the authors studied the fatigue mechanisms of antiferroelectric and proposed a static self-recovery (SSR) method to restore the 2Pr. However, several issues need to be clarified as follows.

[1] Line 86 of page 3: “Note that the changes in FWHM, including increase and decrease, indicate the redistribution of VO.” What is the physical explanation of how changes in FWHM are associated with the redistribution of oxygen vacancies (VO)? Specifically, in the case where the FWHM remains stable, does this imply an increase or decrease in VO concentration due to charge trapping? Suggest material analysis for reference.
[2] Fig. 2d shows the different fatigue behavior of ZrO2 and Hf0.1Zr0.9O2. What are the underlying mechanisms contributing to these differences, and how do they relate to VO?
[3] Fig. 3a indicates shallow and deep fatigue, where the distinction is based on whether the polarization is completely recoverable. The concepts of intrinsic and extrinsic fatigue were also introduced, suggesting that only extrinsic fatigue is fully recoverable. Does the fatigue mechanism analysis for $ZrO_2$ show direct evidence indicating that extrinsic factors dominate to support this recovery behavior?
[4] In Fig. 3c of cited reference 27, there are three VO positions for consideration; however, Fig. 4c only assumes two VO positions. Please comment on the difference in setup between these two simulations.
[5] For Fig. 5c, if I understand correctly, a zero-second break time implies that no recovery method is applied. Why is endurance also improved? Please comment on the possible reasons.
[6] Regarding endurance performance, the cycling data present fewer than $1\times10^9$ cycles. What is the maximum number of cycles achievable using the proposed SSR approach? Is there any experimental data to support potential endurance beyond $10^9$ cycles?
[7] The proposed SSR implies that the waiting time for recovery is necessary. The recovery time makes the method unreliable and impractical for application.
[8] Benchmark comparison with other methods is suggested for readers to understand the merits and disadvantages.

Reviewer #2 (Remarks to the Author):

This manuscript investigates the fatigue phenomenon observed in MIM capacitors utilizing ZrO2-based AFE characteristics. It focuses on a method to recover the degraded 2Pr,p values caused by fatigue by introducing a break time between cycles, based on the conclusion drawn from the analysis of the fatigue mechanism—specifically, the Vo charge trapping phenomenon. The manuscript also aims to elucidate the underlying mechanism of this recovery.

Q1. It seems necessary to include details about the device fabrication process. There is no mention of the precursors used for Hf and Zr deposition, the oxidant used during deposition, or the gases used during annealing. Since the ALD window can vary depending on the precursor, and the Vo concentration—which is critical in this work—can significantly change depending on the type of oxidant, additional information on these points is required.

Q2. The manuscript states that ZrO2 undergoes fatigue with cycling, but recovers after a certain break period, with the 2Pr,p value returning to its initial peak level. While the similarity between the 2Pr,p values after fatigue and after the break period may suggest this indirectly, it would be beneficial to directly confirm whether intrinsic fatigue has occurred due to phase transition or Vo localization in ZrO2, as mentioned in the text, through intrinsic fatigue assessment.

Q3. In Fig. 3(d), fatigue caused by charge trapping is shown to be recovered through the release process up to 10^8 cycles. I am curious whether, if cycling continues to 10^9 or 10^10, the difference in 2Pr,p values between the with- and without-release cases increases further. Additionally, assuming breakdown does not occur, I would like to know whether the degree

of extrinsic fatigue in HZO according to break time (as shown in Fig. 4(f)) aligns with the difference in 2Pr,p values with or without the release. If they do not align, could this indicate that different fatigue mechanisms may emerge depending on the number of cycles?

Q4. The schematic in Fig. 4(g) shows electrons being detrapped from Vo during the recovery of extrinsic fatigue. It also depicts the electrons moving to relatively higher energy levels. I am curious whether this energy level difference is low enough to be overcome by thermal energy alone—i.e., if detrapping is possible simply through break time. Is there a quantitative value provided for this energy level difference?

Reviewer #3 (Remarks to the Author):

**General remarks:**

In this article, the authors present a method they call static self-recovery (SRR) applied to $ZrO_2$-based films. The SSR method allows an increase in remanent polarization after fatigue. The authors also combined this method with Density Functional Theory (DFT) and a three level traps model to understand which mechanism for fatigue plays a major role in their endurance tests for TiN/$ZrO_2$ (10 nm)/TiN and TiN/$Hf_{0.1}Zr_{0.9}O_2$(10 nm)/TiN capacitors.

The article shows interesting results; however, the manuscript suffers from an overuse of emphatic language, such as ″clearly″ (e.g., ″clearly prove″, ″clearly elucidate″) and “precisely” (e.g., “precisely described”), which may overstate the strength of the evidence provided. For expert readers, the current level of physical and mathematical justifications does not always appear sufficiently robust to support such assertive phrasing. This may unintentionally undermine the credibility of the conclusions.

In addition, although the manuscript is visually well-prepared, with high-quality figures and formatting, the scientific depth and rigor of the analysis do not fully match the quality of the presentation. The physical and mathematical modeling, as well as the interpretation of the experimental results, would benefit from clearer justification and possibly stronger experimental backing.

**General questions:**

- For a DRAM, which is the targeted application in this paper, introducing a break time implies that no current should flow through the device for a relatively long duration. Do you think such a condition can realistically be achieved during the power-off phases of electronic devices? Are you confident this would not be detrimental to overall device reliability or performance? Even if the OPCR method described in Extended Data Fig.2 is not ideal, it has the advantage that it can be quickly implemented by an algorithm. The use of break time seems to limit the applicability of the SSR method to real devices.

- Furthermore, if a manufacturer needs to anticipate whether shallow or deep fatigue is likely to occur, which of the two materials presented in this study would you recommend, and why?

- Finally, could the SSR method work for ferroelectric HfO2-based capacitors? And why?

**Specific questions**

- l. 34-35 “One of the key issues is the remnant polarization (Pr) degradation during electrical cycling, which is a concern regarding their reliability.” Pr degradation (fatigue) occurs principally when voltage is decreased or frequency is increased. Did you observe this effect? Or did you consider this in your characterizations?

- On Fig.1, more precisions are requested. For example, please indicate that the curve in dashed lines on figures 1d and 1e is the initial state.

- l. 76 Starting from line 76, you use the acronym Pr to denote the remanent polarization. However, the word “remanent” means “what remains”. So the term "remanent" specifically refers to the polarization that remains in the absence of an external electric field—i.e., the polarization measured at 0 V. In your case, Pr appears to refer to the polarization at the relaxation voltage, which corresponds to the voltage around which the positive (or negative) uni-PUND pulse sequence is centered. While the analogy is understandable, this value does not strictly represent the remanent polarization and should be referred to using a different term to avoid confusion.

- l.81-85 In the presence of a wake-up effect, the peak of the switching current, which corresponds to the coercive voltage, defines the appropriate relaxation voltage. In your case, the relaxation voltage is not explicitly stated. Based on the curve in Fig. 2b, it seems that you may be using half of the total applied voltage (i.e., 3.5 V / 2 = 1.75 V). However, if a wake-up effect is occurring and the coercive field shifts during cycling, using a fixed relaxation voltage may inadvertently distort the symmetry of the hysteresis loop. As a result, some of the observed effects might be attributed to this misalignment rather than to intrinsic material properties. For instance, Magagning et al. ACS NanoLetters (2025) (https://doi.org/10.1021/acs.nanolett.5c00851) suggested using an automatic sequence to determine the relaxation voltage

before using uni-PUND. Do you think it might be relevant or not in your case? And Why?

- l.86-90 The authors state that the FWHM change observed in $ZrO_2$ is attributed solely to charge trapping, without involving oxygen vacancy ($V_o$) redistribution, whereas the FWHM change in $Hf_{0.1}Zr_{0.9}O_2$ follows a different behavior. However, I could not find any experimental evidence or theoretical framework supporting this distinction. Could the authors please elaborate on this point and clarify the basis—experimental, analytical, or otherwise—for this hypothesis?

- l.92 The description of how electric field (E-field) modulation is implemented remains somewhat unclear. Fig. 2b, which appears to illustrate a uni-PUND sequence, does not show any E-field modulation. Given the strong potential of E-field modulation for various applications, it would be helpful if the authors could clarify the measurement protocol or electrical sequence one can use to achieve this modulation.

- l.101-132 Imprint is likely to develop during the break time. Could it be that, ultimately, the SSR method relies on exploiting the imprint effect to re-center the hysteresis around the relaxation point, thereby recovering a higher polarization?

- l.138 “couping” I think there is a mistake. It should be: “coupling”

- l.160 and l.169 From equations (1) and (2), the three-level traps model seems to be very simple. Don’t you think that additional parameters should be taken into account to describe the overall phenomenon occurring in fluorite materials?

- l.181-203 The three-level traps model essentially relies on fitting with three exponential components. However, it is not demonstrated how one can confidently attribute distinct physical mechanisms to these components, given the potential overlap and similarity in their mathematical behavior. Without additional validation, the assignment of specific processes to each level remains speculative. It would strengthen the work to support the model with complementary experimental evidence, such as temperature-dependent measurements, frequency response analysis, or material characterization techniques, that could independently validate the existence and nature of the proposed trap levels.

**Questions about the extended data**

- In the “methods” section, could you precise about how the stoichiometry is determined?

- l.351 The authors are talking about the AFE orthorhombic phase and the non-polar tetragonal phase. To my knowledge, the current theory of antiferroelectricity in ZrO2 suggests that there is a structural phase transition from tetragonal to orthorhombic phase (see for instance, Hoffmann et al. Nature (2022), https://doi.org/10.1038/s41467-022-28860-1 ). I recommend not using the words “antiferroelectric orthorhombic phase” as the interplay between tetragonal and orthorhombic phases remains unclear. And only talking about orthorhombic and tetragonal without specifying the electric behavior.



Version 1:

Decision Letter:



Dear Dr Qian,

Thank you again for submitting your manuscript "Elucidating and Decoupling Diverse Fatigue Mechanisms Toward Static Self-Recovery in ZrO2-Based Antiferroelectrics" to Communications Materials. We have now received reports from the 3 reviewers and, based on their comments, we have decided to invite a further revision of your work. You will find the reviewers' reports below. While they find your work improved, they still raise important points which must be addressed in a revised manuscript.

In particular, we ask that you address the points regarding SSR methods raised by Reviewer 1 and, if possible, those raised by Reviewer 3.

To allow us to move forward with your work, we also ask that you edit your manuscript according to the attached table. **Please read this document carefully as we will be unable to further assess your revised paper until these important points are addressed.**

Please outline all revisions made in the right-hand column and return the completed table with your updated manuscript files as a Related Manuscript file.

**When resubmitting, please also include:**

- A point-by-point response to the reviewers' comments. If you are unable to address specific reviewer requests or find any points invalid, please explain
- A clean version of your revised manuscript with no mark-ups
- A marked-up version of your paper with all changes highlighted in a different colour

Please use the link below to submit your revised files:
Link Redacted

** This url links to your confidential home page and associated information about manuscripts you may have submitted or that your are reviewing for us. If you wish to forward this email to co-authors, please delete the link to your homepage first **

**We hope to receive your revised paper within six weeks, but we understand that the revisions may take longer. Please let us know if you find that the revision process will take substantially more time.**

We are committed to providing a fair and constructive peer-review process. Please do not hesitate to contact me if you have any questions or would like to discuss these revisions further. We look forward to seeing the revised manuscript and thank you for the opportunity to review your work.

Best regards,

Andreja Bencan Golob, PhD
Editorial Board Member
Communications Materials
orcid.org/0000-0002-2116-3779

**Reviewers' comments:**
Reviewer #1 (Remarks to the Author):

This manuscript has been improved after revision. Since the authors proposed a static self-recovery (SSR) method to restore the 2Pr, there are some suggestions as below.

1) The waiting time needs to be performed with 2Pr degradation, and the authors mentioned that a threshold can be predefined. How to realize this concept, like "Self-Tracking Circuit Design for Recovery" [1]. Can the authors propose a circuit to sense the 2Pr degradation threshold?
[1] C.-W. Wu et al, IEDM, 18-2, 2023.

2) The authors claimed SSR has the potential to exceed 10^9 cycles. Recently, many papers show the robust endurance for > 10^10 cycles. The suggestion is that the authors have to demonstrate the outstanding performance of the SSR scheme to convince the readers.

Reviewer #2 (Remarks to the Author):

This manuscript presents a novel approach to addressing the endurance (fatigue) issues in $ZrO_2$-based antiferroelectric (AFE) devices. The authors introduce the concept of Static Self-Recovery (SSR) and systematically analyze the fatigue mechanisms of $ZrO_2$-based AFEs through electrical measurements. They further decouple the contributions of oxygen vacancy ($V_o$) formation and shallow/deep traps, and establish a clear interpretation of the fatigue behavior. Based on this, they propose a three-level trap model to describe the SSR process, which is additionally supported by density functional theory (DFT) calculations.
The reviewers mainly raised questions regarding the contribution of oxygen vacancy traps and the validity of the newly proposed SSR measurement method. The authors responded thoroughly and convincingly, addressing these concerns without undermining the original claims of their work. In particular, the distinction between shallow and deep fatigue and the universality of the three-level trap model were clarified and strongly supported by both experimental data and theoretical analysis.
Therefore, this reviewer concludes that the manuscript presents significant and meaningful results with direct implications for enhancing the endurance of next-generation AFE-based memory devices. The study provides valuable insights and is of sufficient quality for publication. Accordingly, I recommend acceptance of this manuscript.

Reviewer #3 (Remarks to the Author):

The manuscript is overall very interesting, and the results are of clear relevance for the field.

The authors present convincing analyses of the electrical characterizations for memory applications, and the quality of the paper has improved significantly following the reviewers' comments. The work, in its current form, already provides valuable insights, and the study deserves consideration for publication.

That said, the discussion relies mainly on theoretical arguments to support the interpretation of electrical measurements. While these interpretations are logical and often compelling, the absence of complementary experimental evidence (such as deeper analyses in XRD, XPS, TEM, temperature-dependent measurements, etc.) limits the strength of the conclusions. For example, the separation between extrinsic and intrinsic fatigue, or the attribution of FWHM distribution to oxygen vacancy redistribution, would be considerably more convincing if supported by direct experimental proof. At present, some explanations remain hypothetical, particularly as several justifications draw primarily on the authors' own prior publications. More generally, the article interprets complex, multifactorial electrical measurements through largely theoretical support. This approach is not without merit, but additional perspectives would enhance the work. Future studies could benefit from:
• Complementary experimental characterizations to substantiate theoretical hypotheses.
• Engagement with a wider body of literature, beyond the authors' own work (particularly in the first response to reviewers)
• Consideration of alternative mechanisms could provide greater nuance and robustness to the conclusions.



Version 2:

Decision Letter:



Dear Dr Qian,

Thank you once again for submitting your manuscript, "Elucidating and Decoupling Diverse Fatigue Mechanisms Toward Static Self-Recovery in ZrO2-Based Antiferroelectrics," to Communications Materials. It has now been seen again by the referees, whose comments are appended below. The concerns of our reviewers have now been addressed, but there are some amendments needed before we can accept your paper.

We ask that you edit your manuscript according to the attached table. **Please read this document carefully as we will be unable to further assess your revised paper until these important points are addressed.**

Please outline all revisions made in the right-hand column and return the completed table with your updated manuscript files as a Related Manuscript file.

Please use the link below to submit your revised files:
Link Redacted

When resubmitting, please provide a marked-up manuscript with all changes highlighted, as well as a clean version of your paper.

**We hope to receive this updated version of your paper within 1 week, but please let us know if you find that you need more time.**

Best regards,

Andreja Bencan Golob, PhD
Editorial Board Member
Communications Materials
orcid.org/0000-0002-2116-3779

**Reviewers' comments:**
Reviewer #1 (Remarks to the Author):

This manuscript has been improved after revision. The relevance circuit for recovery and projected fatigue under SSR has been added in the supplementary Information. Accordingly, the manuscript is worthy of publication.

Version 3:

Decision Letter:

Dear Dr Qian,

We are delighted to accept your manuscript titled "Elucidating and Decoupling Diverse Fatigue Mechanisms Toward Static Self-Recovery in ZrO2-Based Antiferroelectrics" for publication in Communications Materials. Thank you for choosing to publish your interesting work with us.

**Licence to Publish and Article-Processing Charge**

In approximately 7-10 business days you will receive an email with a link to choose the grant of rights necessary for publishing your paper and – if applicable – to provide payment information for your article-processing charge (APC), either via credit card or by requesting an invoice.

If needed, our Author Services team will be in touch regarding any additional information that may be required.

**In order to avoid any delays, please ensure that you have emails from Springer Nature whitelisted in your mail system.**

If you have any questions about our publishing options, costs, Open Access requirements, or our legal forms, please contact ASJournals@springernature.com

We will edit your manuscript to ensure that it conforms with our house style and send you a link to an online eProof for checking in a separate email to the publishing agreements. Please read your proof with great care to ensure that the sense has not been altered. We also suggest you discuss the proof with your co-authors, but please ensure that only one author communicates with us and that only one set of corrections is returned via the online correction in the eProof. The corresponding (or nominated) author is responsible on behalf of all co-authors for the accuracy of all content, including spelling of names and current affiliations.

To ensure prompt publication, your proofs should be returned within two working days. If there is any period within the next four weeks in which you won't be available, please nominate a co-author with whom we can correspond, and let us know their e-mail address as soon as possible.

**Please note that production will not continue until the Licence to Publish and Article-Processing Charge steps are completed and your proof corrections are submitted.**

Please note that your Supplementary Information files are now finalized. They will be uploaded directly to the Communications Materials website in preparation for publication of the Article. Any requests to make changes will only be considered in exceptional circumstances and will result in a delay to publication.

Acceptance of your manuscript is conditional on all authors' agreement with <a href="https://www.nature.com/commsmat/editorial-policies">our publication policies</a>. In particular, your manuscript must not be published elsewhere and there must be no announcement of the work in the media until the publication date. At this stage, you may wish to make your institution's press office aware of the forthcoming publication, if you wish to bring your work to the media's attention, so that they can start preparing any publicity. Please note that the paper is still under embargo

until it is published in the journal. Further details of our embargo policy can be found here http://www.nature.com/authors/policies/embargo.html.

We will aim to publish your article in a timely manner. Please note there will be no further correspondence about your publication date. When your article is published, you will receive a notification email. **If you are planning an embargoed press release or require a specific publication date, please complete our <a href="https://forms.office.com/e/ed7NBDd08u">scheduling requests form</a>, or contact commsproduction@springernature.com, as soon as possible after acceptance and we will endeavour to accommodate your request.** For further information on the journey of your article from acceptance to publication, please see our <a href="https://www.nature.com/documents/Author_FAQs.pdf">Author FAQs.</a>

If you have any questions about open-access invoicing or payment, please contact authororders@nature.com

You can now use a single sign-on for all your accounts, view the status of all your manuscript submissions and reviews, access usage statistics for your published articles and download a record of your refereeing activity for the Nature journals.

We look forward to publishing your paper.

Best regards,

Andreja Bencan Golob, PhD
Editorial Board Member
Communications Materials
orcid.org/0000-0002-2116-3779

***As a new journal, we would greatly appreciate any comments you have about your experience at Communications Materials. I hope that we have been able to meet your expectations and look forward to working with you again in the future.

We may promote your article on social media once it is published, so please feel free to send me the twitter handles of any authors or departments and we will be sure to tag them accordingly.***

** Visit Nature Research's author and referees' website at <a href="http://www.nature.com/authors">www.nature.com/authors</a> for information about policies, services and author benefits**

# Response to Reviewer's Comments

Title: Elucidating and Decoupling Diverse Fatigue Mechanisms Toward Static Self-Recovery in $ZrO_2$-Based Antiferroelectrics

Authors: Haoji Qian, Rongzong Shen, Jiacheng Xu, Miaomiao Zhang, Minglei Ma, Yian Ding, Xiaoxi Li, Gaobo Lin, Jiani Gu, Ran Cheng, Yan Liu, Chengji Jin, Jiajia Chen, Yue Hao, and Genquan Han

Dear Reviewers,

We really appreciate your important comments on our manuscript entitled: Elucidating and Decoupling Diverse Fatigue Mechanisms Toward Static Self-Recovery in $ZrO_2$-Based Antiferroelectrics. We have carefully revised the manuscript according to the reviewers' comments. The detailed descriptions on the revisions and the point-to-point responses to the reviewers' comments are summarized as below. The revised parts in the new manuscript have been highlighted.

Notably, we have carefully revised our terminology throughout the manuscript to ensure proper usage. **All instances of "$P_{r,p}$" have been replaced with "$P_{s,p}$"** to quantitatively evaluate the AFE properties in actual applications with half-loop operation to accurately reflect the measured switchable polarization in our uni-PUND experiments.

## Reviewer: 1

Comments to the Author

In this manuscript, the authors studied the fatigue mechanisms of antiferroelectric and proposed a static self-recovery (SSR) method to restore the $2P_r$. However, several issues need to be clarified as follows.

**Comment 1:** Line 86 of page 3: "Note that the changes in *FWHM*, including increase and decrease, indicate the redistribution of $V_O$." What is the physical explanation of how changes in *FWHM* are associated with the redistribution of oxygen vacancies ($V_O$)? Specifically, in the case where the *FWHM* remains stable, does this imply an increase or decrease in $V_O$ concentration due to charge trapping? Suggest material analysis for reference.

**Response:** We sincerely appreciate the reviewer's insightful comment regarding the physical association between full-width at half-maximum (*FWHM*) changes and oxygen vacancies ($V_O$) redistribution. $ZrO_2$-based antiferroelectric (AFE) thin films exhibit polycrystalline and multi-domain characteristics, wherein the domain reversal requires overcoming a local nucleation energy barrier corresponding to local coercive fields ($E_c$). The *FWHM* of *I–V* curve manifests the spatial dispersion of local $E_c$ across the film. A small *FWHM* represents collective switching of all domains within a narrow electric field range, indicating a tightly distributed local $E_c$. Conversely, a large *FWHM* signifies asynchronous domain switching at varied electric fields,

reflecting a dispersed local $E_c$ distribution. Various reports have claimed that $V_O$ plays a critical role in governing polarization switching characteristics. The distribution of $V_O$ would significantly modify the local $E_c$, substantially impacting polarization switching energy barriers [1-4]. Thus, when $V_O$ are uniformly distributed, the distribution of local $E_c$ is tight and the *FWHM* is small. Oppositely, the inhomogeneous distributed $V_O$ causes the broader distributed local $E_c$ and a larger *FWHM*. A stable *FWHM* over cycling signifies the maintenance of stationary $V_O$ distribution. On the other hand, the charged $V_O$ generates local internal electric fields ($E_i$), which primarily manifest as a global shift of the local $E_c$ in the *I–V* curve. In summary, the $V_O$ distribution significantly affect the macroscopic polarization-switching behavior, which can be characterized by the distribution of the local $E_c$ in the *I–V* curve.

In response to the reviewer's specific question regarding stable *FWHM* and its implications for $V_O$ evolution, the stable *FWHM* with the shifted *I–V* curve suggests no significant redistribution of $V_O$[4]. The dynamic evolution of $ZrO_2$ capacitors shows that when the *FWHM* of $I_{peak}$ remains almost unchanged while the *I–V* curve shifts, the dominant microscopic physical mechanism is interfacial $V_O$ charge trapping (extrinsic fatigue). In this process, pre-existing $V_O$ at the TiN/$Hf_xZr_{1-x}O_2$ will be charged during continuous uni-directional cycling, creating the $E_i$ that biases the polarization switching without requiring $V_O$ migration or generation inside the film. Therefore, the overall $V_O$ concentration (and spatial distribution) stays effectively constant, neither increasing nor decreasing, while the charge states of $V_O$ altered. This picture agrees with the behavior that has been observed in $ZrO_2$ AFE film after $10^8$ cycles and is likely the leading fatigue mechanism in this system. In contrast, fatigue in $Hf_{0.1}Zr_{0.9}O_2$ may involve a coupling of $V_O$ charge trapping and redistribution, which contributes to a complicated evolution of *FWHM* as the film undergoes the repeated switching process.

**Reference (Response Letter)**

1. Gong, Z. et al. Physical origin of the endurance improvement for $HfO_2$-$ZrO_2$ superlattice ferroelectric film. *Applied Physics Letters* **121**, 242901 (2022).

2. Chen, J. et al. Physical Origin of Recovable Ferroelectric Fatigue and Recovery for Doped-$HfO_2$: Toward Endurance Immunity. in *2023 International Electron Devices Meeting (IEDM)* 18.1.1-18.1.4 (IEEE, San Francisco, CA, USA, 2023).

3. Chen, J. et al. Impact of Oxygen Vacancy on Ferroelectric Characteristics and Its Implication for Wake-Up and Fatigue of $HfO_2$-Based Thin Films. *IEEE Trans. Electron Devices* **69**, 5297-5301 (2022).

4. Qian, H. et al. Dynamic evolution of oxygen vacancies during cycling in antiferroelectric $Hf_xZr_{1-x}O_2$. *Applied Physics Letters* **124**, 243508 (2024).

According to the reviewer's comment, we have added some sentences to describe the physical association between *FWHM* changes and $V_O$ evolution more clearly in the revised manuscript. **The revised sections are as follows.**

## Electrical characteristics of $ZrO_2$-based AFE capacitors

Fig. 2c shows the definition of full width at half maximum (*FWHM*) extracted from the current-voltage (*I*–*V*) curve, which is used to assess the spreading of coercive field ($E_c$) distribution. The *FWHM* of *I*–*V* curve manifests the spatial dispersion of local $E_c$ across the film. A small *FWHM* represents collective switching of all domains within a narrow electric field range, indicating a tightly distributed local $E_c$. Conversely, a large *FWHM* signifies asynchronous domain switching at varied electric fields, reflecting a dispersed local $E_c$ distribution. The distribution of $V_O$ would significantly modify the local $E_c$, substantially impacting polarization switching energy barriers. When $V_O$ are uniformly distributed, the distribution of local $E_c$ is tight and the *FWHM* is small. Oppositely, the inhomogeneous distributed $V_O$ causes the broader distributed local $E_c$ and a larger *FWHM*. A stable *FWHM* over cycling signifies the maintenance of stationary $V_O$ distribution.

**Comment 2:** Fig. 2d shows the different fatigue behavior of $ZrO_2$ and $Hf_{0.1}Zr_{0.9}O_2$. What are the underlying mechanisms contributing to these differences, and how do they relate to $V_O$?

**Response:** We sincerely appreciate this insightful comment. The contrasting fatigue trends in **Fig. 2d** and the corresponding changes in *I*–*V* curves in **Fig. 2e** arise from how Hf doping alters the generation, distribution, charge trapping, and migration kinetics of $V_O$, which in turn affects both extrinsic and intrinsic fatigue mechanisms of $ZrO_2$-based AFE devices. Our previous work[4] systematically tracked the dynamic evolution of $V_O$ during cycling in $Hf_xZr_{1-x}O_2$ AFE capacitors, providing a useful mechanistic framework that we apply to interpret the data in this manuscript.

Three major fatigue mechanisms have been discussed: (i) $V_O$ charge trapping (extrinsic fatigue). Under repeated uni-directional electrical cycling, $V_O$ located near the electrode/$Hf_xZr_{1-x}O_2$ interfaces can be charged. The accumulation of these charged defects produces an additional $E_i$ aligned with the external electric field. $E_i$ lowers the barrier for switching into the field-favored polarization state ($P_{\downarrow\uparrow}\rightarrow P_{\downarrow\downarrow}$) while weakly affecting the reverse process, leading to an asymmetric shrinkage of the lower branch of the AFE half-loop and an apparent loss of switchable polarization. (ii) $V_O$-mediated AFE to FE phase transition (PT) (intrinsic fatigue). The electrical cycling drives redistribution of $V_O$ within the films. When $V_O$ migrate into specific lattice sites, they could promote local AFE grains transforming into FE phase. (iii) $V_O$ localization (intrinsic fatigue). First-principles nudged elastic band (NEB) calculations show that configurations with $V_O$ at tetra-coordinated (IV-O) sites exhibit substantially higher polarization switching barriers (~2.4 eV) than configurations with $V_O$ at tri-coordinated (III-O) sites (~1.8 eV), suppressing the achievable polarization switching and contributing to intrinsic fatigue.

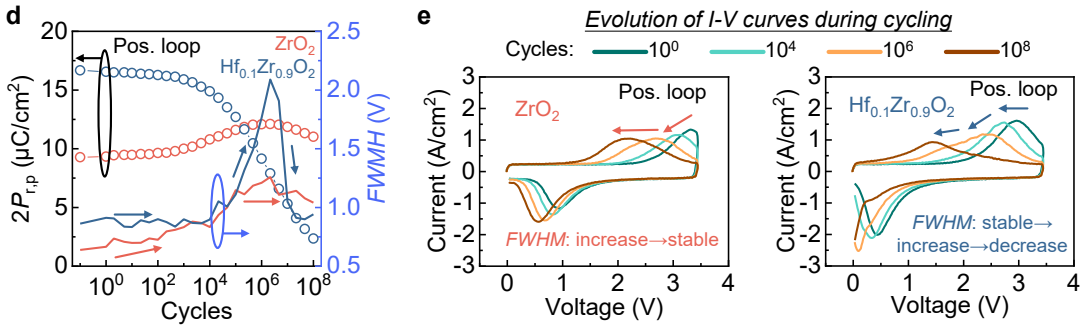


**Fig. 2 d**, Evolution of $2P_{s,p}$ extracted from uni-PUND measurements, and *FWHM* derived from *I–V* measurements for $ZrO_2$ and $Hf_{0.1}Zr_{0.9}O_2$ capacitors under +3.5 V, 200 kHz uni-directional cycling. **e**, Evolution of *I–V* curves for $ZrO_2$ and $Hf_{0.1}Zr_{0.9}O_2$ capacitors during uni-directional $10^8$ cycles, with the trends of $E_c$ and *FWHM* indicated by arrows and annotations. Changes in *FWHM* suggest the redistribution of $V_O$.

**Fig. 4c of Ref. [4]** presents a comparative summary of the three identified fatigue mechanisms as a function of Hf concentration in $Hf_xZr_{1-x}O_2$. The figure clearly illustrates that at lower Hf doping (e.g., HZO-10), extrinsic fatigue dominates, leading to significant charge trapping. In contrast, as the Hf concentration increases (e.g., HZO-20), intrinsic fatigue mechanisms become increasingly dominant. Specifically, higher Hf doping promotes $V_O$ localization at IV-O sites, which raises the switching barrier and impedes polarization switching. Additionally, the AFE to FE PT becomes more pronounced under high Hf concentration, further contributing to intrinsic fatigue. This trend highlights a clear shift from extrinsic to intrinsic fatigue mechanisms with increasing Hf doping.

The different fatigue behaviors observed between $ZrO_2$ and $Hf_{0.1}Zr_{0.9}O_2$ are primarily governed by the evolution of $V_O$ distribution, which are strongly influenced by the presence of Hf. In pure $ZrO_2$, where no Hf is introduced, $V_O$ tend to be charged during electrical cycling, resulting in a dominant extrinsic fatigue, characterized by the shift of *I–V* curves with the limited change in the shapes of the curves. In contrast, in $Hf_{0.1}Zr_{0.9}O_2$, the introduction of Hf enhances the intrinsic fatigue. Specifically, Hf incorporation facilitates partial localization of $V_O$ within the lattice and initiates AFE to FE PT, both of which contribute to intrinsic fatigue, and significantly change the shapes of the *I–V* curves (**Fig. 2e**).

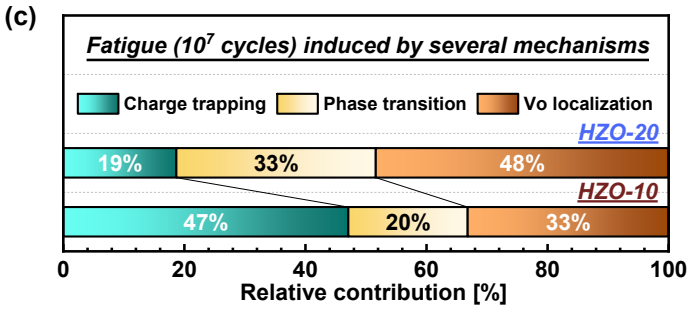


**Fig. 4. (Ref. [4]) c**, Summary of fatigue caused by several mechanisms[4].

**Reference (Response Letter)**

4. Qian, H. et al. Dynamic evolution of oxygen vacancies during cycling in antiferroelectric $Hf_xZr_{1-x}O_2$. *Applied Physics Letters* **124**, 243508 (2024).

According to the reviewer's comment, we have added some sentences to explain the different fatigue behavior of $ZrO_2$ and $Hf_{0.1}Zr_{0.9}O_2$ in the revised manuscript. **The revised sections are as follows.**

## Electrical characteristics of $ZrO_2$-based AFE capacitors

The comparison of $2P_{s,p}$ and *FWHM* evolutions between the $ZrO_2$ and $Hf_{0.1}Zr_{0.9}O_2$ capacitors during Pos. cycling with 3.5 V at 200 kHz is exhibited in Fig. 2d. The $ZrO_2$ capacitor shows wake-up effect with *FWHM* increasing until $2\times10^6$ cycles, then fatigue occurs with the stable *FWHM*. While the $Hf_{0.1}Zr_{0.9}O_2$ capacitor skips the wake-up process and begins fatigue after $5\times10^3$ cycles with *FWHM* first increasing and then decreasing. Fig. 2e shows the evolution of *I*–*V* curves with $10^8$ cycles for the $ZrO_2$ and $Hf_{0.1}Zr_{0.9}O_2$ capacitors. Note that the changes in *FWHM*, including increase and decrease, indicate the redistribution of $V_O$[16,17]. During the cycling process, the stable *FWHM* with the shifted *I*–*V* curve means that charge trapping occurs in the capacitor, without the redistribution of $V_O$, which may be the leading fatigue mechanism in $ZrO_2$ with $10^8$ cycles. While the fatigue in $Hf_{0.1}Zr_{0.9}O_2$ may be induced by the coupling of $V_O$ charge trapping and redistribution. The different fatigue behaviors observed between $ZrO_2$ and $Hf_{0.1}Zr_{0.9}O_2$ are strongly influenced by the presence of Hf. In pure $ZrO_2$, where no Hf is introduced, $V_O$ tend to be charged during electrical cycling, characterized by the shift of *I*–*V* curves with the limited change in the shapes of the curves. In contrast, in $Hf_{0.1}Zr_{0.9}O_2$, the introduction of Hf incorporation facilitates partial localization of $V_O$ within the lattice and initiates AFE to FE PT, contributing to the significant change in the shapes of the *I*–*V* curves.

**Comment 3:** Fig. 3a indicates shallow and deep fatigue, where the distinction is based on whether the polarization is completely recoverable. The concepts of intrinsic and extrinsic fatigue were also introduced, suggesting that only extrinsic fatigue is fully recoverable. Does the fatigue mechanism analysis for $ZrO_2$ show direct evidence indicating that extrinsic factors dominate to support this recovery behavior?

**Response:** We sincerely appreciate the reviewer's insightful comment regarding fatigue mechanisms. By analyzing the evolution of charge-voltage (*Q*–*V*) and *I*–*V* curves during electrical cycling, it is possible to directly identify the dominant physical mechanism in the fatigue process. As illustrated in **Fig. 4b of Ref. [4]**, extrinsic and intrinsic fatigue affect *Q*–*V* curves differently. Extrinsic fatigue primarily causes the shrinking of the *Q*–*V* curve's lower branch due to the accelerated polarization switching from the $P_{\downarrow\uparrow}$ to $P_{\downarrow\downarrow}$ state, while intrinsic fatigue leads to a reduction in the maximum *Q* value ($Q_{max}$). Additionally, two intrinsic fatigue

mechanisms often occur simultaneously since both involve $V_O$ migration.

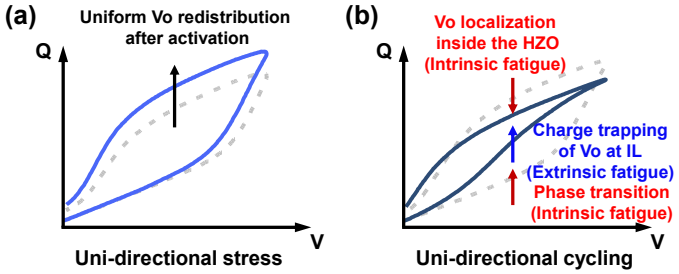


**Fig. 4 (Ref. [4]) a,** Evolution of $Q$–$V$ curves during activation under uni-directional stress. **b,** Evolution of $Q$–$V$ curves during fatigue process under uni-directional cycling.

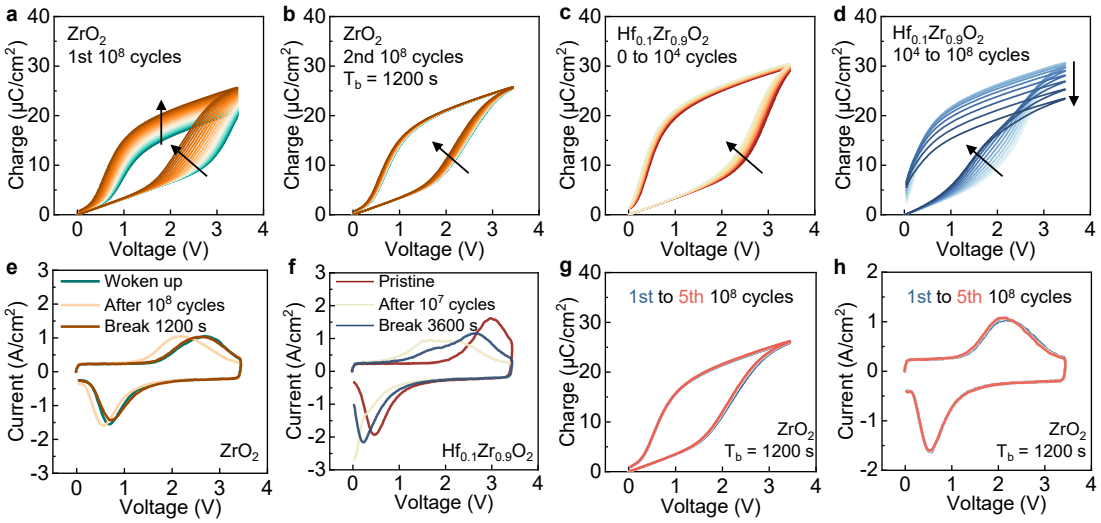


**Fig. R1 Evolutions of the $Q$–$V$ curves for $ZrO_2$ and $Hf_{0.1}Zr_{0.9}O_2$ capacitors. a**, Evolution of the $Q$–$V$ curves during the 1st $10^8$ electrical cycles for $ZrO_2$ capacitors. **b**, Evolution of the $Q$–$V$ curves during the 2nd $10^8$ electrical cycles after SSR process with $T_b$ = 1200 s for $ZrO_2$ capacitors. **c**, Evolution of the $Q$–$V$ curves during the 0 to $10^4$ electrical cycles for $Hf_{0.1}Zr_{0.9}O_2$ capacitors. **d**, Evolution of the $Q$–$V$ curves during the $10^4$ to $10^8$ electrical cycles for $Hf_{0.1}Zr_{0.9}O_2$ capacitors. **e**,f, $I$–$V$ curves of $ZrO_2$ and $Hf_{0.1}Zr_{0.9}O_2$ capacitors in the states before cycling, after cycling, and after SSR. **g,h,** $P$–$V$ and $I$–$V$ curves of 1st to 5th $10^8$ electrical cycles for $ZrO_2$ capacitors.

According to this feature, we analyzed the $Q$–$V$ curve evolution of $ZrO_2$ and $Hf_{0.1}Zr_{0.9}O_2$ capacitors under electrical cycling. For pristine $ZrO_2$ capacitors, the wake-up effect causes the entire $Q$–$V$ curve to shift upward during early cycles, making it difficult to observe fatigue-related changes (**Fig. R1a**). To overcome this challenge, we analyzed $ZrO_2$ capacitors after undergoing SSR with 1200 s break. This approach is justified by the observation that the $2P_{s,p}$ degradation during five consecutive sets of $10^8$ cycles (1st to 5th $10^8$ cycles) remains consistent, as shown in the **Extended Data Fig. 3**, indicating that the fatigue mechanism does not change. As shown in **Fig. R1b**, during the 2th $10^8$ cycles, the shrinking of the $Q$–$V$ curve's lower branch provides direct evidence that extrinsic fatigue is the dominant mechanism. In the case of $Hf_{0.1}Zr_{0.9}O_2$, a similar extrinsic fatigue dominated stage can also be observed. **Fig. R1c** illustrates the $Q$–$V$ curve evolution during the initial $10^4$ cycles, where the shrinking of the $Q$–$V$

curve's lower branch indicates extrinsic fatigue, corresponding to the recovery behavior shown in **Fig. 4a**, where the $2P_{s,p}$ fatigue is totally recoverable at low cycle numbers ($<10^4$). As shown in **Fig. R1d**, with the number of cycles increases to $10^8$, the $Q$–$V$ curve begins to exhibit a reduction in the $Q_{max}$, indicating the onset of intrinsic fatigue, which gradually becomes dominant. At this stage, the $2P_{s,p}$ fatigue becomes partially recoverable. Based on this trend, $ZrO_2$ capacitors under extended cycling (e.g., $10^{11}$ or $10^{12}$ cycles) would likely begin to exhibit intrinsic fatigue dominated stage, resulting in partial recovery of $2P_{s,p}$ fatigue.

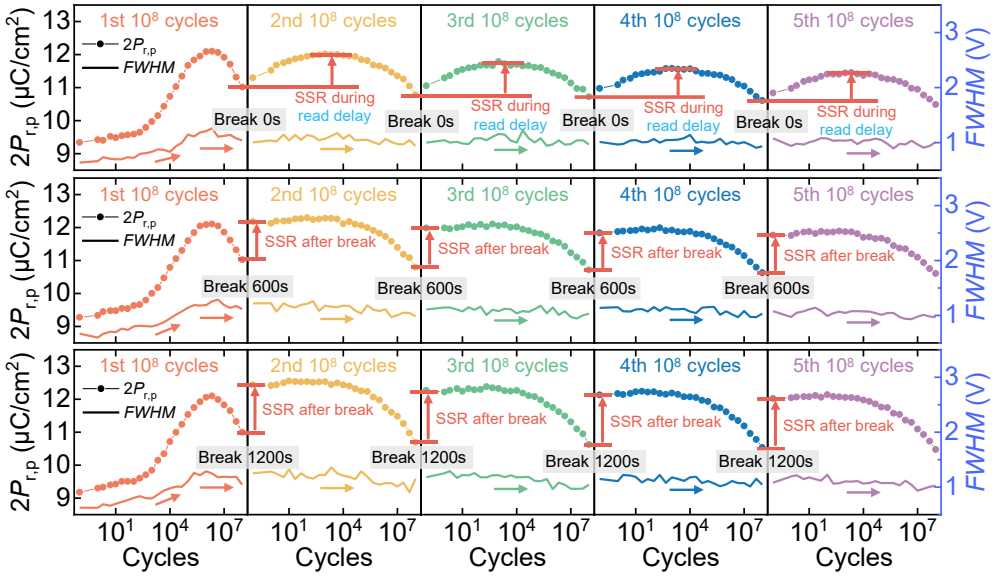


**Extended Data Fig. 3** The evolutions of $2P_{s,p}$ and the corresponding *FWHM* during continuous four SSR processes in $ZrO_2$ capacitors, with the $T_b$ set as 0/600/1200 s.

The comparison of $I$–$V$ curves under fatigue and recovery states provides additional evidence for the dominance of extrinsic mechanisms in recoverable $2P_{s,p}$ fatigue. In **Fig. R1e**, for $ZrO_2$ capacitors, the $I$–$V$ curve after SSR with 1200 s break closely overlaps with the woken up $I$–$V$ curve. In contrast, for $Hf_{0.1}Zr_{0.9}O_2$ capacitors, the $I$–$V$ curve after recovery does not fully overlap with the pristine $I$–$V$ curve (**Fig. R1f**), suggesting that intrinsic fatigue has occurred. Furthermore, for $ZrO_2$ capacitors, the $Q$–$V$ and $I$–$V$ curves after the 1st to 5th $10^8$ cycles (with $T_b$ = 1200 s between adjacent $10^8$ cycles) remain nearly identical, providing direct evidence that intrinsic fatigue does not occur in these cases.

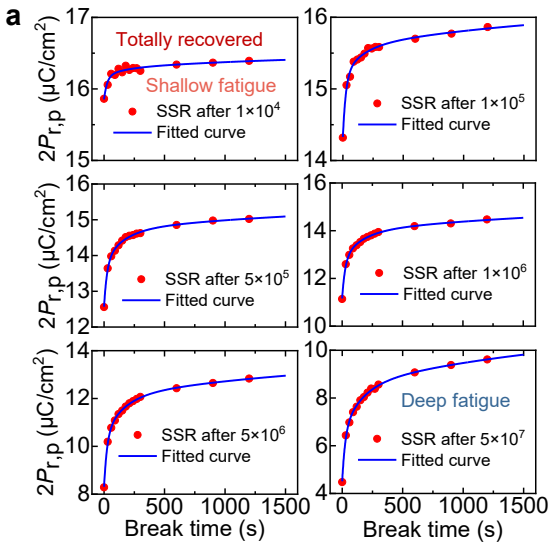


**Fig. 4 a**, Experimental and fitted curves of the SSR processes in $Hf_{0.1}Zr_{0.9}O_2$ capacitors after different fatigue cycles, using the fixed τ parameters extracted from Fig. 3g. The specific fatigue cycles are $1\times10^4$, $1\times10^5$, $5\times10^5$, $1\times10^6$, $5\times10^6$ and $5\times10^7$, respectively.

## Reference (Response Letter)

4. Qian, H. et al. Dynamic evolution of oxygen vacancies during cycling in antiferroelectric $Hf_xZr_{1-x}O_2$. *Applied Physics Letters* **124**, 243508 (2024).

According to the reviewer's comment, we have added **Fig. R1** as **Extended Data Fig. 4** in the revised manuscript to further analyze the fatigue mechanism of $ZrO_2$. **The revised sections are as follows.**

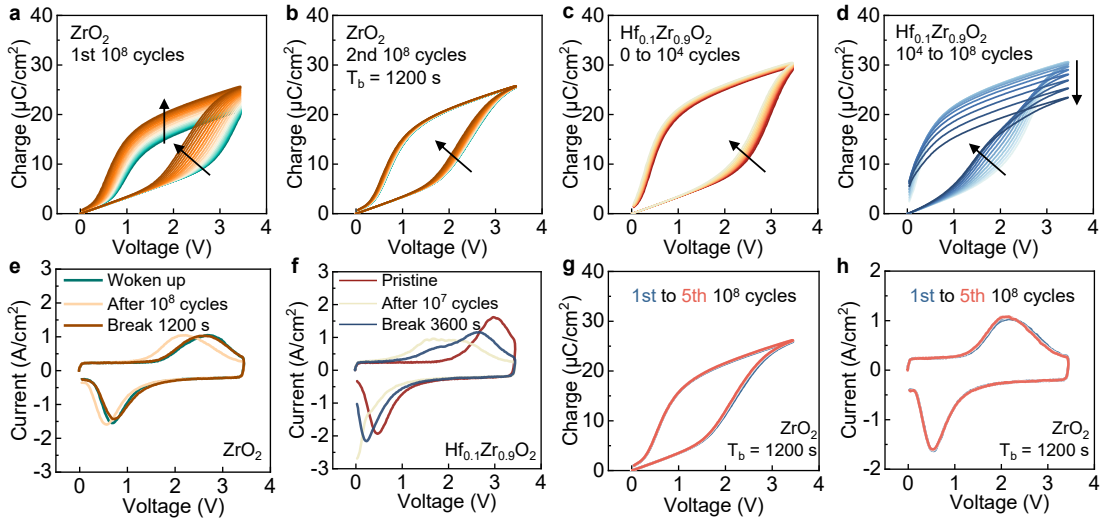


**Extended Data Fig. 4 Evolutions of the *Q–V* curves for $ZrO_2$ and $Hf_{0.1}Zr_{0.9}O_2$ capacitors. a**, Evolution of the *Q–V* curves during the 1st $10^8$ electrical cycles for $ZrO_2$ capacitors. **b**, Evolution of the *Q–V* curves during the 2nd $10^8$ electrical cycles after SSR process with $T_b$ = 1200 s for $ZrO_2$ capacitors. **c**, Evolution of the *Q–V* curves during the 0 to $10^4$ electrical cycles for $Hf_{0.1}Zr_{0.9}O_2$ capacitors. **d**, Evolution of the *Q–V* curves during the $10^4$ to $10^8$ electrical cycles for $Hf_{0.1}Zr_{0.9}O_2$

capacitors. **e**,f, *I*−*V* curves of $ZrO_2$ and $Hf_{0.1}Zr_{0.9}O_2$ capacitors in the states before cycling, after cycling, and after SSR. **g,h,** *P*−*V* and *I*−*V* curves of 1st to 5th $10^8$ electrical cycles for $ZrO_2$ capacitors.

**Comment 4:** In Fig. 3c of cited reference 27, there are three $V_O$ positions for consideration; however, Fig. 4c only assumes two $V_O$ positions. Please comment on these two simulations.

**Response:** The difference in setup between $V_O$ configurations considered in **Fig. 3c of Ref. [4]** (cited reference 27 in the main manuscript) and **Fig. 4c** of the main manuscript arises from the fundamentally distinct computational motivations and modeling strategies in the two works.

The **Ref. [4]** focuses on the polarization switching dynamics in Hf-doped $ZrO_2$, specifically the energy barriers associated with the antiparallel to parallel polarization configurations transition pathways. In this context, the role of $V_O$ is highly site-specific, particularly for $V_O$ located at both III-O sites (III-$V_{OA}$ and III-$V_{OC}$) neighboring IV-O sites, which experience distinct structural environments during polarization switching processes. To put it more intuitively, the difference between the two types of III-O sites lies in whether they reside on the side of polarization switching. As a result, that study considers three nonequivalent $V_O$ configurations to rigorously resolve their respective effects on the intermediate states and energy barriers.

In this work, our primary aim is to evaluate the electronic structure of AFE $ZrO_2$ in its antipolar ground state, with particular emphasis on the energetic position of defect-induced states within the band gap. To this end, we employ a centrosymmetric pure $ZrO_2$ supercell representing the antiparallel polarization configuration. Here, since polarization switching is not considered, the two selected $V_O$ positions (one III-O site and one IV-O site) are sufficient to capture the representative variation in local environments and corresponding defect level distributions, owing to the presence of inversion symmetry. This approach allows us to efficiently characterize the electronic impact of $V_O$ without considering additional symmetry-breaking perturbations.

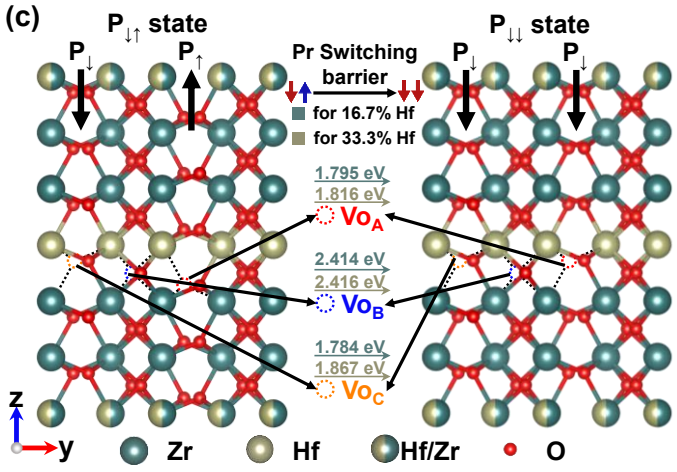


**Fig. 3. (Ref. [4]) c**, Schematic illustration of 16.7/33.3% Hf-doped AFE and FE HZO supercells. The $Vo_A$ (red) and $Vo_C$ (orange) represent for the III-Vo configurations, and the $Vo_B$ (blue) represents for the IV-Vo configuration.

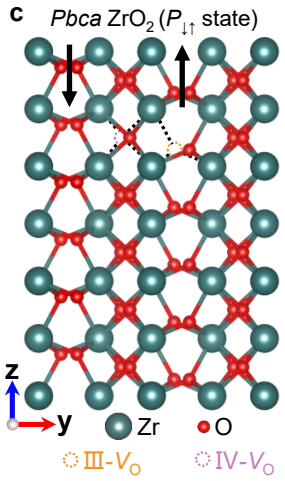


**Fig. 4 c**, Schematic diagram of 1×1×3 *Pbca* $ZrO_2$ supercell, highlighting the locations of neutral III-$V_O$ and IV-$V_O$, marked by orange and purple dashed circles, respectively.

**Reference (Response Letter)**

4. Qian, H. et al. Dynamic evolution of oxygen vacancies during cycling in antiferroelectric $Hf_xZr_{1-x}O_2$. *Applied Physics Letters* **124**, 243508 (2024).

According to the reviewer's comment, we have added some sentences to describe the modeling strategies of $V_O$ configurations in the revised manuscript. **The revised sections are as follows.**

## Development of three level traps model

Furthermore, the three level traps model can be supported by density functional theory (DFT) calculations. Here, 1×1×3 *Pbca* $ZrO_2$ supercells are constructed to theoretically calculate the trap energy level distributions, as shown in Fig. 4c. The O-deficient configurations are constructed by removing one O atom from the supercells, with the orange and purple dashed circles marking the localizations of neutral III-$V_O$ and IV-$V_O$, respectively. Considering the primary aim of evaluating the electronic structure of AFE $ZrO_2$ in its antipolar ground state, the two selected $V_O$ positions (one III-O site and one IV-O site) are sufficient to capture the representative variation in local environments and corresponding defect level distributions, owing to the presence of inversion symmetry. Then, the bulk electronic band structure calculations of supercells with different O-deficient configurations were performed. Fig. 4d and 4e plot the calculated energy-momentum ($E$–$k$) dispersion and density of states (DOS) of $ZrO_2$ supercells with neutral III-$V_O$, IV-$V_O$ and without $V_O$. The band gap between valance band maximum and conduction band minimum is around 3.622 eV, and the localizations of defect energy levels for neutral III-$V_O$ and IV-$V_O$ are confirmed. The formation energies for $V_O$ could be theoretically estimated by:

**Comment 5:** For Fig. 5c, if I understand correctly, a zero-second break time implies that no recovery method is applied. Why is endurance also improved? Please comment on the possible reasons.

**Response:** We thank the reviewer for the thoughtful question. The 0 s break time condition in **Fig. 5c and 5d** is intended to represent continuous cycling without any intentional recovery period. In practice, while we employ Keysight B1530A Waveform Generator to perform the electrical measurements, a brief delay is inherently introduced by the measurement system itself. Specifically, during the automatic switching between the cycling and readout modules within the test sequence, a finite recovery time approximately 0.8 seconds is inevitably incurred. This delay, although not user-defined, can provide partial recovery for the device, thereby contributing to the observed endurance improvement even under nominal 0 s conditions.

We acknowledge that this residual delay may not strictly correspond to an idealized zero-recovery scenario, but it is a practical limitation of the measurement setup. Nevertheless, the trend in endurance with increasing break time remains valid, and the observed endurance enhancement under apparent 0 s conditions can be reasonably attributed to this unavoidable but minimal relaxation period.

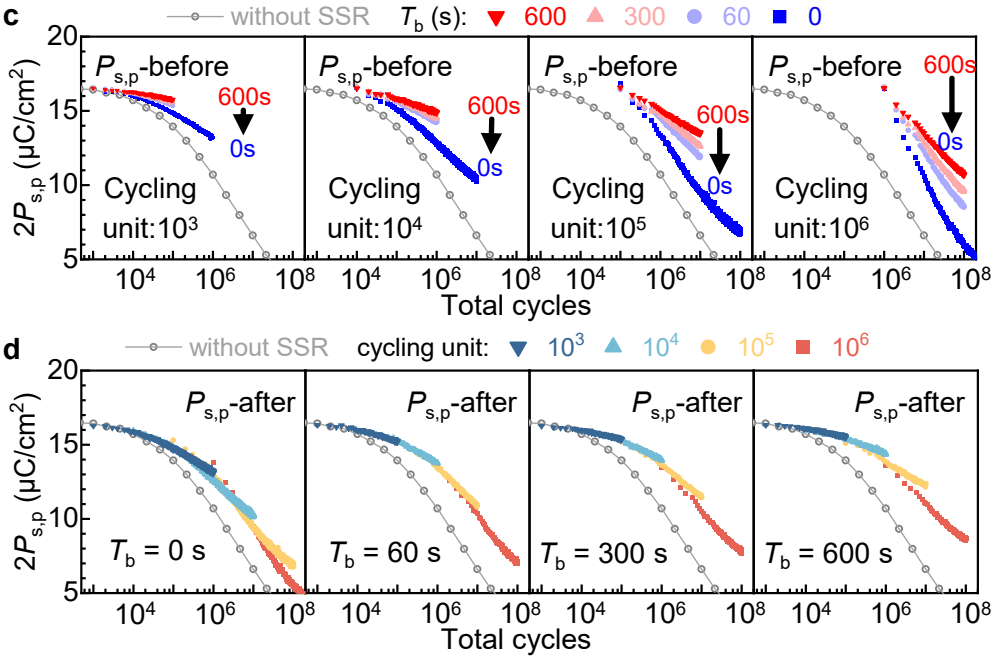


**Fig. 5 c**, Comparison of $P_{s,p}$-before and **d**, $P_{s,p}$-after under different $T_b$ and cycling unit. Both of increasing $T_b$ and decreasing cycling unit can improve endurance.

According to the reviewer's comment, we have added some sentences to describe the modeling strategies of $V_O$ configurations in the revised manuscript. **The revised sections are as follows.**

## Optimization of cycling unit and $T_b$ combination

It is worth considering how to effectively apply SSR to further improve the endurance of devices. Therefore, the abilities of SSR with various combinations of different cycling unit and $T_b$ in $Hf_{0.1}Zr_{0.9}O_2$ capacitors are investigated, in which the cycling unit is defined as several continuous electrical cycles. Fig. 5b shows the measurement scheme, in which the repeat unit is defined as the combination of $T_b$, read before cycling ($P_{s,p}$-before), cycling unit and read after cycling ($P_{s,p}$-after). Different degrees of endurance improvement are realized by applying various combinations of cycling unit ($10^3/10^4/10^5/10^6$ cycles) and $T_b$ (0/60/300/600 s), and the fatigue without SSR is also plotted as a reference. Fig. 5c and 5d show the comparison of $P_{s,p}$-before and $P_{s,p}$-after under different $T_b$ and cycling unit. For fixed cycling unit, the SSR effect is greatly enhanced with increasing $T_b$, shown in Fig. 5c. This means that during the cycling, the more charges trapped in the $ZrO_2$-based AFE devices are released by SSR, thus preventing deep fatigue, the more effective endurance can be enhanced. And for fixed $T_b$, the endurance can be improved with decreasing cycling unit, shown in Fig. 5d. This means that during a single cycling unit, a lower accumulation of trapped charges may enhance the efficacy of SSR in enhancing endurance. Notably, while employing Keysight B1530A Waveform Generator to perform these electrical measurements, a brief delay is inherently introduced by the measurement system itself. Specifically, during the automatic switching between the cycling and readout modules within the test sequence, a finite recovery time approximately 0.8 seconds is inevitably incurred. This delay, although not user-defined, can provide partial recovery for the device, thereby contributing to the observed endurance improvement even under nominal $T_b$ = 0 s conditions. Finally, it has been demonstrated that avoiding deep charge trapping by SSR is effective to the endurance improvement of the $ZrO_2$-based AFE device.

**Comment 6:** Regarding endurance performance, the cycling data present fewer than $1\times10^9$ cycles. What is the maximum number of cycles achievable using the proposed SSR approach? Is there any experimental data to support potential endurance beyond $10^9$ cycles?

**Response:** As shown in **Fig. R2**, through careful analysis of the cycling data presented in **Fig. 5d**, we have performed linear fitting of the endurance performance for the $T_b$ = 600 s, cycling unit = $10^5/10^6$ SSR combinations and extrapolated the results to $10^9$ cycles. This analysis reveals that even under the not that strict SSR optimization parameters ($T_b$ = 600 s, cycling unit = $10^5$), the $Hf_{0.1}Zr_{0.9}O_2$ capacitors maintain a robust $2P_{r,p}$ value of 9.18 μC/cm$^2$ at $10^9$ cycles.
Importantly, our experimental data demonstrates that $Hf_{0.1}Zr_{0.9}O_2$ capacitors subjected to consecutive $10^9$ electrical cycles show no signs of breakdown (gray curve in **Fig. R2**), confirming that the endurance limit indeed exceeds $10^9$ cycles with proper SSR implementation. This finding is particularly significant as it suggests that: (1) the SSR method remains effective at extremely high electrical cycles, and (2) the recovery process continues to mitigate fatigue damage even after prolonged operation. The sustained polarization values and absence of

breakdown at these extreme cycling conditions provide strong evidence for the long-term viability of our proposed SSR approach.

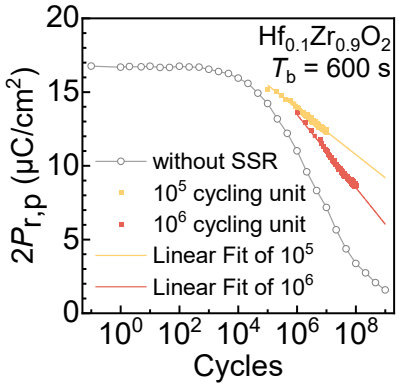


**Fig. R2** Comparison of the endurance performances between the experimental measured data within $10^9$ electrical cycles (gray curve) and the linear fitting for the $T_b$ = 600 s, cycling unit = $10^5$/$10^6$ SSR combinations by extrapolating the results in Fig. 5d to $10^9$ cycles.

According to the reviewer's comment, we have added **Fig. R2** as **Extended Data Fig. 5** in the revised manuscript to further analyze the fatigue mechanism of $ZrO_2$. **The revised sections are as follows.**

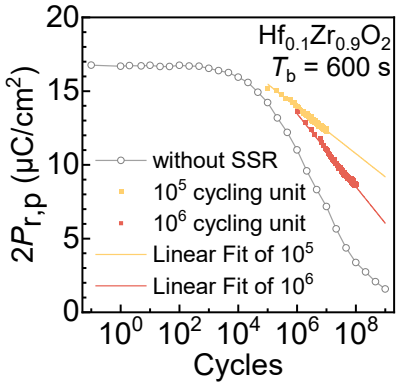


**Extended Data Fig. 5** Comparison of the endurance performances between the experimental measured data within $10^9$ electrical cycles (gray curve) and the linear fitting for the $T_b$ = 600 s, cycling unit = $10^5$/$10^6$ SSR combinations by extrapolating the results in Fig. 5d to $10^9$ cycles.

**Comment 7:** The proposed SSR implies that the waiting time for recovery is necessary. The recovery time makes the method unreliable and impractical for application.

**Response:** We sincerely thank the reviewer for highlighting this important issue. Indeed, the recovery time may affect applications with high real-time performance requirements. However, our proposed recovery strategy does not require the $ZrO_2$-based AFE devices to undergo the SSR process immediately after each write or read operation. The SSR is only triggered when

device monitoring indicates fatigue has exceeded a predefined threshold (e.g., >20% $2P_{s,p}$ degradation). This selective activation significantly reduces operational overhead, as most devices in a memory array requiring SSR infrequently during normal operation.

As demonstrated in **Fig. 4a**, we have conducted optimized measurements combining break time ($T_b$) and the number of single continuous cycles (cycling unit) for $Hf_{0.1}Zr_{0.9}O_2$ devices. It is worth noting that the endurance of $Hf_{0.1}Zr_{0.9}O_2$ is inherently much lower than $ZrO_2$ (line 91, **Fig. 2d**). The measurements in **Fig. 4a** are intended to show that even for devices with relatively poor initial endurance, the SSR method can significantly extend their endurance. When applied to $ZrO_2$ materials, the SSR method is expected to improve endurance by at least four orders of magnitude (to $>10^{12}$ cycles).

Additionally, future work will focus on exploring on-demand recovery strategies and material modifications (e.g., interface engineering) to further shorten the recovery time. Despite this limitation, the current SSR method holds unique value in applications where reliability is a top priority, such as aerospace electronics and medical devices. We are also actively working on system-level designs to minimize the impact of recovery time on practical applications.

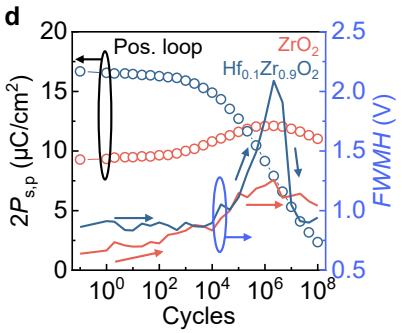


**Fig. 2 d**, Evolution of $2P_{s,p}$ extracted from uni-PUND measurements, and *FWHM* derived from *I–V* measurements for $ZrO_2$ and $Hf_{0.1}Zr_{0.9}O_2$ capacitors under +3.5 V, 200 kHz uni-directional cycling.

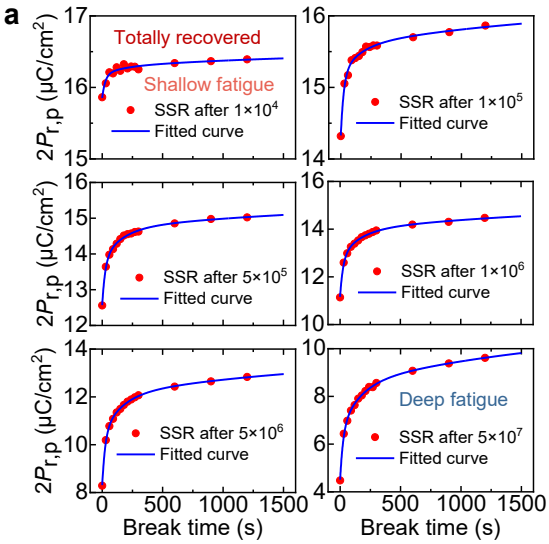


**Fig. 4 a**, Experimental and fitted curves of the SSR processes in $Hf_{0.1}Zr_{0.9}O_2$ capacitors after different fatigue cycles, using the fixed τ parameters extracted from Fig. 3g. The specific fatigue cycles are $1\times10^4$, $1\times10^5$, $5\times10^5$, $1\times10^6$, $5\times10^6$ and $5\times10^7$, respectively.

**Comment 8:** Benchmark comparison with other methods is suggested for readers to understand the merits and disadvantages.

**Response:** We would like to thank the reviewer for the suggestion. There is need to clarify that, to the best of our knowledge, there are currently limited studies focusing on recovery methods specifically for $ZrO_2$-based AFE devices. The most discussed approach in existing literature is Opposite Polarity Cycling Recovery (OPCR)[5], and we have included detailed comparisons between OPCR and our proposed SSR method in **Extended Data Fig. 2**.

The primary focus of this work is to establish the fundamental understanding of SSR methodology and its underlying physical mechanisms in $ZrO_2$ systems. While comprehensive benchmarking would certainly be valuable, the novelty of this field means that standardized comparison methods have not yet been established. We fully agree with the reviewer about the importance of comparative analysis and will include more systematic benchmarking in our future studies as more recovery methods emerge for $ZrO_2$-based devices.

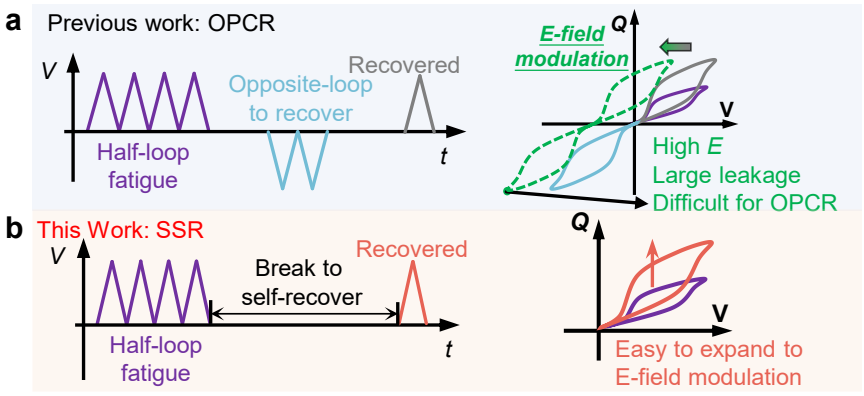


**Extended Data Fig. 2 Comparison between the OPCR and SSR recovery methods. a,** Schematic illustration of previously proposed OPCR method in ref. 20. The half-loop fatigue is recovered by applying opposite-loop pulses, leading to large leakage for the requirement of a high electric field, and limiting its practical applicability. **b**, Schematic illustration of the SSR method proposed in this work. Allowing the device to self-recover after a break period following half-loop fatigue, simplifying the recovery process.

**Reference (Response Letter)**

5. Hsiang, K.-Y. et al. Novel Opposite Polarity Cycling Recovery (OPCR) of $HfZrO_2$ Antiferroelectric-RAM with an Access Scheme Toward Unlimited Endurance. in *2022 International Electron Devices Meeting (IEDM)* 32.5.1-32.54 (IEEE, San Francisco, CA, USA, 2022).

## Reviewer: 2

Comments to the Author

This manuscript investigates the fatigue phenomenon observed in MIM capacitors utilizing $ZrO_2$-based AFE characteristics. It focuses on a method to recover the degraded $2P_{s,p}$ values caused by fatigue by introducing a break time between cycles, based on the conclusion drawn from the analysis of the fatigue mechanism—specifically, the $V_O$ charge trapping phenomenon. The manuscript also aims to elucidate the underlying mechanism of this recovery.

**Comment 1:** It seems necessary to include details about the device fabrication process. There is no mention of the precursors used for Hf and Zr deposition, the oxidant used during deposition, or the gases used during annealing. Since the ALD window can vary depending on the precursor, and the $V_O$ concentration—which is critical in this work—can significantly change depending on the type of oxidant, additional information on these points is required.

**Response:** We sincerely appreciate the reviewer's helpful suggestion. We would like to add more details about the device fabrication process in the **Methods of revised manuscript**. The fabrication of $ZrO_2/Hf_{0.1}Zr_{0.9}O_2$ AFE capacitors starts from silicon (Si) substrate. After conventional RCA wet clean, a 50 nm-thick TiN layer is deposited as bottom electrode (BE) on Si substrate by reactive sputtering. Then, the samples are loaded into the atomic layer deposition (ALD) chamber. Next, 10 nm $ZrO_2/Hf_{0.1}Zr_{0.9}O_2$ AFE film is in situ deposited via ALD using tetrakis-dimethylamino hafnium (TDMAHf) and tetrakis-dimethylamino zirconium (TDMAZr) as precursors, and $H_2O$ as oxidant at 250 ℃. The growth rates of $HfO_2$ and $ZrO_2$ are 0.71 and 0.67 Å/cycle, respectively. During the deposition of $Hf_{0.1}Zr_{0.9}O_2$ AFE film, $HfO_2$ cycles are uniformly inserted in $ZrO_2$ cycles, and one $HfO_2$ cycle followed by nine $ZrO_2$ cycles as a supercycle is employed. Subsequently, 50 nm-thick TiN is deposited by reactive sputtering and patterned for top electrode (TE). The size of characterized devices is 11304 $\mu m^2$. Finally, post-metallization annealing (PMA) at 500 ℃ for 30 s in $N_2$ atmosphere is performed to crystallize $ZrO_2/Hf_{0.1}Zr_{0.9}O_2$ films.

According to the reviewer's comment, we have added some sentences to describe the details about device fabrication process in the revised manuscript. **The revised sections are as follows.**

### Methods

#### Device Fabrication

The fabrication of $ZrO_2/Hf_{0.1}Zr_{0.9}O_2$ AFE capacitors starts from silicon (Si) substrate. After conventional RCA wet clean, a 50 nm-thick TiN layer is deposited as bottom electrode (BE) on Si substrate by reactive sputtering. Then, the samples are loaded into the atomic layer deposition (ALD)

chamber for 10 min $O_3$ treatment on TiN BE[23]. Next, 10 nm $ZrO_2$/$Hf_{0.1}Zr_{0.9}O_2$ AFE film is in situ deposited via ALD using tetrakis-dimethylamino hafnium (TDMAHf) and tetrakis-dimethylamino zirconium (TDMAZr) as precursors, and $H_2O$ as oxidant at 250 ℃. The growth rates of $HfO_2$ and $ZrO_2$ are 0.71 and 0.67 Å/cycle, respectively. During the deposition of $Hf_{0.1}Zr_{0.9}O_2$ AFE film, $HfO_2$ cycles are uniformly inserted in $ZrO_2$ cycles, and one $HfO_2$ cycle followed by nine $ZrO_2$ cycles as a supercycle is employed. Subsequently, 50 nm-thick TiN is deposited by reactive sputtering and patterned for top electrode (TE). The size of characterized devices is 11304 μm$^2$. Finally, post-metallization annealing (PMA) at 500 ℃ for 30 s in $N_2$ atmosphere is performed to crystallize $ZrO_2$/$Hf_{0.1}Zr_{0.9}O_2$ films.

**Comment 2:** The manuscript states that $ZrO_2$ undergoes fatigue with cycling, but recovers after a certain break period, with the $2P_{s,p}$ value returning to its initial peak level. While the similarity between the $2P_{s,p}$ values after fatigue and after the break period may suggest this indirectly, it would be beneficial to directly confirm whether intrinsic fatigue has occurred due to phase transition or $V_O$ localization in $ZrO_2$, as mentioned in the text, through intrinsic fatigue assessment.

**Response:** We sincerely appreciate the reviewer's insightful comment regarding fatigue mechanisms. By analyzing the evolution of charge-voltage ($Q$–$V$) and $I$–$V$ curves during electrical cycling, it is possible to directly identify the dominant physical mechanism in the fatigue process. As illustrated in **Fig. 4b of Ref. [4]**, extrinsic and intrinsic fatigue affect $Q$–$V$ curves differently. Extrinsic fatigue primarily causes the shrinking of the $Q$–$V$ curve's lower branch due to the accelerated polarization switching from the $P_{\downarrow\uparrow}$ to $P_{\downarrow\downarrow}$ state, while intrinsic fatigue leads to a reduction in the maximum $Q$ value ($Q_{max}$). Additionally, two intrinsic fatigue mechanisms often occur simultaneously since both involve $V_O$ migration.

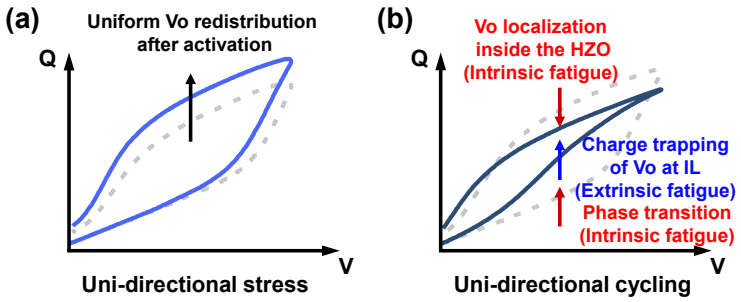


**Fig. 4 (Ref. [4]) a,** Evolution of $Q$–$V$ curves during activation under uni-directional stress. **b,** Evolution of $Q$–$V$ curves during fatigue process under uni-directional cycling.

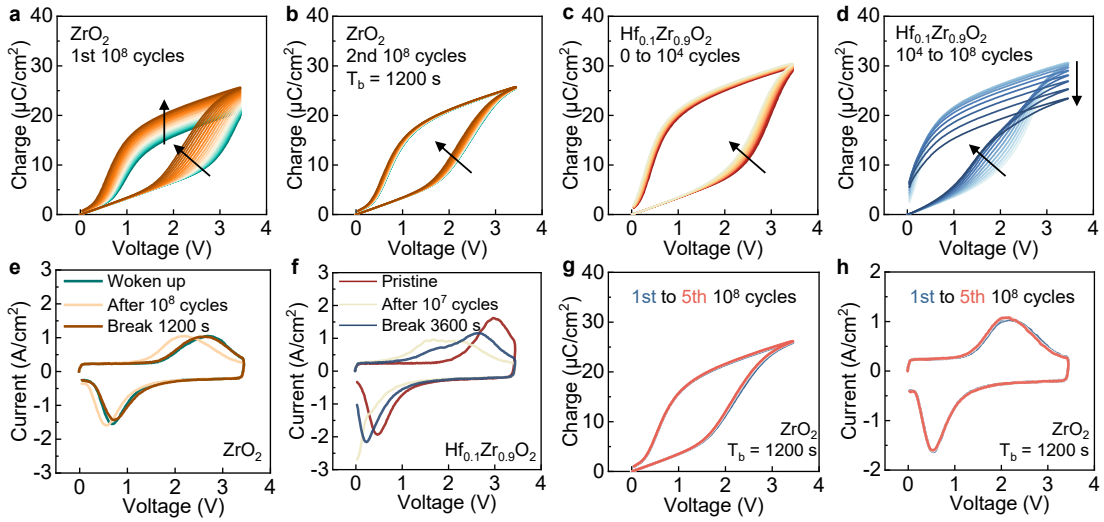


**Fig. R1 Evolutions of the *Q–V* curves for $ZrO_2$ and $Hf_{0.1}Zr_{0.9}O_2$ capacitors. a**, Evolution of the *Q–V* curves during the 1st $10^8$ electrical cycles for $ZrO_2$ capacitors. **b**, Evolution of the *Q–V* curves during the 2nd $10^8$ electrical cycles after SSR process with $T_b$ = 1200 s for $ZrO_2$ capacitors. **c**, Evolution of the *Q–V* curves during the 0 to $10^4$ electrical cycles for $Hf_{0.1}Zr_{0.9}O_2$ capacitors. **d**, Evolution of the *Q–V* curves during the $10^4$ to $10^8$ electrical cycles for $Hf_{0.1}Zr_{0.9}O_2$ capacitors. **e**,f, *I–V* curves of $ZrO_2$ and $Hf_{0.1}Zr_{0.9}O_2$ capacitors in the states before cycling, after cycling, and after SSR. **g,h,** *P–V* and *I–V* curves of 1st to 5th $10^8$ electrical cycles for $ZrO_2$ capacitors.

According to this feature, we analyzed the *Q–V* curve evolution of $ZrO_2$ and $Hf_{0.1}Zr_{0.9}O_2$ capacitors under electrical cycling. For pristine $ZrO_2$ capacitors, the wake-up effect causes the entire *Q–V* curve to shift upward during early cycles, making it difficult to observe fatigue-related changes (**Fig. R1a**). To overcome this challenge, we analyzed $ZrO_2$ capacitors after undergoing SSR with 1200 s break. This approach is justified by the observation that the $2P_{s,p}$ degradation during five consecutive sets of $10^8$ cycles (1st to 5th $10^8$ cycles) remains consistent, as shown in the **Extended Data Fig. 3**, indicating that the fatigue mechanism does not change. As shown in **Fig. R1b**, during the 2th $10^8$ cycles, the shrinking of the *Q–V* curve's lower branch provides direct evidence that extrinsic fatigue is the dominant mechanism. In the case of $Hf_{0.1}Zr_{0.9}O_2$, a similar extrinsic fatigue dominated stage can also be observed. **Fig. R1c** illustrates the *Q–V* curve evolution during the initial $10^4$ cycles, where the shrinking of the *Q–V* curve's lower branch indicates extrinsic fatigue, corresponding to the recovery behavior shown in **Fig. 4a**, where the $2P_{s,p}$ fatigue is totally recoverable at low cycle numbers ($<10^4$). As shown in **Fig. R1d**, with the number of cycles increases to $10^8$, the *Q–V* curve begins to exhibit a reduction in the $Q_{max}$, indicating the onset of intrinsic fatigue, which gradually becomes dominant. At this stage, the $2P_{s,p}$ fatigue becomes partially recoverable. Based on this trend, $ZrO_2$ capacitors under extended cycling (e.g., $10^{11}$ or $10^{12}$ cycles) would likely begin to exhibit intrinsic fatigue dominated stage, resulting in partial recovery of $2P_{s,p}$ fatigue.

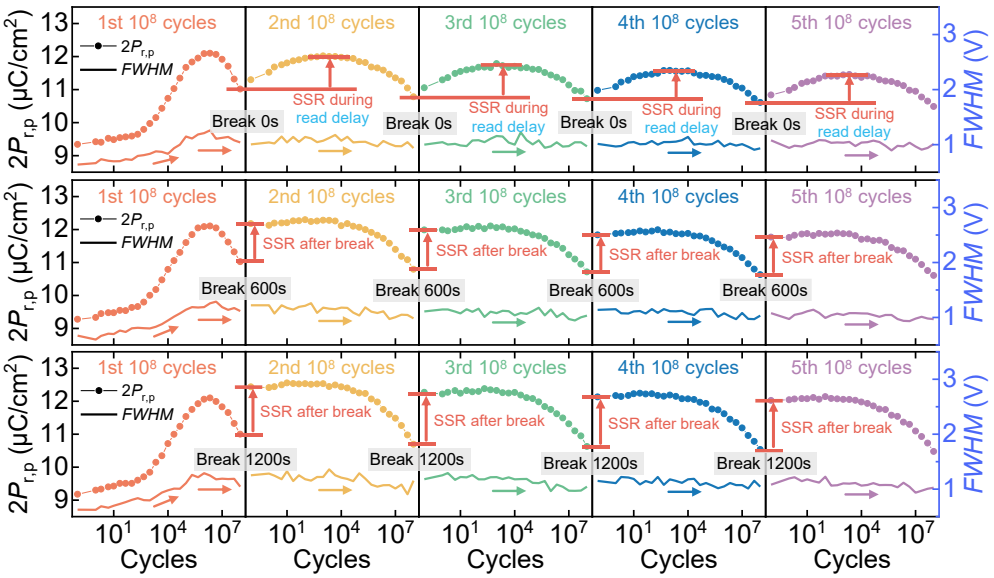


**Extended Data Fig. 3** The evolutions of $2P_{s,p}$ and the corresponding *FWHM* during continuous four SSR processes in $ZrO_2$ capacitors, with the $T_b$ set as 0/600/1200 s.

The comparison of *I–V* curves under fatigue and recovery states provides additional evidence for the dominance of extrinsic mechanisms in recoverable $2P_{s,p}$ fatigue. In **Fig. R1e**, for $ZrO_2$ capacitors, the *I–V* curve after SSR with 1200 s break closely overlaps with the woken up *I–V* curve. In contrast, for $Hf_{0.1}Zr_{0.9}O_2$ capacitors, the *I–V* curve after recovery does not fully overlap with the pristine *I–V* curve (**Fig. R1f**), suggesting that intrinsic fatigue has occurred. Furthermore, for $ZrO_2$ capacitors, the *Q–V* and *I–V* curves after the 1st to 5th $10^8$ cycles (with $T_b$ = 1200 s between adjacent $10^8$ cycles) remain nearly identical, providing direct evidence that intrinsic fatigue does not occur in these cases.

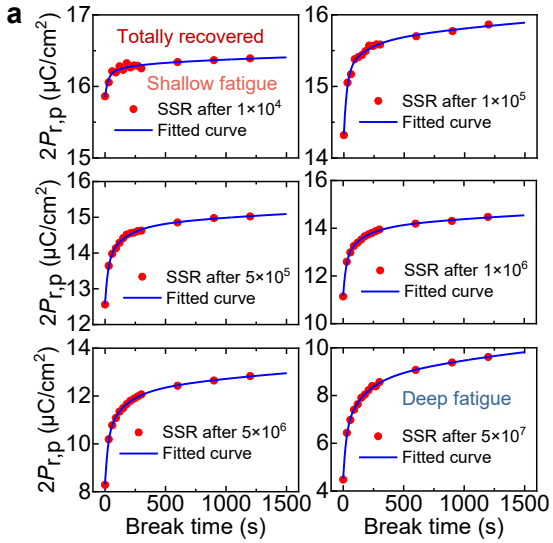


**Fig. 4 a**, Experimental and fitted curves of the SSR processes in $Hf_{0.1}Zr_{0.9}O_2$ capacitors after different fatigue cycles, using the fixed τ parameters extracted from Fig. 3g. The specific fatigue cycles are $1\times10^4$, $1\times10^5$, $5\times10^5$, $1\times10^6$, $5\times10^6$ and $5\times10^7$, respectively.

## Reference (Response Letter)

4. Qian, H. et al. Dynamic evolution of oxygen vacancies during cycling in antiferroelectric $Hf_xZr_{1-x}O_2$. *Applied Physics Letters* **124**, 243508 (2024).

According to the reviewer's comment, we have added **Fig. R1** as **Extended Data Fig. 4** in the revised manuscript to further analyze the fatigue mechanism of $ZrO_2$. **The revised sections are as follows.**

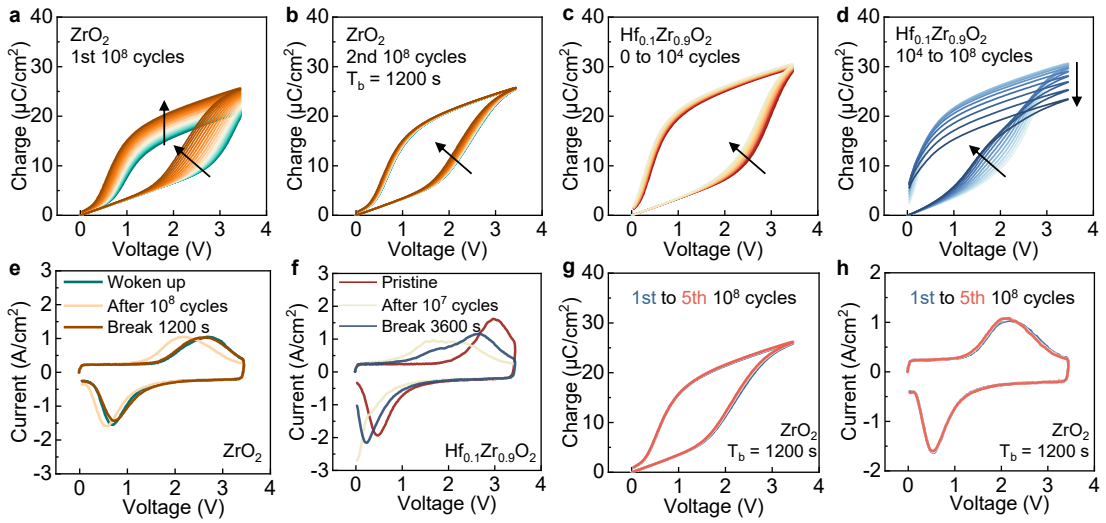


**Extended Data Fig. 4 Evolutions of the *Q–V* curves for $ZrO_2$ and $Hf_{0.1}Zr_{0.9}O_2$ capacitors. a**, Evolution of the *Q*–*V* curves during the 1st $10^8$ electrical cycles for $ZrO_2$ capacitors. **b**, Evolution of the *Q*–*V* curves during the 2nd $10^8$ electrical cycles after SSR process with $T_b$ = 1200 s for $ZrO_2$ capacitors. **c**, Evolution of the *Q*–*V* curves during the 0 to $10^4$ electrical cycles for $Hf_{0.1}Zr_{0.9}O_2$ capacitors. **d**, Evolution of the *Q*–*V* curves during the $10^4$ to $10^8$ electrical cycles for $Hf_{0.1}Zr_{0.9}O_2$ capacitors. **e**,f, *I*–*V* curves of $ZrO_2$ and $Hf_{0.1}Zr_{0.9}O_2$ capacitors in the states before cycling, after cycling, and after SSR. **g**,**h**, *P*–*V* and *I*–*V* curves of 1st to 5th $10^8$ electrical cycles for $ZrO_2$ capacitors.

**Comment 3:** In Fig. 3d, fatigue caused by charge trapping is shown to be recovered through the release process up to $10^8$ cycles. I am curious whether, if cycling continues to $10^9$ or $10^{10}$, the difference in $2P_{s,p}$ values between the with- and without-release cases increases further. Additionally, assuming breakdown does not occur, I would like to know whether the degree of extrinsic fatigue in HZO according to break time (as shown in Fig. 3f) aligns with the difference in $2P_{s,p}$ values with or without the release. If they do not align, could this indicate that different fatigue mechanisms may emerge depending on the number of cycles?

**Response:** We sincerely appreciate the reviewer's insightful comment regarding the long-term cycling behavior and fatigue mechanisms in $Hf_{0.1}Zr_{0.9}O_2$ capacitors. In response to this important query, we have conducted additional experiments extending the endurance measurements to $10^9$ cycles and carefully analyzed the recovery characteristics following the methodology established in **Fig. 3f**. As shown in **Fig. R3**, the newly measured experimental

data reveals that the recoverable $2P_{s,p}$ value (7.54 μC/cm$^2$) shows excellent agreement with the measured extrinsic fatigue (7.22 μC/cm$^2$), with only a minor 4.4% difference. This close correspondence strongly supports our original finding that the self-recoverable fatigue in $ZrO_2$-based AFE capacitors stems from extrinsic fatigue caused by $V_O$ charge trapping.

The alignment between these values at such high cycle counts provides compelling evidence that the break-time-dependent recovery process remains effective and that no significant new fatigue mechanisms emerge in this cycling regime. The minor deviation observed is not statistically significant and does not indicate any fundamental change in the underlying physics. Rather, it confirms the robustness of our proposed model where $V_O$ charge trapping can be effectively addressed through our SSR strategy. Finally, **we would like to incorporate these new findings into the revised manuscript as Extended Data Fig. 4**, which demonstrates that the SSR method maintains its effectiveness even under extreme cycling conditions, significantly strengthening the manuscript's conclusions regarding the long-term reliability of $ZrO_2$-based AFE devices.

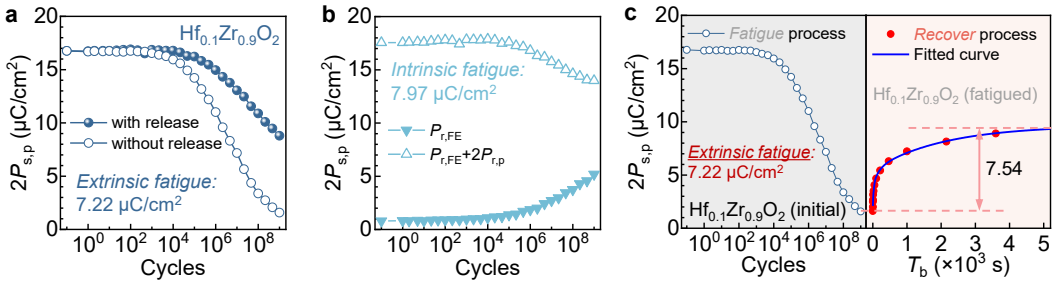


**Fig. R3 SSR characteristics and fatigue mechanisms analysis for $Hf_{0.1}Zr_{0.9}O_2$ capacitors with $10^9$ electrical cycles. a**, Endurance characteristics of the $Hf_{0.1}Zr_{0.9}O_2$ capacitors, with and without charge release. **b**, Evolution of $P_{r,FE}$ and $P_{r,FE}+2P_{s,p}$ read by PUND and uni-PUND methods during $10^9$ electrical cycling. **c**, Fatigue and recover processes of $Hf_{0.1}Zr_{0.9}O_2$ capacitors under $10^9$ cycles, with $T_b$ of 3600 s

According to the reviewer's comment, we have added **Fig. R3** as **Extended Data Fig. 6 and** some sentences to describe the details about the figure in the revised manuscript. **The revised sections are as follows.**

## Development of three level traps model

After figuring out the proportional contributions of different mechanisms in deep fatigue situation of $Hf_{0.1}Zr_{0.9}O_2$, further analysis of the SSR capability at varying $T_b$ is conducted, as illustrated by the red scatter plot in the right panel of Fig. 3f. The maximum self-recoverable polarization through SSR can be approximately estimated at 6.11 μC/cm$^2$ (the difference between the recovered $2P_{s,p}$ after SSR with a 3600 s break and the fatigued $2P_{s,p}$ after $10^7$ cycles), nearly equivalent to the magnitude of extrinsic fatigue extracted from Fig. 3d, which is 6.21 μC/cm$^2$ for $10^7$ cycles. This indicates that SSR can fully recover the extrinsic fatigue caused by charge trapping but has limited

effectiveness in recovering intrinsic fatigue. Additional experiments on $Hf_{0.1}Zr_{0.9}O_2$ capacitors have been conducted to extend the endurance measurements to $10^9$ cycles. As shown in Extended Data Fig. 6, it is revealed that the recoverable $2P_{s,p}$ value (7.54 μC/cm$^2$) shows excellent agreement with the measured extrinsic fatigue (7.22 μC/cm$^2$), with a minor 4.4% difference. The alignment between these values at such high cycle counts provides compelling evidence that the break-time-dependent SSR process remains effective and that no significant new fatigue mechanisms emerge in this cycling regime.

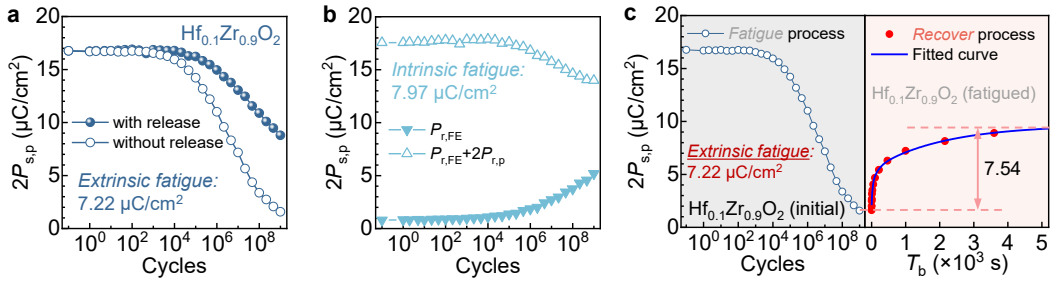


**Extended Data Fig. 6 SSR characteristics and fatigue mechanisms analysis for $Hf_{0.1}Zr_{0.9}O_2$ capacitors with $10^9$ electrical cycles. a**, Endurance characteristics of the $Hf_{0.1}Zr_{0.9}O_2$ capacitors, with and without charge release. **b**, Evolution of $P_{r,FE}$ and $P_{r,FE}+2P_{s,p}$ read by PUND and uni-PUND methods during $10^9$ electrical cycling. **c**, Fatigue and recover processes of $Hf_{0.1}Zr_{0.9}O_2$ capacitors under $10^9$ cycles, with $T_b$ of 3600 s

**Comment 4:** The schematic in Fig. 4g shows electrons being detrapped from $V_O$ during the recovery of extrinsic fatigue. It also depicts the electrons moving to relatively higher energy levels. I am curious whether this energy level difference is low enough to be overcome by thermal energy alone—i.e., if detrapping is possible simply through break time. Is there a quantitative value provided for this energy level difference?

**Response:** We sincerely appreciate the reviewer's insightful comment. The energy level differences associated with electron detrapping from $V_O$ during the self-recovery of extrinsic fatigue are indeed thermally surmountable through two key mechanisms: (1) The effective detrapping rate from deep traps (~1.0-1.2 eV) follows a Boltzmann distribution where a small but non-zero fraction of carriers ($\exp(-E_a/k_BT)$) can overcome the barrier at room temperature, especially given the high attempt frequency (~$10^{12}$ s$^{-1}$) in oxide materials, (2) the observed recovery of deep fatigue occurs over macroscopic timescales ($10^2$-$10^3$ s), allowing sufficient time for statistically rare thermal excitation events to accumulate. This is evidenced by our three-level trap model's excellent fit to the recovery kinetics (with $\tau_1$~24.85 s, $\tau_2$~159.86 s, $\tau_3$~2074.18 s) inherently accounts for thermally activated detrapping processes. Through Arrhenius analysis (assuming a typical phonon attempt frequency of $10^{12}$ s$^{-1}$), these time constants correspond to trap depths of ~0.6-1.0 eV, which are fully consistent with: (1) the thermal energy available at room temperature ($k_BT \approx 0.026$ eV, considering the Boltzmann

distribution of carrier energies), and (2) calculated $V_O$ energy levels in $ZrO_2$ systems.
Our theoretical framework supported by the quantitative agreement between modeled and observed recovery behavior already establishes that the detrapping occurs through thermal activation. The referenced work by Chen & Xu (J. Appl. Phys. **106**, 123707 (2009), Ref. [29]) further validates this interpretation for similar dielectric materials. We believe the current analysis sufficiently demonstrates that the energy level differences can be overcome by thermal energy during break time, which is the key physical mechanism underlying the observed recovery phenomenon.

According to the reviewer's comment, we have added some sentences to describe the details about the thermally activated detrapping processes in the revised manuscript. **The revised sections are as follows.**

### Development of three level traps model

The calculated formation energies of the different charged $V_O$ as a function of $\mu_e$ are illustrated in Fig. 4f, and three transition levels are confirmed as $E_{III}^{2+/0}$, $E_{III}^{0/2-}$ and $E_{IV}^{2+/0}$, indicating $V_O$ are more likely to be charged at three trap energy levels during cycling, which are named as $E_{D-1}^{2+}$, $E_{D-2}^{2+}$ and $E_{D-3}^{2-}$. Assuming that these three trap energy levels are all above the middle of band gap, and their relative positions are schematically illustrated in Fig. 4g. Possible $V_O$ detrapping routes for $E_{D-1}^{2+}$ are: (i) electrons transition from conduction band ($E_c$), (iv) electrons transition from $E_{D-3}^{2-}$ to $E_{D-1}^{2+}$, (vii) tunneling electrons from electrodes; for $E_{D-2}^{2+}$ are: (ii) electrons transition from $E_c$, (v) electrons transition from $E_{D-3}^{2-}$ to $E_{D-2}^{2+}$, (vi) tunneling electrons from electrodes; for $E_{D-3}^{2-}$ are: (iii) electrons transition from $E_{D-3}^{2-}$ to $E_c$, (iv) electrons transition from $E_{D-3}^{2-}$ to $E_{D-1}^{2+}$, (v) electrons transition from $E_{D-3}^{2-}$ to $E_{D-2}^{2+}$. The energy level differences associated with electron detrapping from $V_O$ during the self-recovery of extrinsic fatigue are indeed thermally surmountable through two key mechanisms: (1) The effective detrapping rate from deep traps (~1.0-1.2 eV) follows a Boltzmann distribution where a small but non-zero fraction of carriers ($\exp(-E_a/k_BT)$) can overcome the barrier at room temperature, especially given the high attempt frequency (~$10^{12}$ $s^{-1}$) in oxide materials, (2) the observed recovery of deep fatigue occurs over macroscopic timescales ($10^2$-$10^3$ s), allowing sufficient time for statistically rare thermal excitation events to accumulate. This is evidenced by our three-level trap model's excellent fit to the recovery kinetics (with $\tau_1$~24.85 s, $\tau_2$~159.86 s, $\tau_3$~2074.18 s) inherently accounts for thermally activated detrapping processes.

## Reviewer: 3:

### I. General remarks:

In this article, the authors present a method they call static self-recovery (SSR) applied to $ZrO_2$-based films. The SSR method allows an increase in remanent polarization after fatigue. The authors also combined this method with Density Functional Theory (DFT) and a three level traps model to understand which mechanism for fatigue plays a major role in their endurance tests for TiN/$ZrO_2$ (10 nm)/TiN and TiN/$Hf_{0.1}Zr_{0.9}O_2$(10 nm)/TiN capacitors.

The article shows interesting results; however, the manuscript suffers from an overuse of emphatic language, such as “clearly” (e.g., “clearly prove”, “clearly elucidate”) and “precisely” (e.g., “precisely described”), which may overstate the strength of the evidence provided. For expert readers, the current level of physical and mathematical justifications does not always appear sufficiently robust to support such assertive phrasing. This may unintentionally undermine the credibility of the conclusions.

In addition, although the manuscript is visually well-prepared, with high-quality figures and formatting, the scientific depth and rigor of the analysis do not fully match the quality of the presentation. The physical and mathematical modeling, as well as the interpretation of the experimental results, would benefit from clearer justification and possibly stronger experimental backing.

Re: We sincerely appreciate the reviewer’s thoughtful evaluation of our manuscript. We acknowledge that the original wording may have occasionally overstated the strength of our evidence, and we have carefully revised the manuscript to adopt a more measured and precise language throughout. All instances of emphatic terms like “clearly” and “precisely” have been replaced with more objective phrasing that better reflects the actual evidence presented.

While we maintain that the SSR method represents a significant advancement for $ZrO_2$-based AFE devices, we have revised the discussion to more carefully qualify our conclusions and explicitly acknowledge alternative interpretations. The connection between experimental observations and theoretical models has been clarified, with particular attention to identifying the limitations of our current understanding. These revisions have been implemented throughout the manuscript while preserving the key findings about the effectiveness of the SSR approach.

We are grateful for the reviewer’s suggestions, which have helped us improve both the presentation and scientific rigor of our work. The revised manuscript provides a more balanced and thoroughly supported account of our research while maintaining its novel contributions to the field of antiferroelectric memory devices.

According to the reviewer’s suggestions, we have made some changes to reduce the use of emphatic language in the revised manuscript. **The revised sections are as follows.**

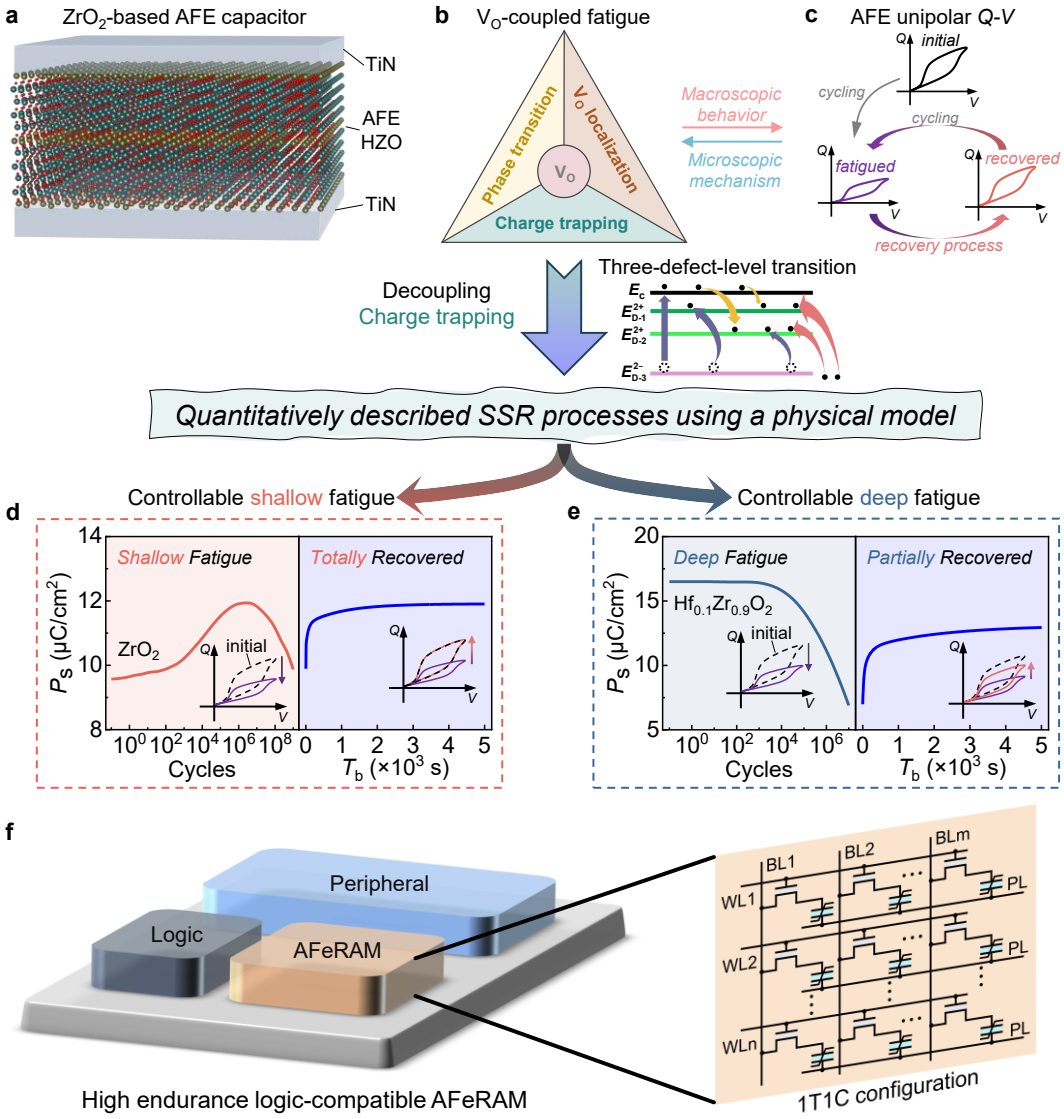


**Fig. 1 Proposal of the SSR method through elucidation of device fatigue mechanisms. a**, Schematic illustration of the AFE TiN/HZO/TiN capacitors. **b**, $V_O$-coupled fatigue mechanisms in $ZrO_2$-based AFE capacitors. **c**, Schematic diagram of the endurance enhancement in half-loop operated AFE devices via the recovery method. **d**,**e**, Development of predictable SSR method under (d) shallow and (e) deep fatigue situations in $ZrO_2$-based AFE capacitors by decoupling $V_O$ charge trapping. Left panels are fatigue processes, and the right panels are recovery processes. The $Q$–$V$ curves of initial states are illustrated by black dashed lines. **f**, Application of SSR method in high endurance logic-compatible AFeRAM utilizing half-loop operation with low operating voltage.

## Optimization of cycling unit and $T_b$ combination

It has been proved above that the shallow fatigue can be totally recovered by SSR, and for deep fatigue, the extrinsic $P_r$ degradation caused by charge trapping can also be totally recovered by SSR, while the intrinsic one cannot. Fig. 5a presents the schematic diagrams

illustrating $V_O$ evolutions during both shallow and deep fatigue conditions, as well as the corresponding SSR processes. These visualizations elucidate the mechanisms that lead to both totally and partially recovered polarization degradation.

## II. General questions:

**Comment 1:** For a DRAM, which is the targeted application in this paper, introducing a break time implies that no current should flow through the device for a relatively long duration. Do you think such a condition can realistically be achieved during the power-off phases of electronic devices? Are you confident this would not be detrimental to overall device reliability or performance? Even if the OPCR method described in Extended Data Fig.2 is not ideal, it has the advantage that it can be quickly implemented by an algorithm. The use of break time seems to limit the applicability of the SSR method to real devices.

**Response:** We sincerely appreciate the reviewer's important question regarding the concern about power-off phases of electronic devices. We would like to address this concern in greater detail. First, AFE capacitors can achieve non-volatile storage through electric field modulation as shown in Fig. 2a, primarily implemented by engineering work function differences between top and bottom electrodes. Second, we emphasize that the break time in our proposed SSR method does not necessarily require the entire AFeRAM to be fully powered off. Instead, the key requirement is to place the target device in an antiparallel polarization configuration. It should be emphasized that the SSR process is not required after every write/read operation. Our proposed SSR method activates only when significant fatigue is detected (typically >20% polarization degradation), which occurs relatively infrequently during normal operation. Given the inherently high endurance of pristine $ZrO_2$ AFE devices (>$10^{10}$ cycles), SSR triggering would be exceptionally rare in practical applications. This design ensures minimal impact on device operation while maintaining reliable performance. Third, to address the reviewer's point regarding practical implementation, we propose that the SSR method can also be integrated with algorithms and peripheral circuitry to selectively trigger recovery operations. When performance degradation is detected in specific memory cells, the algorithm could initiate SSR operations to recover performance. Compared to the OPCR method, this approach offers simpler implementation, as it avoids the need for electrical cycling on the opposite half-loop.

According to the reviewer's suggestions, we have made some changes in the revised manuscript. **The revised sections are as follows.**

In comparison, $ZrO_2$-based antiferroelectric (AFE) devices exhibit more excellent endurance performance as reported[22-26]. Despite this, their endurance properties remain insufficient for dynamic random-access memory (DRAM)-level applications. The fundamental challenge lies in the limited understanding of the correlation between microscopic fatigue mechanisms and macroscopic

electrical behavior in $ZrO_2$-based AFE devices, which hinders further advancements in their reliability and performance optimization. It has been revealed that the evolution of oxygen vacancies ($V_O$) plays a crucial role in the fatigue process of the metal-AFE-metal capacitor (Fig. 1a), which could be concluded as the coupling of $V_O$ charge trapping, AFE to FE phase transition (PT) and $V_O$ localization (Fig. 1b)[27]. A comprehensive understanding and decoupling of these three mechanisms will enable the development of a robust physical model, offering predictive and regulatory insights into the fatigue and recovery behaviors of $ZrO_2$-based AFE capacitors while potentially unveiling intriguing underlying physical phenomena (Fig. 1c).

## Electrical characteristics of $ZrO_2$-based AFE capacitors

AFE capacitors with the same top electrode (TE) and bottom electrode (BE) materials would show double hysteresis loop and zero spontaneous polarization. A lower operating voltage can be achieved by utilizing half-loop operation through electric field bias modulation, as shown by schematic charge-voltage ($Q$–$V$) curves in Fig. 2a, primarily realized by engineering work function differences between TE and BE[24-26]. Therefore, investigating the electrical properties of half-loop is vital to the application of AFE capacitors.

**Comment 2:** Furthermore, if a manufacturer needs to anticipate whether shallow or deep fatigue is likely to occur, which of the two materials presented in this study would you recommend, and why?

**Response:** We sincerely appreciate the reviewer's thoughtful question. Both $ZrO_2$ and $Hf_{0.1}Zr_{0.9}O_2$ exhibit similar fatigue evolution pathways during electrical cycling, progressing from shallow (extrinsic mechanisms dominant) fatigue to deep (intrinsic mechanisms dominant) fatigue stages. The key difference lies in their inherent endurance characteristics, which leads to distinct cycle-count thresholds for this transition, as clearly demonstrated in **Fig. R1**.

For $ZrO_2$ capacitors, our data shows that extrinsic fatigue remains dominant even after $10^8$ electrical cycles, evidenced by the characteristic shrinking of the lower $Q$–$V$ branch without significant $Q_{max}$ reduction (**Fig. R1b**). In contrast, $Hf_{0.1}Zr_{0.9}O_2$ transitions to intrinsic fatigue dominance at much lower cycle counts (~$10^4$ cycles), showing clear $Q_{max}$ reduction at $10^8$ cycles (**Fig. R1d**). This indicates that while both materials follow similar fatigue progression patterns, $ZrO_2$ maintains its extrinsic fatigue characteristics for significantly longer cycling periods.

Based on these observations, we recommend that for applications requiring $<10^4$ cycles, $Hf_{0.1}Zr_{0.9}O_2$ may be suitable due to its larger $2P_{r,p}$. While for applications requiring $>10^8$ cycles, $ZrO_2$ is superior due to its delayed transition to intrinsic fatigue. The $Q$–$V$ evolution patterns provide direct experimental evidence for these recommendations, showing how material choice affects the fatigue behavior under different cycling conditions.

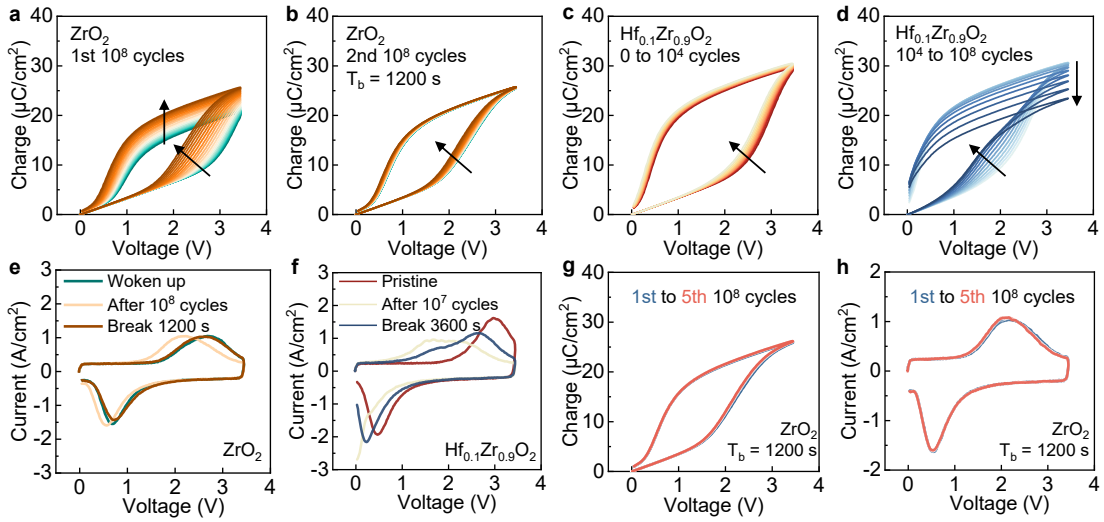


**Fig. R1 Evolutions of the *Q–V* curves for $ZrO_2$ and $Hf_{0.1}Zr_{0.9}O_2$ capacitors. a**, Evolution of the *Q*−*V* curves during the 1st $10^8$ electrical cycles for $ZrO_2$ capacitors. **b**, Evolution of the *Q*−*V* curves during the 2nd $10^8$ electrical cycles after SSR process with $T_b$ = 1200 s for $ZrO_2$ capacitors. **c**, Evolution of the *Q*−*V* curves during the 0 to $10^4$ electrical cycles for $Hf_{0.1}Zr_{0.9}O_2$ capacitors. **d**, Evolution of the *Q*−*V* curves during the $10^4$ to $10^8$ electrical cycles for $Hf_{0.1}Zr_{0.9}O_2$ capacitors. **e**,f, *I*−*V* curves of $ZrO_2$ and $Hf_{0.1}Zr_{0.9}O_2$ capacitors in the states before cycling, after cycling, and after SSR. **g,h,** *P*−*V* and *I*−*V* curves of 1st to 5th $10^8$ electrical cycles for $ZrO_2$ capacitors.

According to the reviewer's suggestions, we have made some changes in the revised manuscript.

**The revised sections are as follows.**

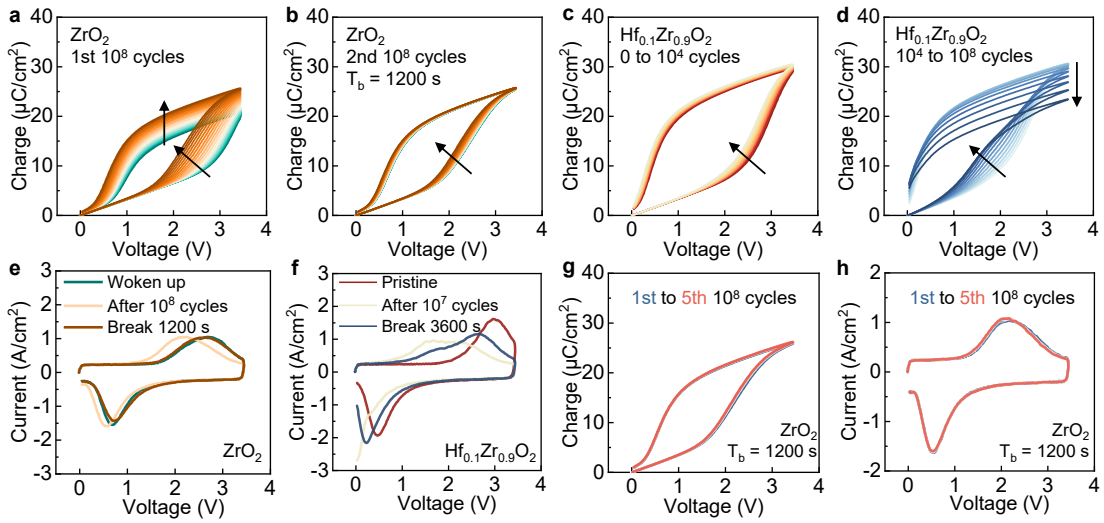


**Extended Data Fig. 4 Evolutions of the *Q–V* curves for $ZrO_2$ and $Hf_{0.1}Zr_{0.9}O_2$ capacitors. a**, Evolution of the *Q*−*V* curves during the 1st $10^8$ electrical cycles for $ZrO_2$ capacitors. **b**, Evolution of the *Q*−*V* curves during the 2nd $10^8$ electrical cycles after SSR process with $T_b$ = 1200 s for $ZrO_2$ capacitors. **c**, Evolution of the *Q*−*V* curves during the 0 to $10^4$ electrical cycles for $Hf_{0.1}Zr_{0.9}O_2$ capacitors. **d**, Evolution of the *Q*−*V* curves during the $10^4$ to $10^8$ electrical cycles for $Hf_{0.1}Zr_{0.9}O_2$ capacitors. **e**,f, *I*−*V* curves of $ZrO_2$ and $Hf_{0.1}Zr_{0.9}O_2$ capacitors in the states before cycling, after cycling, and after SSR. **g,h,** *P*−*V* and *I*−*V* curves of 1st to 5th $10^8$ electrical cycles for $ZrO_2$ capacitors.

**Comment 3:** Finally, could the SSR method work for ferroelectric $HfO_2$-based capacitors? And why?

**Response:** We sincerely appreciate the reviewer's insightful question regarding the potential applicability of SSR to $HfO_2$-based ferroelectric capacitors. Our experimental results and theoretical analysis demonstrate that the SSR phenomenon is material-dependent, with fundamentally different fatigue mechanisms operating in $ZrO_2$-based antiferroelectrics compared to $HfO_2$-based ferroelectrics. In $ZrO_2$-based antiferroelectrics, the observed SSR stems from the dominant role of $V_O$ charge trapping in the fatigue process, which constitutes an extrinsic and reversible polarization degradation mechanism. In contrast, $HfO_2$-based ferroelectrics exhibit completely different fatigue behavior dominated by irreversible in-plane $V_O$ redistribution[1-3], where charge trapping effects are not dominant. This fundamental difference in the underlying fatigue mechanisms precludes the manifestation of SSR effects in $HfO_2$-based FE capacitors. The distinct material physics governing these two systems explains why our proposed SSR approach, while effective for $ZrO_2$-based antiferroelectrics, cannot be directly extended to $HfO_2$-based FE devices.

**Reference (Response Letter)**

1. Gong, Z. et al. Physical origin of the endurance improvement for $HfO_2$-$ZrO_2$ superlattice ferroelectric film. *Applied Physics Letters* **121**, 242901 (2022).

2. Chen, J. et al. Physical Origin of Recovable Ferroelectric Fatigue and Recovery for Doped-$HfO_2$: Toward Endurance Immunity. in *2023 International Electron Devices Meeting (IEDM)* 18.1.1-18.1.4 (IEEE, San Francisco, CA, USA, 2023).

3. Chen, J. et al. Impact of Oxygen Vacancy on Ferroelectric Characteristics and Its Implication for Wake-Up and Fatigue of $HfO_2$-Based Thin Films. *IEEE Trans. Electron Devices* **69**, 5297-5301 (2022).

According to the reviewer's suggestions, we have made some changes in the revised manuscript. **The revised sections are as follows.**

## Impact of fatigue mechanisms on the SSR characteristics

Endurance is a vital characteristic for memory devices. However, the endurance of AFE HZO devices reported so far is still insufficient to support DRAM-level applications. It has been extensively reported that recovery method is one of the most effective technologies to improve the endurance properties in FE and AFE materials. Fig. 1c shows the schematic diagram of a typical recovery process. For $HfO_2$-based FE materials, higher electric field cycling is employed to recover the $P_r$ fatigue caused by low electric field cycling, with its physical origin attributed to the redistribution of Vo[16]. The fatigue behaviors of $HfO_2$-based FE devices are fundamentally different

with the ones of $ZrO_2$-based antiferroelectrics, where $V_O$ charge trapping is not dominant. The $ZrO_2$-based AFE materials undergo a more complex phase transition process and fatigue mechanism, and the physical nature of its recovery has yet to be fully elucidated. In this article, guided by the exploration of the fatigue and recovery mechanism, an SSR method is proposed for $ZrO_2$-based AFE capacitors. As shown in Extended Data Fig. 2b, the proposed SSR process can be briefly described as performing a certain period of break after cycling, realizing the self-recovery of polarization.

## III. Specific questions

**Comment 4:** (l. 34-35) "One of the key issues is the remnant polarization ($P_r$) degradation during electrical cycling, which is a concern regarding their reliability." $P_r$ degradation (fatigue) occurs principally when voltage is decreased or frequency is increased. Did you observe this effect? Or did you consider this in your characterizations?

**Response:** We sincerely appreciate the reviewer's insightful comment. Our experimental results confirm the observed phenomenon that polarization degradation occurs principally when operating voltage is decreased or frequency is increased, which could be attributed to partial polarization switching under these electrical conditions. The voltage-dependent polarization degradation behavior emerges because reduced electric fields lead to incomplete domain switching, resulting in gradual polarization loss over successive cycles. Similarly, increased frequencies limit the available time for domain reversal during each cycle, causing the measured polarization degradation. This behavior has been carefully considered in our reliability measurements and physical mechanism investigations, where we maintained strictly consistent readout parameters throughout all cycling experiments to ensure data comparability and reliability.

According to the reviewer's suggestions, we have made some changes to clarify the measurement parameters in the revised manuscript. **The revised sections are as follows.**

### Electrical characteristics of $ZrO_2$-based AFE capacitors

AFE capacitors with the same top electrode (TE) and bottom electrode (BE) materials would show double hysteresis loop and zero spontaneous polarization. A lower operating voltage can be achieved by utilizing half-loop operation through build-in electric field modulation, as shown by schematic charge-voltage ($Q$–$V$) curves in Fig. 2a, primarily realized by engineering work function differences between TE and BE[24-26]. Therefore, investigating the electrical properties of half loop is vital to the application of AFE capacitors. Fig. 2b shows the measured polarization-voltage ($P$–$V$) curves of fabricated AFE $Hf_xZr_{1-x}O_2$ (HZO) capacitors by uni-directional positive-up-negative-down (uni-PUND) method, in which the positive (Pos.) and negative (Neg.) loops

were recorded by applying +3.5 V and −3.5 V at 10 kHz, with the relax voltage ($V_{relax}$) maintained at +1.75 V and −1.75 V, respectively[28]. Here, $2P_{s,p}$ is used to quantitatively evaluate the AFE properties in actual applications with half-loop operation, as defined by the black arrow in the Pos. loop shown in Fig. 2b. The initial $2P_{s,p}$ value of $ZrO_2$ capacitor is 12.79 μC/cm$^2$, which is quite smaller than the one of $Hf_{0.1}Zr_{0.9}O_2$ capacitor (16.64 μC/cm$^2$). Fig. 2c shows the definition of full width at half maximum (*FWHM*) extracted from the current-voltage (*I*–*V*) curve, which is used to assess the spreading of coercive field ($E_c$) distribution.

## References


28. Magagnin, G. *et al.* An Original Positive-Up-Negative-Down Protocol for Electrical Characterization of Antiferroelectric Materials. *Nano Lett.* **25**, 6686-6692 (2025).

29. Chen, G. & Xu, Z. Charge trapping and detrapping in polymeric materials. *Journal of Applied Physics* **106**, 123707 (2009).

30. Kresse, G. & Hafner, J. Ab initio molecular dynamics for liquid metals. *Phys. Rev. B* **47**, 558 (1993).

31. Kresse, G. & Furthmüller, J. Efficient iterative schemes for ab initio total-energy calculations using a plane-wave basis set. *Phys. Rev. B* **54**, 11169 (1996).

32. Kresse, G. & Joubert, D. From ultrasoft pseudopotentials to the projector augmented-wave method. *Phys. Rev. B* **59**, 1758 (1999).


**Comment 5:** On Fig.1, more precisions are requested. For example, please indicate that the curve in dashed lines on figures 1d and 1e is the initial state.

**Response:** We sincerely appreciate the reviewer for this helpful suggestion to improve the clarity of **Fig. 1**. In the revised manuscript, we have explicitly indicated in both the figure and captions that the dashed lines in Fig. 1d and 1e represent the initial state of the devices before electrical cycling. This clarification has been added to ensure readers can immediately identify the baseline characteristics for comparison with the post-cycling measurements (shown as solid lines). We appreciate this opportunity to improve the clarity of our data presentation.

According to the reviewer's suggestions, we have made some changes to Fig. 1 and captions in the revised manuscript. **The revised sections are as follows.**

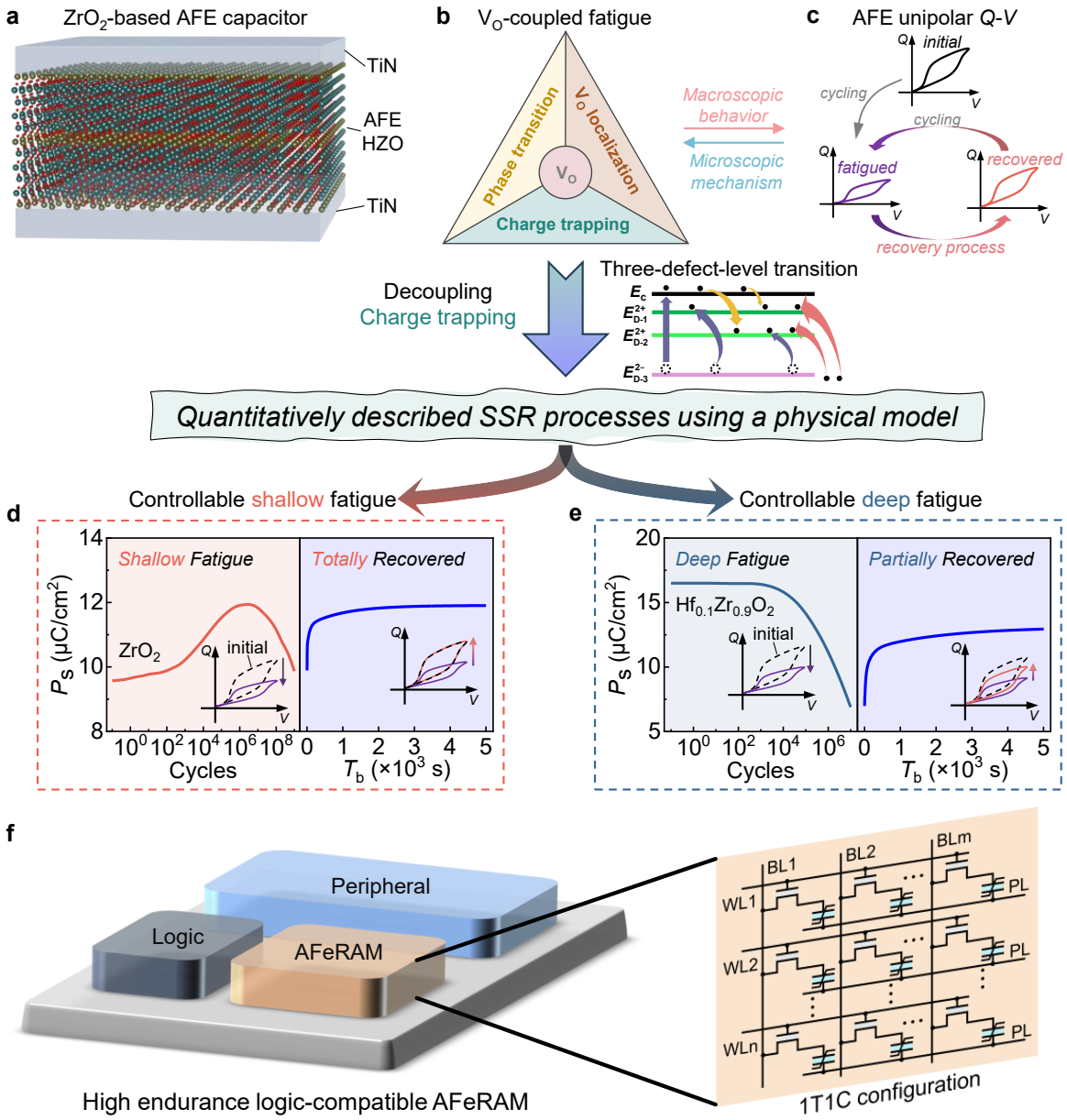


**Fig. 1 Proposal of the SSR method through elucidation of device fatigue mechanisms. a**, Schematic illustration of the AFE TiN/HZO/TiN capacitors. **b**, $V_O$-coupled fatigue mechanisms in $ZrO_2$-based AFE capacitors. **c**, Schematic diagram of the endurance enhancement in half-loop operated AFE devices via the recovery method. **d**,**e**, Development of predictable SSR method under (d) shallow and (e) deep fatigue situations in $ZrO_2$-based AFE capacitors by decoupling $V_O$ charge trapping. Left panels are fatigue processes, and the right panels are recovery processes. The $Q$–$V$ curves of initial states are illustrated by black dashed lines. **f**, Application of SSR method in high endurance logic-compatible AFeRAM utilizing half-loop operation with low operating voltage.

**Comment 6:** (l. 76) Starting from line 76, you use the acronym $P_r$ to denote the remanent polarization. However, the word "remanent" means "what remains". So the term "remanent" specifically refers to the polarization that remains in the absence of an external electric field—

i.e., the polarization measured at 0 V. In your case, $P_r$ appears to refer to the polarization at the relaxation voltage, which corresponds to the voltage around which the positive (or negative) uni-PUND pulse sequence is centered. While the analogy is understandable, this value does not strictly represent the remanent polarization and should be referred to using a different term to avoid confusion.

**Response:** We sincerely appreciate the reviewer's helpful suggestion. The reviewer is absolutely correct that the term "remanent polarization" ($P_r$) should strictly refer to the polarization measured at zero electric field. In our original manuscript, we had used $P_{r,p}$ to denote the switchable polarization measured by uni-PUND method (half-loop of AFE double hysteresis curve), which does not fully conform to the standard definition.

In response to this valuable comment, we have carefully revised our terminology throughout the manuscript to ensure proper usage. All instances of "$P_{r,p}$" have been replaced with "switchable polarization ($P_{s,p}$)" to accurately reflect the measured quantity in our half-loop experiments. We have also added explanatory text in the revised manuscript (Line ) to clarify this distinction and explicitly define $P_{s,p}$ as the switchable polarization measured by uni-PUND method. This change maintains the scientific rigor of our work while preventing any potential confusion about the measured parameters.

We thank the reviewer for bringing this important technical distinction to our attention, as it has helped improve the precision and clarity of our manuscript. The revised terminology better aligns with standard FE characterization conventions while still accurately representing our experimental measurements.

According to the reviewer's suggestions, we have made some changes to Fig. 1 and captions in the revised manuscript. **The revised sections are as follows.**

The axis label of "$2P_{r,p}$ ($\mu C/cm^2$)" in Fig. 1 to Extended Data Fig. 3 are modified as "$2P_{s,p}$ ($\mu C/cm^2$)", and the description of "$2P_{r,p}$" in figure captions are modified as "$2P_{s,p}$".

All instances of "$P_{r,p}$" in the main text have been replaced with "$P_{s,p}$" to quantitatively evaluate the AFE properties in actual applications with half-loop operation to accurately reflect the measured switchable polarization in our uni-PUND experiments.

**Comment 7:** (l.81-85) In the presence of a wake-up effect, the peak of the switching current, which corresponds to the coercive voltage, defines the appropriate relaxation voltage. In your case, the relaxation voltage is not explicitly stated. Based on the curve in Fig. 2b, it seems that you may be using half of the total applied voltage (i.e., 3.5 V/2 = 1.75 V). However, if a wake-up effect is occurring and the coercive field shifts during cycling, using a fixed relaxation voltage may inadvertently distort the symmetry of the hysteresis loop. As a result, some of the

observed effects might be attributed to this misalignment rather than to intrinsic material properties. For instance, Magagning et al. ACS NanoLetters (2025) (https://doi.org/10.1021/acs.nanolett.5c00851) suggested using an automatic sequence to determine the relaxation voltage before using uni-PUND. Do you think it might be relevant or not in your case? And Why?

**Response:** We sincerely appreciate the reviewer's insightful comments. As shown in **Fig. 2b**, the symmetric double hysteresis loops in both $ZrO_2$ and $Hf_{0.1}Zr_{0.9}O_2$ films demonstrate the absence of significant internal electric fields in these AFE systems. For the half-loop measurements, while we observe a symmetric distribution of coercive voltages ($V_c$) about the midpoint of applied voltage for woken-up $ZrO_2$, a slight intrinsic asymmetry of $I_{peak}$ in $I$–$V$ curves persists. This minor asymmetry stems from the marginally higher activation energy required for switching from antiparallel to parallel polarization states compared to the reverse switching process.

As correctly noted by the reviewer, Magagning et al. (ACS NanoLetters 2025) suggested an automatic sequence to determine relaxation voltage before using uni-PUND, which would indeed be necessary for $ZrO_2$ with significant wake-up effects. In our study, we evaluated the relaxation voltage ($V_{relax}$) for woken-up $ZrO_2$ using the proposed method, obtaining $V_{relax} \approx (2.763+0.731)/2 = 1.747$ V. This closely matches our fixed $V_{relax}$ of 1.75 V, confirming that no asymmetric testing conditions are introduced in our measurement for our subsequent analyses. Regarding reliability measurements, maintaining consistent readout parameters during cycling is essential, which precludes dynamic adjustment of $V_{relax}$. Our methodology ensures measurement reproducibility while still capturing intrinsic material behavior, showing the observed polarization degradation and recovery phenomena are genuine material responses rather than measurement artifacts. While protocols like those proposed by Magagning et al. offer value for fundamental switching dynamics studies, our fixed-voltage approach provides the necessary consistency for reliability assessment. The physical insights we report remain valid within this experimental framework, though we acknowledge alternative measurement schemes could provide complementary information for future studies.

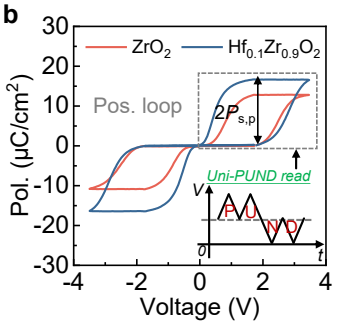


**Fig. 2 b**, Measured $P$–$V$ curve and $2P_{s,p}$ extracted from the Pos. loop, with the uni-PUND scheme shown in the inset.

According to the reviewer's suggestions, we have made some changes to clarify the measurement parameters in the revised manuscript. **The revised sections are as follows.**

## Electrical characteristics of $ZrO_2$-based AFE capacitors

AFE capacitors with the same top electrode (TE) and bottom electrode (BE) materials would show double hysteresis loop and zero spontaneous polarization. A lower operating voltage can be achieved by utilizing half-loop operation through build-in electric field modulation, as shown by schematic charge-voltage ($Q$–$V$) curves in Fig. 2a, primarily realized by engineering work function differences between TE and BE[24-26]. Therefore, investigating the electrical properties of half loop is vital to the application of AFE capacitors. Fig. 2b shows the measured polarization-voltage ($P$–$V$) curves of fabricated AFE $Hf_xZr_{1-x}O_2$ (HZO) capacitors by uni-directional positive-up-negative-down (uni-PUND) method, in which the positive (Pos.) and negative (Neg.) loops were recorded by applying +3.5 V and −3.5 V at 10 kHz, with the relax voltage ($V_{relax}$) maintained at +1.75 V and −1.75 V, respectively[28]. Here, $2P_{s,p}$ is used to quantitatively evaluate the AFE properties in actual applications with half-loop operation, as defined by the black arrow in the Pos. loop shown in Fig. 2b. The initial $2P_{s,p}$ value of $ZrO_2$ capacitor is 12.79 μC/cm$^2$, which is quite smaller than the one of $Hf_{0.1}Zr_{0.9}O_2$ capacitor (16.64 μC/cm$^2$). Fig. 2c shows the definition of full width at half maximum (*FWHM*) extracted from the current-voltage ($I$–$V$) curve, which is used to assess the spreading of coercive field ($E_c$) distribution.

## References


28. Magagnin, G. *et al.* An Original Positive-Up-Negative-Down Protocol for Electrical Characterization of Antiferroelectric Materials. *Nano Lett.* **25**, 6686-6692 (2025).

29. Chen, G. & Xu, Z. Charge trapping and detrapping in polymeric materials. *Journal of Applied Physics* **106**, 123707 (2009).

30. Kresse, G. & Hafner, J. Ab initio molecular dynamics for liquid metals. *Phys. Rev. B* **47**, 558 (1993).

31. Kresse, G. & Furthmüller, J. Efficient iterative schemes for ab initio total-energy calculations using a plane-wave basis set. *Phys. Rev. B* **54**, 11169 (1996).

32. Kresse, G. & Joubert, D. From ultrasoft pseudopotentials to the projector augmented-wave method. *Phys. Rev. B* **59**, 1758 (1999).


**Comment 8:** (l.86-90) The authors state that the *FWHM* change observed in $ZrO_2$ is attributed solely to charge trapping, without involving oxygen vacancy ($V_O$) redistribution, whereas the *FWHM* change in $Hf_{0.1}Zr_{0.9}O_2$ follows a different behavior. However, I could not find any experimental evidence or theoretical framework supporting this distinction. Could the authors please elaborate on this point and clarify the basis—experimental, analytical, or otherwise—

for this hypothesis?

**Response:** We sincerely appreciate the reviewer's insightful comment regarding the physical association between *FWHM* changes and oxygen vacancies ($V_O$) redistribution. $ZrO_2$-based AFE thin films exhibit polycrystalline and multi-domain characteristics, wherein the domain reversal requires overcoming a local nucleation energy barrier corresponding to local $E_c$. The *FWHM* of *I–V* curve manifests the spatial dispersion of local $E_c$ across the film. A small *FWHM* represents collective switching of all domains within a narrow electric field range, indicating a tightly distributed local $E_c$. Conversely, a large *FWHM* signifies asynchronous domain switching at varied electric fields, reflecting a dispersed local $E_c$ distribution. Various reports have claimed that $V_O$ plays a critical role in governing polarization switching characteristics. The distribution of $V_O$ would significantly modify the local $E_c$, substantially impacting polarization switching energy barriers [1-4]. Thus, when $V_O$ are uniformly distributed, the distribution of local $E_c$ is tight and the *FWHM* is small. Oppositely, the inhomogeneous distributed $V_O$ causes the broader distributed local $E_c$ and a larger *FWHM*. A stable *FWHM* over cycling signifies the maintenance of stationary $V_O$ distribution. On the other hand, the charged $V_O$ generates local internal electric fields ($E_i$), which primarily manifest as a global shift of the local $E_c$ in the *I–V* curve. In summary, the $V_O$ distribution significantly affect the macroscopic polarization-switching behavior, which can be characterized by the distribution of the local $E_c$ in the *I–V* curve.

In response to the reviewer's specific question regarding stable *FWHM* and its implications for $V_O$ evolution, the stable *FWHM* with the shifted *I–V* curve suggests no significant redistribution of $V_O$[4]. The dynamic evolution of $ZrO_2$ capacitors shows that when the *FWHM* of $I_{peak}$ remains almost unchanged while the *I–V* curve shifts, the dominant microscopic physical mechanism is interfacial $V_O$ charge trapping (extrinsic fatigue). In this process, pre-existing $V_O$ at the $TiN/Hf_xZr_{1-x}O_2$ will be charged during continuous uni-directional cycling, creating the $E_i$ that biases the polarization switching without requiring $V_O$ migration or generation inside the film. Therefore, the overall $V_O$ concentration (and spatial distribution) stays effectively constant, neither increasing nor decreasing, while the charge states of $V_O$ altered. This picture agrees with the behavior that has been observed in $ZrO_2$ AFE film after $10^8$ cycles and is likely the leading fatigue mechanism in this system. In contrast, fatigue in $Hf_{0.1}Zr_{0.9}O_2$ may involve a coupling of $V_O$ charge trapping and redistribution, which contributes to a complicated evolution of *FWHM* as the film undergoes the repeated switching process.

We hope this clarifies the distinction we are making in terms of the mechanisms behind the *FWHM* behavior in $ZrO_2$ and $Hf_{0.1}Zr_{0.9}O_2$, and we thank the reviewer for the opportunity to elaborate on this point.

**Reference (Response Letter)**

1. Gong, Z. et al. Physical origin of the endurance improvement for $HfO_2$-$ZrO_2$ superlattice ferroelectric film. *Applied Physics Letters* **121**, 242901 (2022).
2. Chen, J. et al. Physical Origin of Recovable Ferroelectric Fatigue and Recovery for Doped-$HfO_2$: Toward Endurance Immunity. in *2023 International Electron Devices Meeting (IEDM)* 18.1.1-18.1.4 (IEEE, San Francisco, CA, USA, 2023).
3. Chen, J. et al. Impact of Oxygen Vacancy on Ferroelectric Characteristics and Its Implication for Wake-Up and Fatigue of $HfO_2$-Based Thin Films. *IEEE Trans. Electron Devices* **69**, 5297-5301 (2022).
4. Qian, H. et al. Dynamic evolution of oxygen vacancies during cycling in antiferroelectric $Hf_xZr_{1-x}O_2$. *Applied Physics Letters* **124**, 243508 (2024).

According to the reviewer's comment, we have added some sentences to describe the physical association between *FWHM* changes and $V_O$ evolution more clearly in the revised manuscript. **The revised sections are as follows.**

### Electrical characteristics of $ZrO_2$-based AFE capacitors

Fig. 2c shows the definition of full width at half maximum (*FWHM*) extracted from the current-voltage (*I*–*V*) curve, which is used to assess the spreading of coercive field ($E_c$) distribution. The *FWHM* of *I*–*V* curve manifests the spatial dispersion of local $E_c$ across the film. A small *FWHM* represents collective switching of all domains within a narrow electric field range, indicating a tightly distributed local $E_c$. Conversely, a large *FWHM* signifies asynchronous domain switching at varied electric fields, reflecting a dispersed local $E_c$ distribution. The distribution of $V_O$ would significantly modify the local $E_c$, substantially impacting polarization switching energy barriers. When $V_O$ are uniformly distributed, the distribution of local $E_c$ is tight and the *FWHM* is small. Oppositely, the inhomogeneous distributed $V_O$ causes the broader distributed local $E_c$ and a larger *FWHM*. A stable *FWHM* over cycling signifies the maintenance of stationary $V_O$ distribution.

**Comment 9:** (l.92) The description of how electric field (*E*-field) modulation is implemented remains somewhat unclear. Fig. 2b, which appears to illustrate a uni-PUND sequence, does not show any *E*-field modulation. Given the strong potential of *E*-field modulation for various applications, it would be helpful if the authors could clarify the measurement protocol or electrical sequence one can use to achieve this modulation.

**Response:** The non-volatile storage in AFE capacitors, as illustrated in **Fig. 2a**, could be primarily achieved by **engineering work function differences between the top and bottom electrodes**. This approach centers the half-loop of the AFE materials. When an appropriate external electric field is applied, the AFE material switches between two distinct polarization states, typically one parallel polarization configuration ($P_{\downarrow\downarrow}$, logical "1") and one antiparallel polarization configuration ($P_{\downarrow\uparrow}$, logical "0"), maintaining its state upon field removal due to the

intrinsic energy landscape of the AFE phase.

In this work, we employed symmetric electrode structures ($TiN/ZrO_2/TiN$ and $TiN/Hf_{0.1}Zr_{0.9}O_2/TiN$) to investigate the fundamental polarization switching behavior from $P_{\downarrow\uparrow}$ to $P_{\downarrow\downarrow}$ states using a half-loop characterization approach. This methodology provides crucial insights into the polarization dynamics under external electric field. Specifically, the half-loop measurements reveal essential characteristics including intrinsic AFE behavior, material response to repeated cycling, and the SSR characteristics after various break time. This foundational knowledge is essential for informing future device optimization efforts involving more complex electrode engineering, which we are currently investigating in follow-up studies. The insights gained from this work provide the necessary framework for developing advanced AFE-based memory devices with optimized performance characteristics.

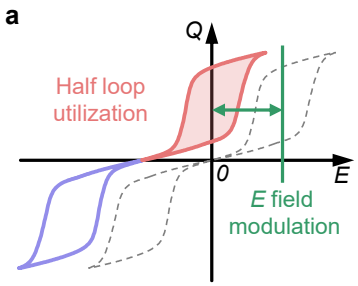


**Fig. 2 a**, Evolution of the $Q-V$ curve utilizing the half loop method for AFeRAM via electric field modulation.

According to the reviewer's suggestions, we have made some changes to clarify conventional *E*-field modulation method in the revised manuscript. **The revised sections are as follows.**

## Electrical characteristics of $ZrO_2$-based AFE capacitors

AFE capacitors with the same top electrode (TE) and bottom electrode (BE) materials would show double hysteresis loop and zero spontaneous polarization. A lower operating voltage can be achieved by utilizing half-loop operation through build-in electric field modulation, as shown by schematic charge-voltage ($Q-V$) curves in Fig. 2a, primarily realized by engineering work function differences between TE and BE[24-26]. Therefore, investigating the electrical properties of half loop is vital to the application of AFE capacitors.

**Comment 10:** (l.101-132) Imprint is likely to develop during the break time. Could it be that, ultimately, the SSR method relies on exploiting the imprint effect to re-center the hysteresis around the relaxation point, thereby recovering a higher polarization?

**Response:** We sincerely appreciate the reviewer's thoughtful question regarding the relationship between the SSR method and imprint effects. Our analysis suggests that while the extrinsic fatigue mechanism in $ZrO_2$-based AFE devices involves charge trapping processes

conceptually similar to imprint, where localized charge accumulation creates internal bias fields that shift the hysteresis loop, there are fundamental differences in the underlying physics and reversibility of these phenomena.

The key distinction lies in the microscopic processes involved. In conventional imprints, defect redistribution and dipole alignment create relatively stable internal fields that are difficult to reverse. In contrast, our $ZrO_2$-based AFE system exhibits a more reversible form of charge trapping at pre-existing $V_O$ sites near interfaces, which can be effectively released through SSR processes. This is evidenced by the complete restoration of the centered hysteresis after SSR process (**Fig. 4g**, top panel).

The effect of SSR does involve re-centering the hysteresis loop by removing internal bias fields, like what the reviewer described. The mechanism operates through detrapping of charges rather than establishing new imprints. This distinction is crucial because it explains the excellent recoverability observed in our devices and suggests different fundamental limits for endurance compared to systems dominated by classical imprint.

**Comment 11:** (l.138) "couping" I think there is a mistake. It should be: "coupling"

**Response:** We sincerely appreciate the reviewer's careful reading and helpful correction. The reviewer is absolutely right. It is indeed a typographical error, and the correct term should be "coupling" rather than "couping". We have carefully reviewed the manuscript and corrected this mistake in all instances where it appeared.

This correction has been implemented in the revised version of the manuscript, along with a thorough proofreading to ensure no similar errors remain. We thank the reviewer for bringing this to our attention and helping us improve the accuracy and professionalism of our manuscript.

**Comment 12:** (l.160 and l.169) From equations (1) and (2), the three-level traps model seems to be very simple. Don't you think that additional parameters should be taken into account to describe the overall phenomenon occurring in fluorite materials?

**Response:** The SSR behavior in $ZrO_2$ and $Hf_{0.1}Zr_{0.9}O_2$ capacitors is fundamentally tied to $V_O$ charge detrapping dynamics, as highlighted by the multi-level defect detrapping model in Ref. [6]. That work established that charge decay in dielectrics follows multi-exponential kinetics due to traps with distinct energy depths (shallow vs. deep), where detrapping rates depend on temperature and defect energy levels:

$$k_{\text{th}} = N_c \nu_{\text{th}} \sigma_c \exp\left(-\frac{E_t}{kT}\right), \qquad \text{(Eq. 6 in Ref. [6])}$$

Inspired by this framework, we proposed a three-level trap model (Eq. 1) to describe the self-recoverable $2P_{s,p}$ during SSR. Our model extends Ref. [6]'s principles to oxide systems, with

$\tau_1$, $\tau_2$, and $\tau_3$ representing the effective lifetimes of charges released from progressively deeper traps.

$$2P_{r,p}(t) = 2P_{r,0} - P_1 e^{-t/\tau_1} - P_2 e^{-t/\tau_2} - P_3 e^{-t/\tau_3}, \quad (1)$$

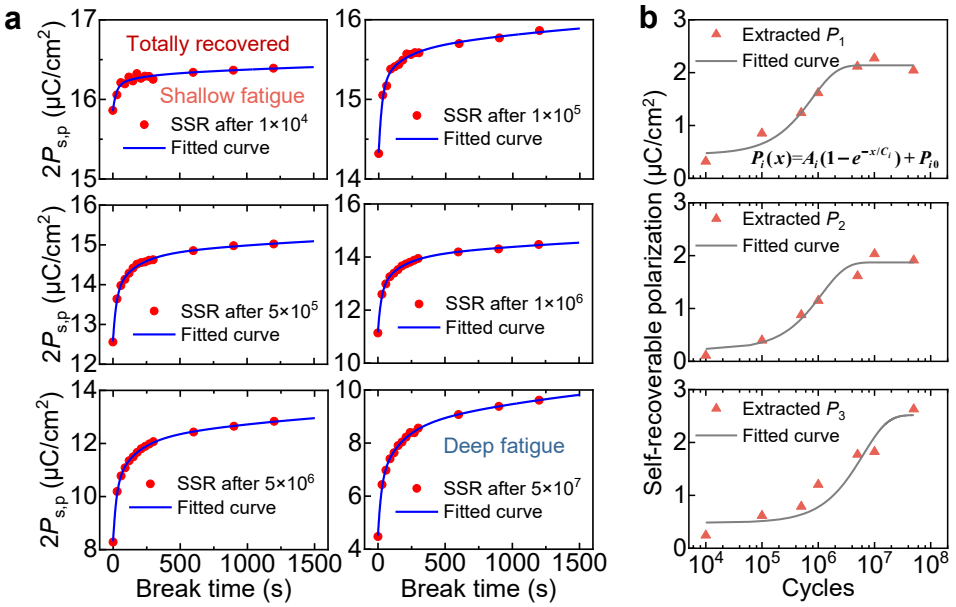


**Fig. 4 a**, Experimental and fitted curves of the SSR processes in $Hf_{0.1}Zr_{0.9}O_2$ capacitors after different fatigue cycles, using the fixed $\tau$ parameters extracted from Fig. 3g. The specific fatigue cycles are $1\times10^4$, $1\times10^5$, $5\times10^5$, $1\times10^6$, $5\times10^6$ and $5\times10^7$, respectively. **b**, Extracted values of $P_1$, $P_2$ and $P_3$ as a function of electrical cycles and their respective fitting curves.

The experimental SSR curves for $Hf_{0.1}Zr_{0.9}O_2$ (**Fig. 4a**) align precisely with this model, showing initial rapid recovery (shallow traps) followed by slower dynamics (deep traps), mirroring Ref. [6]'s observations in polymers. Further, the dependency of self-recoverable $2P_{s,p}$ on electrical cycles (Eq. 2 and **Fig. 4b**) reflects how trap filling influences detrapping, indicating a concept central to Ref. [6]'s discussion of injection and trapping processes (Eqs. 14-15 in Ref. [6]). The universality of this behavior is underscored by the identical SSR trends in $ZrO_2$ and the controlled extrinsic fatigue in $Hf_{0.1}Zr_{0.9}O_2$, captured by our model. We've clarified these connections in the revised manuscript and appreciate the reviewer's opportunity to strengthen this discussion.

$$P_i(x) = A_i(1 - e^{-x/C_i}) + P_{i0}, \quad (2)$$

$$n_1(t) = \frac{A_1 N_1}{A_1 + k_1}\left\{1 - \exp\left[-(A_1 + k_1)t\right]\right\}, \quad \text{(Eq. 14 in Ref. [6])}$$

$$n_2(t) = \frac{A_2 N_2}{A_2 + k_2}\left\{1 - \exp\left[-(A_2 + k_2)t\right]\right\}, \quad \text{(Eq. 15 in Ref. [6])}$$

**Reference (Response Letter)**

6. Chen, G. & Xu, Z. Charge trapping and detrapping in polymeric materials. *Journal of Applied Physics* **106**, 123707 (2009).

According to the reviewer's suggestions, we have made some changes to clarify conventional *E*-field modulation method in the revised manuscript. **The revised sections are as follows.**

## Development of three level traps model

After figuring out the proportional contributions of different mechanisms in deep fatigue situation of $Hf_{0.1}Zr_{0.9}O_2$, further analysis of the SSR capability at varying $T_b$ is conducted, as illustrated by the red scatter plot in the right panel of Fig. 3f. The maximum self-recoverable polarization through SSR can be approximately estimated at 6.11 μC/cm$^2$ (the difference between the recovered $2P_{s,p}$ after SSR with a 3600 s break and the fatigued $2P_{s,p}$ after $10^7$ cycles), nearly equivalent to the magnitude of extrinsic fatigue extracted from Fig. 3d, which is 6.21 μC/cm$^2$ for $10^7$ cycles. This indicates that SSR can fully recover the extrinsic fatigue caused by charge trapping but has limited effectiveness in recovering intrinsic fatigue. Additional experiments on $Hf_{0.1}Zr_{0.9}O_2$ capacitors have been conducted to extend the endurance measurements to $10^9$ cycles. As shown in Extended Data Fig. 6, it is revealed that the recoverable $2P_{s,p}$ value (7.54 μC/cm$^2$) shows excellent agreement with the measured extrinsic fatigue (7.22 μC/cm$^2$), with a minor 4.4% difference. The alignment between these values at such high cycle counts provides compelling evidence that the break-time-dependent SSR process remains effective and that no significant new fatigue mechanisms emerge in this cycling regime. Notably, the totally self-recoverable shallow fatigue observed in $ZrO_2$ capacitors may also stem from $V_O$ charge trapping. Due to the strong correlation between the SSR process and charge detrapping, the multi-level defect detrapping model is referenced in this article[29]. The charge decay in dielectrics follows multi-exponential kinetics due to traps with distinct energy depths, where detrapping rates depend on temperature and defect energy levels. A three level traps model is proposed, which successfully reproduces the evolution of $2P_{s,p}$ during SSR process in $ZrO_2$ and $Hf_{0.1}Zr_{0.9}O_2$ capacitors (Fig. 1d,e):

$$2P_{s,p}(t) = 2P_{s,0} - P_1 e^{-t/\tau_1} - P_2 e^{-t/\tau_2} - P_3 e^{-t/\tau_3}, \quad (1)$$

where $P_{s,0}$, $P_i$ and $\tau_i$ ($i$ = 1, 2, 3) represent for the saturated polarization value after sufficiently long SSR, the self-recoverable polarization and the effective lifespan for the corresponding trap energy level, respectively.

**Comment 13:** (l.181-203) The three-level traps model essentially relies on fitting with three exponential components. However, it is not demonstrated how one can confidently attribute distinct physical mechanisms to these components, given the potential overlap and similarity in their mathematical behavior. Without additional validation, the assignment of specific

processes to each level remains speculative. It would strengthen the work to support the model with complementary experimental evidence, such as temperature-dependent measurements, frequency response analysis, or material characterization techniques, that could independently validate the existence and nature of the proposed trap levels.

**Response:** We sincerely appreciate the reviewer's helpful suggestions regarding the need for additional experimental validation to further support the three-level traps model. Indeed, complementary measurements such as temperature-dependent frequency analysis would strengthen the robustness of our conclusions. However, due to current equipment limitations, performing these measurements is unfortunately not feasible in this study.

Although we are unable to implement temperature-dependent frequency measurements, we would like to make some predictions regarding the potential results of temperature-dependent frequency measurements employed in $ZrO_2$-based AFE thin films. It should be noted that $ZrO_2$-based AFE thin films would suffer from potential AFE to FE PT during temperature variations, complicating the temperature-dependent electrical characterization, as demonstrated in $Hf_xZr_{1-x}O_2$ AFE materials[7-11]. The phenomenon can significantly modify defect distributions, inducing changes in internal strain, and alter dielectric properties, all of which may hinder the precise determination of trap energy levels using conventional variable-temperature frequency analysis. These possible factors may interfere with the implementation of temperature-dependent frequency measurements and affect the accurate determination of trap energy levels.

The three-level traps model is fundamentally grounded in the charge trapping/detrapping dynamics, building upon the framework established in Ref. [6] while providing new insights specific to $ZrO_2$-based antiferroelectrics. Crucially, as demonstrated in the discussions of our manuscript through comprehensive electrical characterization, we have established that the self-recoverable portion of fatigue is dominated by extrinsic mechanisms involving $V_O$ charge trapping. The SSR process physically represents the detrapping of charged $V_O$. Our DFT calculations (**Fig. 4c-f**) qualitatively indicate the presence of three $V_O$ energy levels that could participate in these processes. The shallowest trap ($\tau_1$) aligns with weakly trapped charge, while the intermediate ($\tau_2$) and slowest ($\tau_3$) components reflect progressively deeper traps.

The model's physical validity is reinforced by the excellent agreement between the DFT calculated transition levels and the experimentally observed detrapping kinetics. Moreover, the schematic in **Fig. 4g** illustrates seven possible inter-trap transitions that collectively explain the complete SSR behavior, demonstrating how our model captures the actual physical processes rather than serving as mere mathematical fitting. We have strengthened the manuscript to better highlight these connections between the electrical measurements and the underlying physical processes.

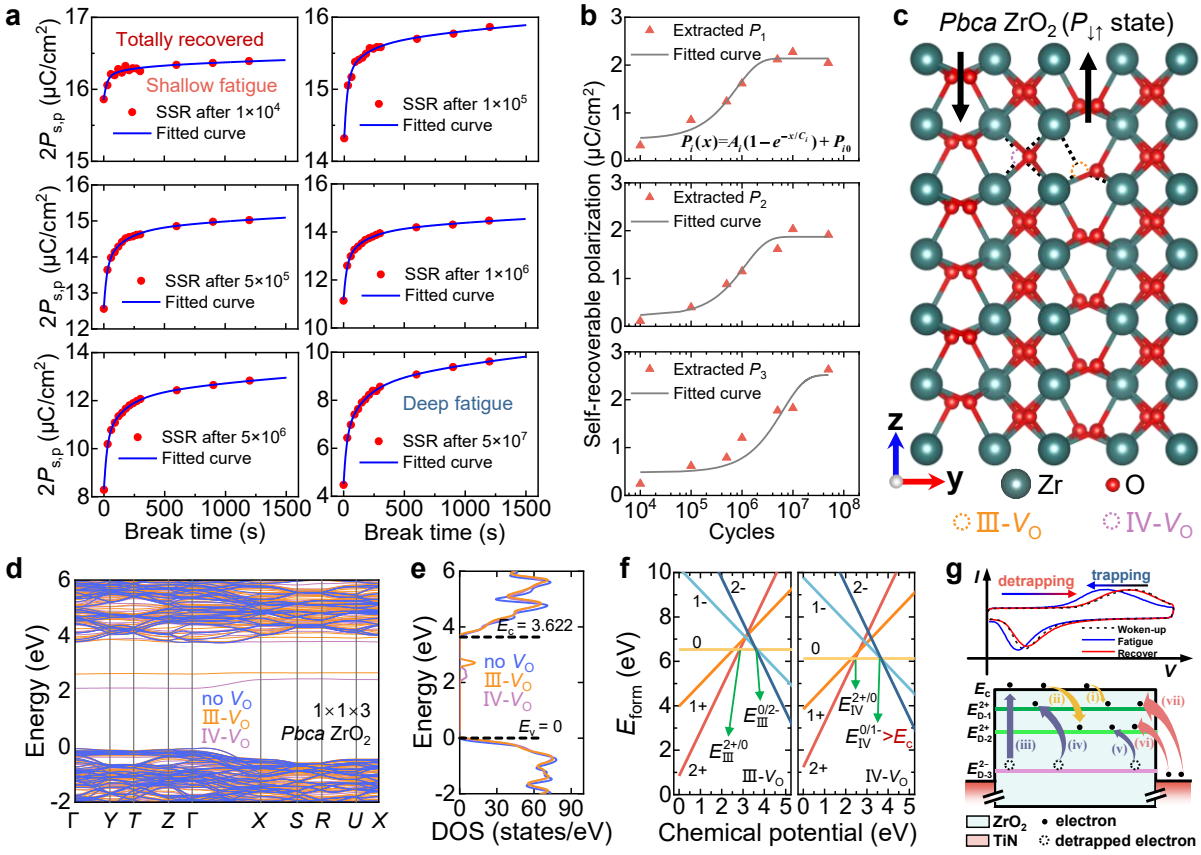


**Fig. 4 Theoretical demonstrations for three level traps model. a**, Experimental and fitted curves of the SSR processes in $Hf_{0.1}Zr_{0.9}O_2$ capacitors after different fatigue cycles, using the fixed τ parameters extracted from Fig. 3g. The specific fatigue cycles are $1\times10^4$, $1\times10^5$, $5\times10^5$, $1\times10^6$, $5\times10^6$ and $5\times10^7$, respectively. **b**, Extracted values of $P_1$, $P_2$ and $P_3$ as a function of electrical cycles and their respective fitting curves. **c**, Schematic diagram of 1×1×3 *Pbca* $ZrO_2$ supercell, highlighting the locations of neutral III-$V_O$ and IV-$V_O$, marked by orange and purple dashed circles, respectively. **d,e**, First-principles calculated *E*–*k* dispersion and DOS spectra for supercells with various O-deficient configurations. **f**, Plot of the formation energy of different charged $V_O$ as a function of the chemical potential. **g**, Schematic illustration of mechanism for SSR and possible detrapping routes for $E^{2+}_{D-1}$ : (i), (iv), (vii); $E^{2+}_{D-2}$ : (ii), (v), (vi); $E^{2-}_{D-3}$ : (iii), (iv), (v).

## References (Response Letter)


6. Chen, G. & Xu, Z. Charge trapping and detrapping in polymeric materials. *Journal of Applied Physics* **106**, 123707 (2009).

7. Wang, Z. et al. Cryogenic Characterization of Antiferroelectric Zirconia down to 50 mK. in 2019 Device Research Conference (DRC) 85–86 (IEEE, Ann Arbor, MI, USA, 2019).

8. Park, M. H. & Hwang, C. S. Fluorite-structure antiferroelectrics. *Rep. Prog. Phys.* **82**, 124502 (2019).

9. Cheema, S. S. *et al.* Ultrathin ferroic $HfO_2$–$ZrO_2$ superlattice gate stack for advanced transistors. *Nature* **604**, 65–71 (2022).

10. Xing, Y. *et al.* Improved Ferroelectricity in Cryogenic Phase Transition of $Hf_{0.5}Zr_{0.5}O_2$. *IEEE J. Electron Devices Soc.* **10**, 996–1002 (2022).
11. Hsiang, K.-Y. *et al.* Cryogenic Endurance of Anti-ferroelectric and Ferroelectric $Hf_{1-x}Zr_xO_2$ for Quantum Computing Applications. in *2023 IEEE International Reliability Physics Symposium (IRPS)* 1–4 (IEEE, Monterey, CA, USA, 2023).

According to the reviewer's suggestions, we have made some changes to clarify conventional *E*-field modulation method in the revised manuscript. **The revised sections are as follows.**

## Development of three level traps model

After figuring out the proportional contributions of different mechanisms in deep fatigue situation of $Hf_{0.1}Zr_{0.9}O_2$, further analysis of the SSR capability at varying $T_b$ is conducted, as illustrated by the red scatter plot in the right panel of Fig. 3f. The maximum self-recoverable polarization through SSR can be approximately estimated at 6.11 μC/cm$^2$ (the difference between the recovered $2P_{s,p}$ after SSR with a 3600 s break and the fatigued $2P_{s,p}$ after $10^7$ cycles), nearly equivalent to the magnitude of extrinsic fatigue extracted from Fig. 3d, which is 6.21 μC/cm$^2$ for $10^7$ cycles. This indicates that SSR can fully recover the extrinsic fatigue caused by charge trapping but has limited effectiveness in recovering intrinsic fatigue. Additional experiments on $Hf_{0.1}Zr_{0.9}O_2$ capacitors have been conducted to extend the endurance measurements to $10^9$ cycles. As shown in Extended Data Fig. 6, it is revealed that the recoverable $2P_{s,p}$ value (7.54 μC/cm$^2$) shows excellent agreement with the measured extrinsic fatigue (7.22 μC/cm$^2$), with a minor 4.4% difference. The alignment between these values at such high cycle counts provides compelling evidence that the break-time-dependent SSR process remains effective and that no significant new fatigue mechanisms emerge in this cycling regime. Notably, the totally self-recoverable shallow fatigue observed in $ZrO_2$ capacitors may also stem from $V_O$ charge trapping. Due to the strong correlation between the SSR process and charge detrapping, the multi-level defect detrapping model is referenced in this article[29]. The charge decay in dielectrics follows multi-exponential kinetics due to traps with distinct energy depths, where detrapping rates depend on temperature and defect energy levels. A three level traps model is proposed, which successfully reproduces the evolution of $2P_{s,p}$ during SSR process in $ZrO_2$ and $Hf_{0.1}Zr_{0.9}O_2$ capacitors (Fig. 1d,e):

$$2P_{s,p}(t) = 2P_{s,0} - P_1e^{-t/\tau_1} - P_2e^{-t/\tau_2} - P_3e^{-t/\tau_3}, \quad (1)$$

where $P_{s,0}$, $P_i$ and $\tau_i$ ($i$ = 1, 2, 3) represent for the saturated polarization value after sufficiently long SSR, the self-recoverable polarization and the effective lifespan for the corresponding trap energy level, respectively.

## Questions about the extended data

**Comment 14:** In the "methods" section, could you precise about how the stoichiometry is determined?

**Response:** We sincerely appreciate the reviewer's helpful suggestion. We would like to add more details about the device fabrication process in the **Methods section of revised manuscript**. The fabrication of $ZrO_2/Hf_{0.1}Zr_{0.9}O_2$ AFE capacitors starts from silicon (Si) substrate. After conventional RCA wet clean, a 50 nm-thick TiN layer is deposited as bottom electrode (BE) on Si substrate by reactive sputtering. Then, the samples are loaded into the atomic layer deposition (ALD) chamber. Next, 10 nm $ZrO_2/Hf_{0.1}Zr_{0.9}O_2$ AFE film is in situ deposited via ALD using tetrakis-dimethylamino hafnium (TDMAHf) and tetrakis-dimethylamino zirconium (TDMAZr) as precursors, and $H_2O$ as oxidant at 250 ℃. The growth rates of $HfO_2$ and $ZrO_2$ are 0.71 and 0.67 Å/cycle, respectively. During the deposition of $Hf_{0.1}Zr_{0.9}O_2$ AFE film, $HfO_2$ cycles are uniformly inserted in $ZrO_2$ cycles, and one $HfO_2$ cycle followed by nine $ZrO_2$ cycles as a supercycle is employed. Subsequently, 50 nm-thick TiN is deposited by reactive sputtering and patterned for top electrode (TE). The size of characterized devices is 11304 $\mu m^2$. Finally, post-metallization annealing (PMA) at 500 ℃ for 30 s in $N_2$ atmosphere is performed to crystallize $ZrO_2/Hf_{0.1}Zr_{0.9}O_2$ films.

According to the reviewer's comment, we have added some sentences to describe the details about device fabrication process in the revised manuscript. **The revised sections are as follows.**

## Methods

### Device Fabrication

The fabrication of $ZrO_2/Hf_{0.1}Zr_{0.9}O_2$ AFE capacitors starts from silicon (Si) substrate. After conventional RCA wet clean, a 50 nm-thick TiN layer is deposited as bottom electrode (BE) on Si substrate by reactive sputtering. Then, the samples are loaded into the atomic layer deposition (ALD) chamber for 10 min $O_3$ treatment on TiN BE[23]. Next, 10 nm $ZrO_2/Hf_{0.1}Zr_{0.9}O_2$ AFE film is in situ deposited via ALD using tetrakis-dimethylamino hafnium (TDMAHf) and tetrakis-dimethylamino zirconium (TDMAZr) as precursors, and $H_2O$ as oxidant at 250 ℃. The growth rates of $HfO_2$ and $ZrO_2$ are 0.71 and 0.67 Å/cycle, respectively. During the deposition of $Hf_{0.1}Zr_{0.9}O_2$ AFE film, $HfO_2$ cycles are uniformly inserted in $ZrO_2$ cycles, and one $HfO_2$ cycle followed by nine $ZrO_2$ cycles as a supercycle is employed. Subsequently, 50 nm-thick TiN is deposited by reactive sputtering and patterned for top electrode (TE). The size of characterized devices is 11304 $\mu m^2$. Finally, post-metallization annealing (PMA) at 500 ℃ for 30 s in $N_2$ atmosphere is performed to crystallize $ZrO_2/Hf_{0.1}Zr_{0.9}O_2$ films.

**Comment 15:** (l.351) The authors are talking about the AFE orthorhombic phase and the non-polar tetragonal phase. To my knowledge, the current theory of antiferroelectricity in $ZrO_2$ suggests that there is a structural phase transition from tetragonal to orthorhombic phase (see

for instance, Hoffmann et al. Nature (2022), https://doi.org/10.1038/s41467-022-28860-1). I recommend not using the words "antiferroelectric orthorhombic phase" as the interplay between tetragonal and orthorhombic phases remains unclear. And only talking about orthorhombic and tetragonal without specifying the electric behavior.

**Response:** We sincerely appreciate the reviewer's insightful comment. As indicated by the reviewer, the origin of antiferroelectricity in $ZrO_2$-based materials needs to be discussed. Actually, several studies have experimentally demonstrated the existence of the antiparallel polarization configuration orthorhombic phase (*Pbca* space group) in $ZrO_2$-based AFE films[12-14]. (for instance, Cheng, Y. *et al. Nat Commun* **13**, 645 (2022); Li, X. *et al*. *Advanced Materials* **35**, 2207736 (2023); Weng, Z. et al. *IEEE Electron Device Lett.* **44**, 1780–1783 (2023).).

As the structural basis for AFE characteristics, with particular emphasis on its antipolar *Pbca* structure (o-I phase) where oxygen displacements exhibit an antiparallel arrangement. This is fundamentally distinct from the polar orthorhombic $Pca2_1$ phase (o-III phase) observed in $HfO_2$-based ferroelectrics. The conclusions are firmly supported by atomic-resolution STEM imaging and ab initio simulations, which directly correlate the *Pbca* phase with AFE properties in $Hf_xZr_{1-x}O_2$, especially in thinner films.

We acknowledge the reviewer's concern about the ongoing discussion regarding the interplay between tetragonal and orthorhombic phases in $ZrO_2$-based systems, as highlighted by Hoffmann et al. While their work emphasizes the t-to-o transition's role in AFE behavior, our findings demonstrate that the *Pbca* phase itself with its inherent antipolar oxygen ordering represents a stable configuration contributing to AFE properties in $Hf_xZr_{1-x}O_2$. This perspective is further reinforced by recent studies. Cheng et al. observed reversible transitions between polar ($Pca2_1$) and antipolar (*Pbca*) phases under electric fields, consistent with the AFE to FE PT fatigue mechanism in $ZrO_2$-based antiferroelectrics. Li et al. visualized unit-cell-scale antipolar-to-polar transitions in $ZrO_2$. These collective findings suggest that while phase transitions between tetragonal and orthorhombic structures may contribute to AFE-like behavior in certain conditions, the antipolar *Pbca* phase itself plays a crucial and distinct role in establishing AFE characteristics in $ZrO_2$-based systems. We will revise our manuscript to more clearly articulate this distinction and to better integrate these complementary perspectives on the origins of AFE behavior in fluorite-structure oxides.

**References (Response Letter)**

12. Cheng, Y. *et al.* Reversible transition between the polar and antipolar phases and its implications for wake-up and fatigue in $HfO_2$-based ferroelectric thin film. *Nat Commun* **13**, 645 (2022).

13. Li, X. *et al.* Polarization Switching and Correlated Phase Transitions in Fluorite-Structure $ZrO_2$ Nanocrystals. *Advanced Materials* **35**, 2207736 (2023).

14. Weng, Z., Zhao, L., Lee, C. & Zhao, Y. Phase Transitions and Anti-Ferroelectric Behaviors in $Hf_{1-x}Zr_xO_2$ Films. *IEEE Electron Device Lett.* **44**, 1780–1783 (2023).

According to the reviewer's comment, we have added some sentences to describe the details about device fabrication process in the revised manuscript. **The revised sections are as follows.**

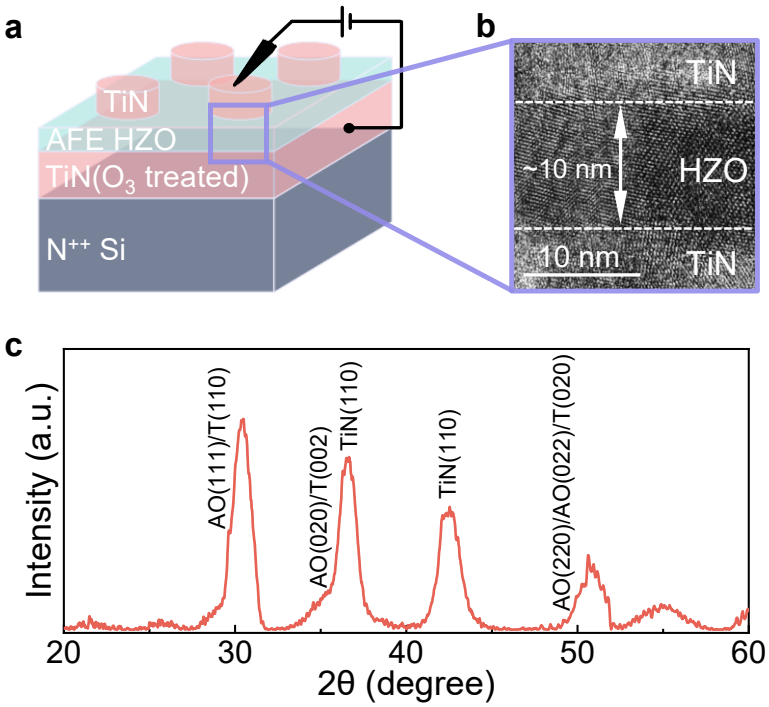


**Extended Data Fig. 1 Structural Characteristics. a**, Schematic illustration of the AFE TiN/HZO/TiN capacitors. **b**, Cross-sectional TEM images of the HZO film. **c**, GIXRD spectra measured for a $ZrO_2$ capacitor.

***Moreover, we have extensively checked the manuscripts and corrected both minor typos and grammatical errors. Also, we have reformatted all paragraphs in order to include the required revisions.***

***We hope that the revised version of the manuscript can now meet the reviewers' expectations and can be accepted for publication; otherwise, we are open to new improvements.***

Best regards,

Haoji Qian
on behalf of all authors

# Response to Reviewer's Comments

Title: Elucidating and Decoupling Diverse Fatigue Mechanisms Toward Static Self-Recovery in $ZrO_2$-Based Antiferroelectrics

Authors: Haoji Qian, Rongzong Shen, Jiacheng Xu, Miaomiao Zhang, Minglei Ma, Yian Ding, Xiaoxi Li, Gaobo Lin, Jiani Gu, Ran Cheng, Yan Liu, Chengji Jin, Jiajia Chen, Yue Hao, and Genquan Han

Dear Reviewers,

We really appreciate your important comments on our manuscript entitled: Elucidating and Decoupling Diverse Fatigue Mechanisms Toward Static Self-Recovery in $ZrO_2$-Based Antiferroelectrics. We have carefully revised the manuscript according to the reviewers' comments. The detailed descriptions on the revisions and the point-to-point responses to the reviewers' comments are summarized as below. The revised parts in the new manuscript have been highlighted.

## Reviewer: 1

Comments to the Author

This manuscript has been improved after revision. Since the authors proposed a static self-recovery (SSR) method to restore the $2P_r$, there are some suggestions as below.

**Comment 1:** The waiting time needs to be performed with $2P_r$ degradation, and the authors mentioned that a threshold can be predefined. How to realize this concept, like "Self-Tracking Circuit Design for Recovery" [1]. Can the authors propose a circuit to sense the $2P_r$ degradation threshold? [1] C.-W. Wu et al, IEDM, 18-2, 2023

**Response:** We sincerely thank the reviewer for raising this important point. To address the concern regarding the realization of the $2P_r$ degradation detection, we have designed a self-sensing circuit for static self-recovery (SSR) operation, as illustrated in **Fig. R1**. This circuit enables dynamic detection of the $2P_r$ degradation level by leveraging differential sensing through two reference cells. The circuit utilizes two sets of sense amplifier (SA) connected to reference cells. REF1 and REF2 represent the minimum signal of the "1" state and the sensed signal for executing the SSR operation, respectively. The design enables the delimitation of a degradation zone by comparing the outputs of the two SAs during a controlled read operation. Specifically, the reference cells are selected such that their readout voltages reflect different degradation thresholds. The output pattern (SA_OUT1 = 0, SA_OUT2 = 0) corresponds to a condition where the degraded target cell has crossed the predefined threshold, while the fresh cell remains readable. This pattern defines the SSR zone, indicating that the memory cell has entered a state requiring recovery. Once the SSR zone is detected, a recovery enable signal (REC_EN = 1) is asserted through a NOR gate, and the system can initiate appropriate SSR

actions to recover the target cell. The detection logic is implemented using a simple digital comparator and control circuitry, allowing seamless integration into existing memory read paths. The proposed SSR circuit demonstrates robust self-monitoring capability and offers a low-overhead solution for enhancing memory reliability. This design provides a practical and scalable solution for in-situ degradation monitoring, and aligns with the concept of self-tracking recovery proposed in **Ref. [1]**, while being tailored to our memory architecture.

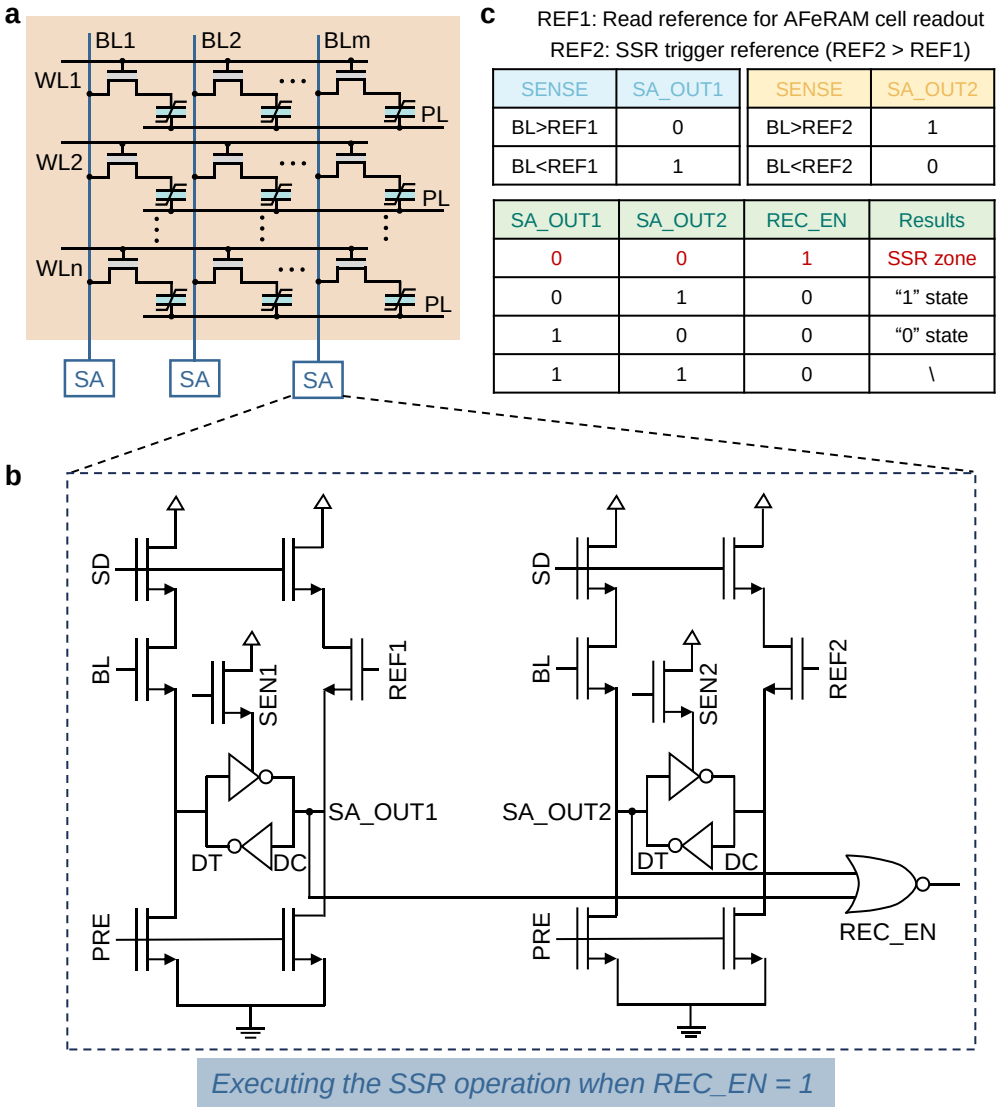


c

REF1: Read reference for AFeRAM cell readout
REF2: SSR trigger reference (REF2 > REF1)

| SENSE | SA_OUT1 |
|---|---|
| BL>REF1 | 0 |
| BL<REF1 | 1 |

| SENSE | SA_OUT2 |
|---|---|
| BL>REF2 | 1 |
| BL<REF2 | 0 |

| SA_OUT1 | SA_OUT2 | REC_EN | Results |
|---|---|---|---|
| 0 | 0 | 1 | SSR zone |
| 0 | 1 | 0 | “1” state |
| 1 | 0 | 0 | “0” state |
| 1 | 1 | 0 | \ |

**Fig. R1**, **Self-sensing circuit for SSR operation. a**, Circuit architecture of $ZrO_2$-based AFeRAM array cooperated with **b**, sensing amplifiers to achieve self-sensing SSR scheme. **c**, SSR operation will be triggered when the output of REC_EN is “1”.

## Reference (Response Letter)


1. Wu, C. et al. Robust Recovery Scheme for MFIS-FeFETs at Optimal Timing with Prolonged Endurance: Fast-Unipolar Pulsing (100 ns), Nearly Zero Memory Window Loss (0.02 %), and Self-Tracking Circuit Design. in *2023 International Electron Devices Meeting (IEDM)* 18.2.1-18.2.4 (IEEE, San Francisco, CA, USA, 2023).

According to the reviewer's comment, we have added the designed circuit (**Fig. R1**) as **Supplementary Figure 8** in the revised Supplementary Information. **The revised sections are as follows.**

## Supplementary Information

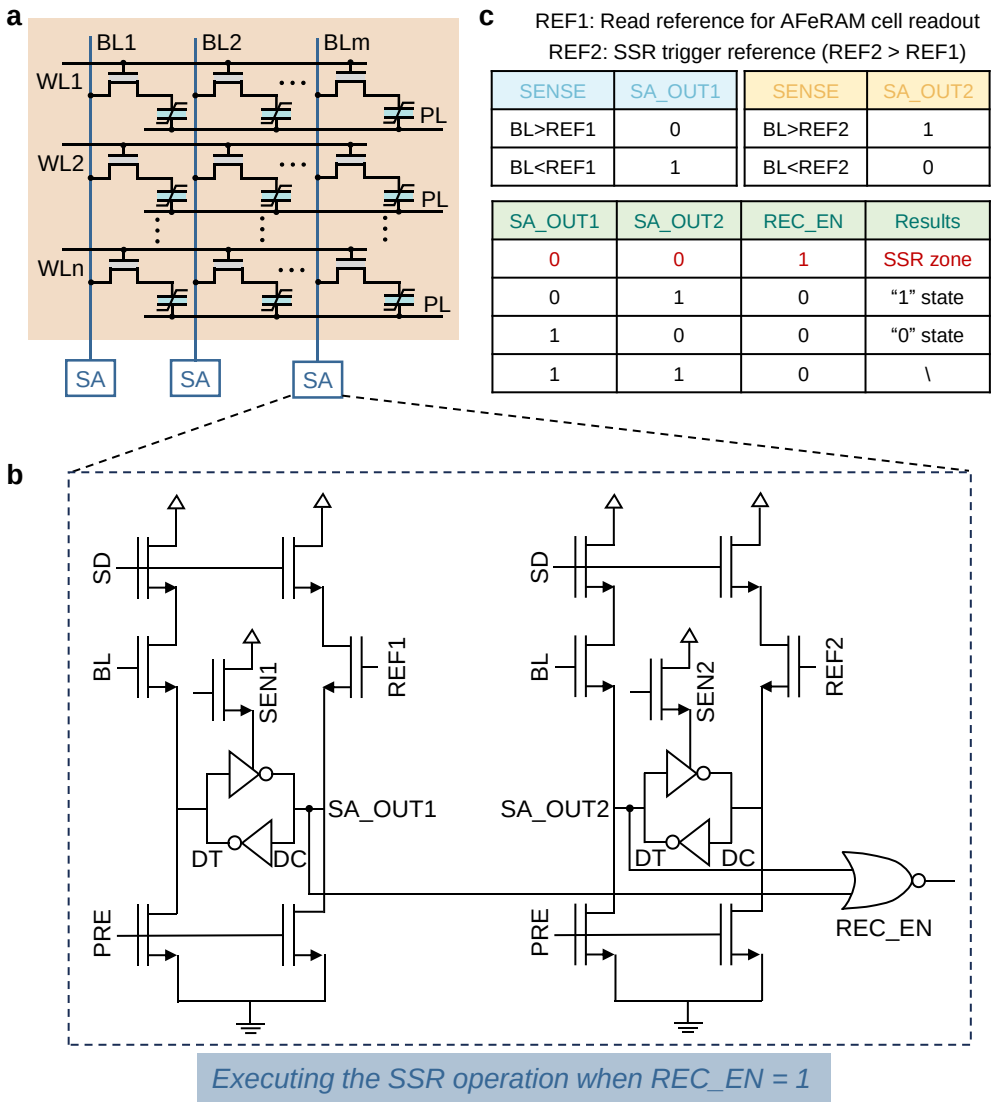


c

REF1: Read reference for AFeRAM cell readout
REF2: SSR trigger reference (REF2 > REF1)

| SENSE | SA_OUT1 | SENSE | SA_OUT2 |
|---|---|---|---|
| BL>REF1 | 0 | BL>REF2 | 1 |
| BL<REF1 | 1 | BL<REF2 | 0 |

| SA_OUT1 | SA_OUT2 | REC_EN | Results |
|---|---|---|---|
| 0 | 0 | 1 | SSR zone |
| 0 | 1 | 0 | "1" state |
| 1 | 0 | 0 | "0" state |
| 1 | 1 | 0 | \ |

**Supplementary Figure 8 Self-sensing circuit for SSR operation. a**, Circuit architecture of $ZrO_2$-based AFeRAM array cooperated with **b**, sensing amplifiers to achieve self-sensing SSR scheme. **c**, SSR operation will be triggered when the output of REC_EN is "1".

As illustrated in Supplementary Figure 8, a self-sensing circuit for static self-recovery (SSR) operation has been designed. This circuit enables dynamic detection of the polarization degradation level by leveraging differential sensing through two reference cells. The circuit utilizes two sets of sense amplifier (SA) connected to reference cells. REF1 and REF2 represent the minimum signal of the "1" state and the sensed signal for executing the SSR operation, respectively. The design enables the delimitation of a degradation zone by comparing the outputs of the two SAs during a controlled read operation. Specifically, the reference cells are selected such that their readout voltages reflect different degradation thresholds. The output pattern (SA_OUT1 = 0, SA_OUT2 = 0) corresponds to a condition where the degraded target cell has crossed the predefined threshold, while the fresh cell remains readable. This pattern defines the SSR zone, indicating that the memory cell has entered a state requiring recovery. Once the SSR zone is detected, a recovery enable signal (REC_EN = 1) is asserted through a NOR gate, and the system can initiate appropriate SSR actions to recover the target cell. The detection logic is implemented using a simple digital comparator and control circuitry, allowing seamless integration into existing memory read paths. This design provides a practical and scalable solution for in-situ degradation monitoring, and aligns with the concept of self-tracking recovery proposed in ref. 2, while being tailored to our memory architecture.

**Comment 2:** The authors claimed SSR has the potential to exceed $10^9$ cycles. Recently, many papers show the robust endurance for > $10^{10}$ cycles. The suggestion is that the authors have to demonstrate the outstanding performance of the SSR scheme to convince the readers.

**Response:** We sincerely thank the reviewer for this valuable suggestion. To address the concern, we have added a more detailed discussion on the application scope and significance of the SSR scheme.

It is true that recent studies have reported endurance exceeding $10^{10}$ cycles, which can be achieved through interface engineering or doping optimization of the ferroelectric (FE) or antiferroelectric (AFE) thin films. However, the SSR method is not in conflict with such intrinsic endurance improvements. On the contrary, SSR can be synergistically combined with high-endurance devices to further enhance overall reliability.

In our current work, the presented $ZrO_2$-based AFE devices are fabricated using standard processes without specific interface optimization. In particular, the $Hf_{0.1}Zr_{0.9}O_2$ capacitors

typically suffer from limited endurance ($2P_{s,p}$ decrease to 5 μC/cm$^2$ after $2\times10^6$ cycles). Nevertheless, by applying the SSR scheme, we demonstrate that the endurance of $Hf_{0.1}Zr_{0.9}O_2$ samples can be extended to beyond $10^9$ cycles.

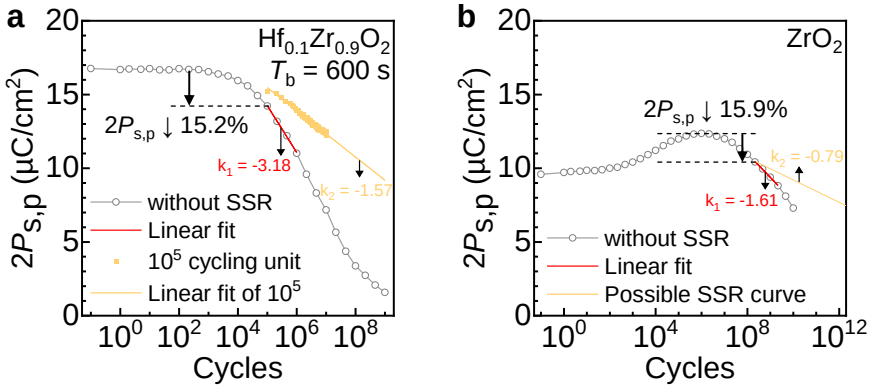


**Fig. R2 Fatigue mitigation in $Hf_{0.1}Zr_{0.9}O_2$ and $ZrO_2$ AFE capacitors via SSR strategy. a**, Endurance performances of $Hf_{0.1}Zr_{0.9}O_2$ samples, comparing the experimental measured data up to $10^9$ electrical cycles (grey curve) and the linear fitting for the $T_b$ = 600 s, cycling unit = $10^6$ SSR combinations by extrapolating the results in Fig. 5d to $10^9$ cycles. The fatigue rate is quantified by $k_1$ and $k_2$. **b**, Endurance performances of $ZrO_2$ samples, showing experimental measured data up to $10^{10}$ electrical cycles (grey curve), the linear fitted fatigue trend at $2\times10^8$ cycles without SSR (red curve) and the projected fatigue behavior under SSR application.

For devices with inherently better endurance, such as $ZrO_2$ capacitors in this work, with $2P_{s,p}$ values > 5 μC/cm$^2$ even after $10^{10}$ cycles (**Fig. R2**), the SSR method can still provide substantial benefits. Although direct SSR (with different cycling unit and $T_b$) combination measurements on $ZrO_2$ devices are constrained by long measurement durations, we have evaluated the potential endurance enhancement through a simplified analogy based on the observed polarization degradation trend. As shown in **Fig. R2a**, experimental data from $Hf_{0.1}Zr_{0.9}O_2$ samples indicate that at $10^5$ cycles, the fatigue level reaches ~15.2%. Applying a combined strategy of $10^5$ cycling units combing $T_b$ = 600 s can reduce the fatigue rate by approximately 49.7% (from $k_1 = -3.12$ to $k_2 = -1.57$).

Considering the similar fatigue mechanisms in these two types of $ZrO_2$-based AFE capacitors, by identifying a comparable fatigue point in $ZrO_2$ devices at ~$2\times10^8$ cycles (with ~15.9% $2P_{s,p}$ degradation), we estimate that applying the SSR strategy ($10^8$ cycling units and $T_b$ = 600 s) could also achieve ~50% fatigue rate delay (from $k_1 = -1.61$ to $k_2 = -0.79$). Under this condition, the device is expected to retain the $2P_{s,p}$ of ~7 μC/cm$^2$ even after $10^{12}$ cycles, indicating a significant improvement in endurance.

In conclusion, the SSR scheme is not only effective for improving the reliability of devices with limited intrinsic endurance but also offers substantial enhancement for high-endurance AFE systems. We have added this analysis to the revised manuscript to clarify the broader applicability and performance advantage of SSR.

According to the reviewer's comment, we have added some sentences in the revised manuscript and replaced **Supplementary Figure 6** in in the revised Supplementary Information by **Fig. R2** to further demonstrate the outstanding performance of the SSR scheme. **The revised sections are as follows.**

## Development of three level traps model

After figuring out the proportional contributions of different mechanisms in deep fatigue situation of $Hf_{0.1}Zr_{0.9}O_2$, further analysis of the SSR capability at varying $T_b$ is conducted, as illustrated by the red scatter plot in the right panel of Fig. 3f. The maximum self-recoverable polarization through SSR can be approximately estimated at 6.11 μC/cm$^2$ (the difference between the recovered $2P_{s,p}$ after SSR with a 3600 s break and the fatigued $2P_{s,p}$ after $10^7$ cycles), nearly equivalent to the magnitude of extrinsic fatigue extracted from Fig. 3d, which is 6.21 μC/cm$^2$ for $10^7$ cycles. This indicates that SSR can fully recover the extrinsic fatigue caused by charge trapping but has limited effectiveness in recovering intrinsic fatigue. Additional experiments on $Hf_{0.1}Zr_{0.9}O_2$ capacitors have been conducted to extend the endurance measurements to $10^9$ cycles, and the $ZrO_2$ capacitors with inherently better endurance is expected to retain the $2P_{s,p}$ of ~7 μC/cm$^2$ even after $10^{12}$ cycles via proper SSR strategy (Supplementary Figure 6).

## Supplementary Information

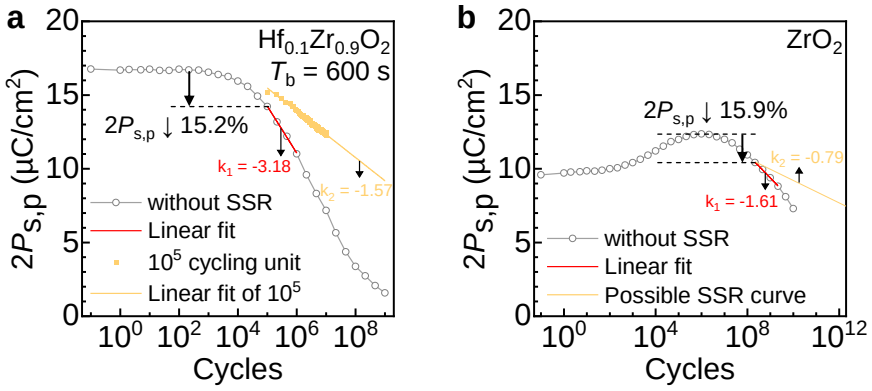


**Supplementary Figure 6 Fatigue mitigation in $Hf_{0.1}Zr_{0.9}O_2$ and $ZrO_2$ AFE capacitors via SSR strategy. a**, Endurance performances of $Hf_{0.1}Zr_{0.9}O_2$ samples, comparing the experimental measured data up to $10^9$ electrical cycles (grey curve) and the linear fitting for the $T_b$ = 600 s, cycling unit = $10^6$ SSR combinations by extrapolating the results in Fig. 5d to $10^9$ cycles. The fatigue rate is quantified by $k_1$ and $k_2$. **b**, Endurance performances of $ZrO_2$ samples, showing experimental

measured data up to $10^{10}$ electrical cycles (grey curve), the linear fitted fatigue trend at $2\times10^{8}$ cycles without SSR (red curve) and the projected fatigue behavior under SSR application.

## Reviewer: 2

Comments to the Author

This manuscript presents a novel approach to addressing the endurance (fatigue) issues in $ZrO_2$-based antiferroelectric (AFE) devices. The authors introduce the concept of Static Self-Recovery (SSR) and systematically analyze the fatigue mechanisms of $ZrO_2$-based AFEs through electrical measurements. They further decouple the contributions of oxygen vacancy ($V_O$) formation and shallow/deep traps, and establish a clear interpretation of the fatigue behavior. Based on this, they propose a three-level trap model to describe the SSR process, which is additionally supported by density functional theory (DFT) calculations.

The reviewers mainly raised questions regarding the contribution of oxygen vacancy traps and the validity of the newly proposed SSR measurement method. The authors responded thoroughly and convincingly, addressing these concerns without undermining the original claims of their work. In particular, the distinction between shallow and deep fatigue and the universality of the three-level trap model were clarified and strongly supported by both experimental data and theoretical analysis.

Therefore, this reviewer concludes that the manuscript presents significant and meaningful results with direct implications for enhancing the endurance of next-generation AFE-based memory devices. The study provides valuable insights and is of sufficient quality for publication. Accordingly, I recommend acceptance of this manuscript.

**Response:** We sincerely thank the reviewer for the positive and thoughtful comments. We appreciate your recognition of the SSR concept, the three trap model, and our combined experimental and theoretical analysis. Your support and recommendation for acceptance are deeply appreciated.

## Reviewer: 3

Comments to the Author

The authors present convincing analyses of the electrical characterizations for memory applications, and the quality of the paper has improved significantly following the reviewers' comments. The work, in its current form, already provides valuable insights, and the study deserves consideration for publication.

That said, the discussion relies mainly on theoretical arguments to support the interpretation of electrical measurements. While these interpretations are logical and often compelling, the absence of complementary experimental evidence (such as deeper analyses in XRD, XPS, TEM, temperature-dependent measurements, etc.) limits the strength of the conclusions. For example, the separation between extrinsic and intrinsic fatigue, or the attribution of FWHM distribution to oxygen vacancy redistribution, would be considerably more convincing if supported by direct experimental proof. At present, some explanations remain hypothetical, particularly as several justifications draw primarily on the authors' own prior publications. More generally, the article interprets complex, multifactorial electrical measurements through largely theoretical support. This approach is not without merit, but additional perspectives would enhance the work. Future studies could benefit from:

- Complementary experimental characterizations to substantiate theoretical hypotheses.
- Engagement with a wider body of literature, beyond the authors' own work (particularly in the first response to reviewers)
- Consideration of alternative mechanisms could provide greater nuance and robustness to the conclusions.

**Response:** We sincerely appreciate the reviewer's thoughtful feedback and agree that complementary experimental evidence can significantly strengthen the interpretation of electrical measurements. To address this concern, we have conducted additional electron energy loss spectroscopy (EELS) analysis to investigate the oxygen vacancies ($V_O$) distribution in $Hf_{0.1}Zr_{0.9}O_2$ capacitors before and after electrical cycling. The energy-loss near-edge structure (ELNES) of the oxygen (O) K-edge obtained from EELS spectrum imaging is analyzed. As reported in prior studies, the O K-edge typically exhibits a characteristic doublet with peaks labeled *a* (~534 eV) and *b* (~538 eV), which is shown in **Fig. R3a**[2]. The relative intensity ratio of the peak *a* and *b* (*a*/*b*) is highly sensitive to the local chemical environment and coordination symmetry. A more uniform and stoichiometric O distribution tends to produce a well-defined doublet with balanced *a*/*b* values. In contrast, the presence of $V_O$ and structural disorder such as those induced by cycling can lead to a suppressed peak *a*, resulting in a smaller *a*/*b* ratio.
As shown in **Fig. R3c**, the EELS mapping of pristine $Hf_{0.1}Zr_{0.9}O_2$ AFE film reveals a relatively uniform distribution of $V_O$, which correlates with the narrow full width at half maximum (*FWHM*) observed in the initial *I*–*V* characteristics. After $10^6$ electrical cycles, the EELS mapping shows a clear localization of $V_O$, consistent with the broader *FWHM* measured after cycling (**Fig. R3d**). The detailed average (AVG) and standard deviation (STD) over Region 1-6 of the pristine and $10^6$ cycled states are shown in **Fig. R3e and R3f**. This spectral evolution provides direct experimental evidence for the redistribution of $V_O$, and supports our explanation of the *FWHM* broadening observed in the electrical measurements.

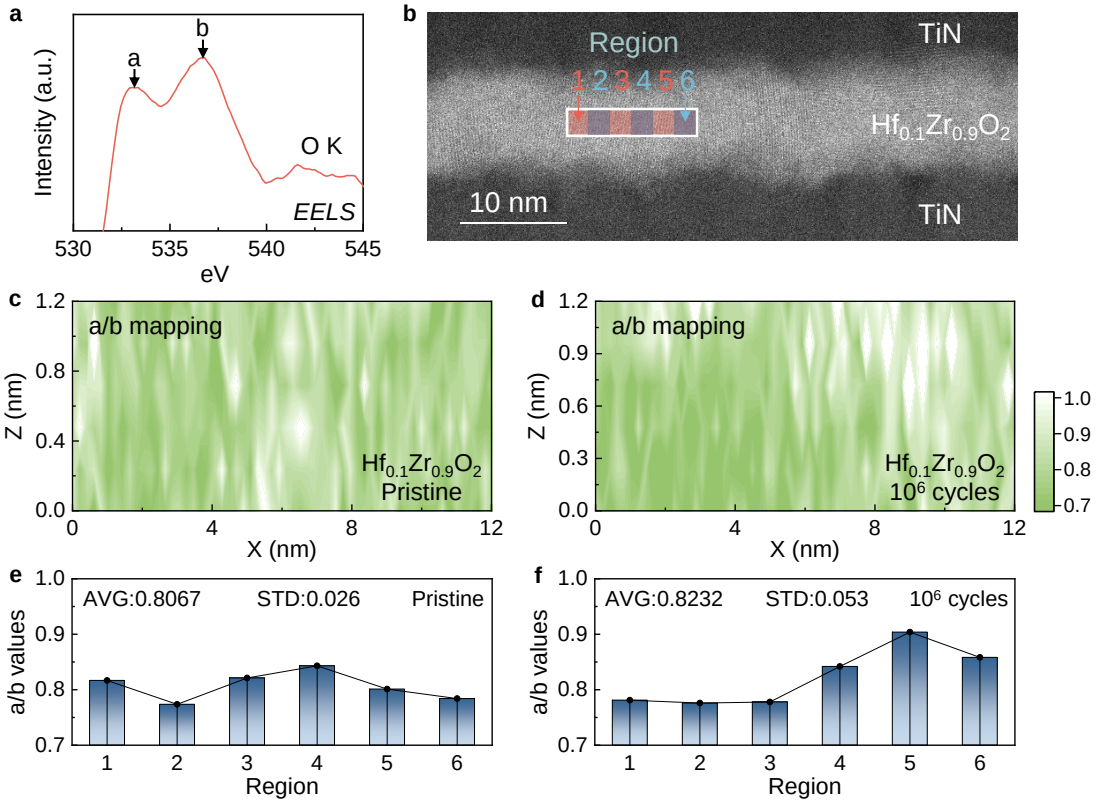


**Fig. R3 Evolution of $V_O$ distribution in $Hf_{0.1}Zr_{0.9}O_2$ capacitors. a**, Typical O K EELS spectra averaged over the $Hf_{0.1}Zr_{0.9}O_2$ film. **b**, Device structure of $Hf_{0.1}Zr_{0.9}O_2$ capacitors and the schematic regions for EELS mapping. **c**,**d**, Maps of *a*/*b* ratio in O K EELS for pristine and $10^6$ cycled $Hf_{0.1}Zr_{0.9}O_2$ samples, respectively. **e**,**f**, The average *a*/*b* ratio and standard deviation over region 1-6 of the pristine and $10^6$ cycled $Hf_{0.1}Zr_{0.9}O_2$ samples, respectively.

**References (Response Letter)**

2. Kang, D., Lee, S., Kim, Y. et al. Highly enhanced ferroelectricity in $HfO_2$-based ferroelectric thin film by light ion bombardment. *Science* **376**, 731–738 (2022).

According to the reviewer's comment, we have added some sentences to describe the O K EELS measurements in the revised manuscript and Supplementary Information. **The revised sections are as follows.**

## Electrical characteristics of $ZrO_2$-based AFE capacitors

Note that the changes in *FWHM*, including increase and decrease, indicate the redistribution of $V_O$[16,17]. During the cycling process, the stable *FWHM* with the shifted *I*−*V* curve means that charge

trapping occurs in the capacitor, without the redistribution of $V_O$, which may be the leading fatigue mechanism in $ZrO_2$ with $10^8$ cycles. While the fatigue in $Hf_{0.1}Zr_{0.9}O_2$ may be induced by the coupling of $V_O$ charge trapping and redistribution. The experimental measured electron energy loss spectroscopy (EELS) maps shown in Supplementary Figure 2 provides direct evidence for the $V_O$ redistribution by extracting the evolution of oxygen (O) K-edge doublet (*a*/*b* ratio) and supports the explanation of the *FWHM* broadening observed in the electrical measurements. The different fatigue behaviors observed between $ZrO_2$ and $Hf_{0.1}Zr_{0.9}O_2$ are strongly influenced by the presence of Hf. In pure $ZrO_2$, where no Hf is introduced, $V_O$ tend to be charged during electrical cycling, characterized by the shift of *I*–*V* curves with the limited change in the shapes of the curves. In contrast, in $Hf_{0.1}Zr_{0.9}O_2$, the introduction of Hf incorporation facilitates partial localization of $V_O$ within the lattice and initiates AFE to FE PT, contributing to the significant change in the shapes of the *I*–*V* curves.

## Supplementary Information

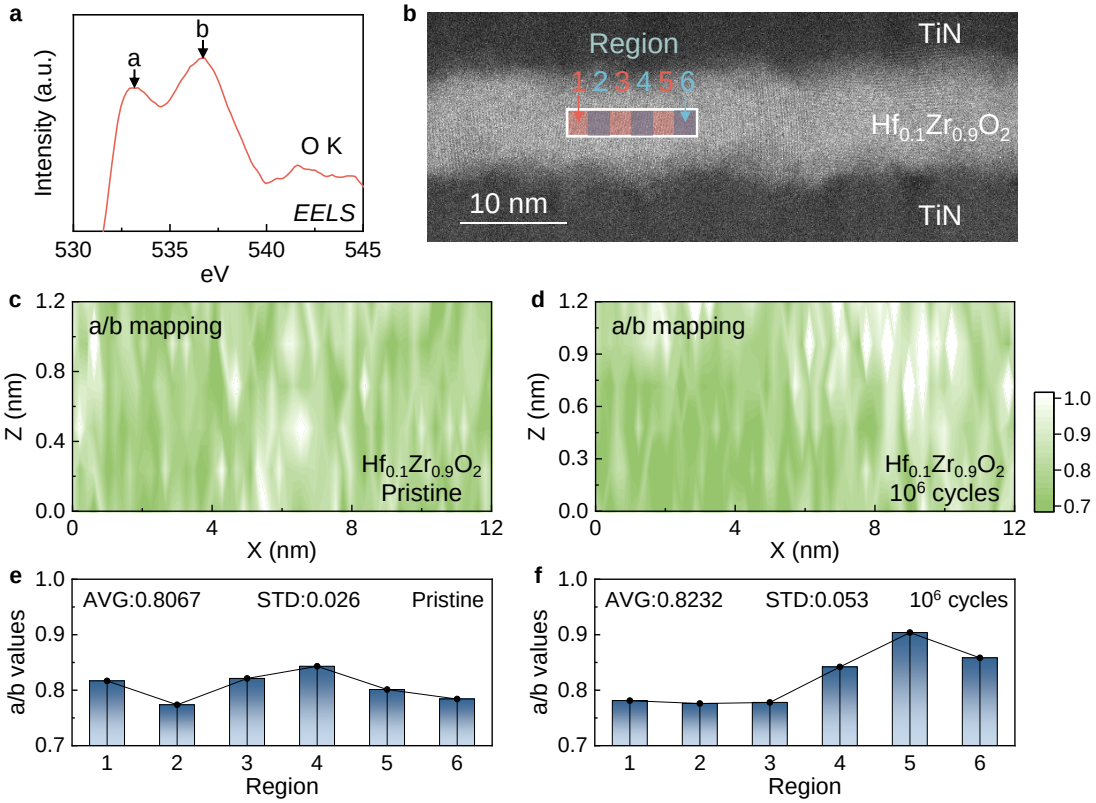

**Supplementary Figure 2 Evolution of $V_O$ distribution in $Hf_{0.1}Zr_{0.9}O_2$ capacitors. a**, Typical O K EELS spectra averaged over the $Hf_{0.1}Zr_{0.9}O_2$ film. **b**, Device structure of $Hf_{0.1}Zr_{0.9}O_2$ capacitors and the schematic regions for EELS mapping. **c**,**d**, Maps of *a*/*b* ratio in O K EELS for pristine and $10^6$ cycled $Hf_{0.1}Zr_{0.9}O_2$ samples, respectively. **e**,**f**, The average *a*/*b* ratio and standard deviation over region 1-6 of the pristine and $10^6$ cycled $Hf_{0.1}Zr_{0.9}O_2$ samples, respectively.

The electron energy loss spectroscopy (EELS) analysis is performed to investigate the oxygen vacancies ($V_O$) distribution in $Hf_{0.1}Zr_{0.9}O_2$ capacitors before and after electrical cycling. The energy-loss near-edge structure (ELNES) of the oxygen (O) K-edge obtained from EELS spectrum imaging is analyzed. As reported in prior studies[1], the O K-edge typically exhibits a characteristic doublet with peaks labeled *a* (~534 eV) and *b* (~538 eV), which is shown in Supplementary Figure 2a. The relative intensity ratio of the peak *a* and *b* (*a*/*b*) is highly sensitive to the local chemical environment and coordination symmetry. A more uniform and stoichiometric O distribution tends to produce a well-defined doublet with balanced *a*/*b* values. In contrast, the presence of $V_O$ and structural disorder such as those induced by cycling can lead to a suppressed peak *a*, resulting in a smaller *a*/*b* ratio.

As shown in Supplementary Figure 2c, the EELS mapping of pristine $Hf_{0.1}Zr_{0.9}O_2$ AFE film reveals a relatively uniform distribution of $V_O$, which correlates with the narrow full width at half maximum (*FWHM*) observed in the initial *I*–*V* characteristics. After $10^6$ electrical cycles, the EELS mapping shows a clear localization of $V_O$, consistent with the broader *FWHM* measured after cycling (Supplementary Figure 2d). The detailed average (AVG) and standard deviation (STD) over Region 1-6 of the pristine and $10^6$ cycled states are shown in Supplementary Figure 3e and Supplementary Figure 2f. This spectral evolution provides direct experimental evidence for the redistribution of $V_O$, and supports our explanation of the *FWHM* broadening observed in the electrical measurements.

***Moreover, we have extensively checked the manuscripts and corrected both minor typos and grammatical errors. Also, we have reformatted all paragraphs in order to include the required revisions.***

***We hope that the revised version of the manuscript can now meet the reviewers' expectations and can be accepted for publication; otherwise, we are open to new improvements.***

Best regards,

Haoji Qian
on behalf of all authors